Dissertation

Turbulence Modeling of Stably Stratified Wall-Bounded Flows

Submitted by

Farid Karimpour

Department of Civil and Environmental Engineering

In partial fulfillment of the requirements

For the Degree of Doctor of Philosophy

Colorado State University

Fort Collins, Colorado

Fall 2014

Doctoral Committee:

Advisor: Subhas K. Venayagamoorthy

Thomas Birner
Brian P. Bledsoe
Pierre Y. Julien

Abstract

Turbulence Modeling of Stably Stratified Wall-Bounded Flows

The subject of wall-bounded flows has been a matter of discussion and has received considerable attention in the past few decades. This is mainly attributed to the fact that the presence of the solid wall has profound effects on the turbulence and hence results in anomalous mixing and transport of momentum, scalar and heat in environmental flows. This is much more intense in the vicinity of the solid wall commonly known as the near-wall region compared to regions away from the wall. This effect will be more complicated in the presence of density stratification which has a strong influence on the development of turbulence. Therefore, numerous field, laboratory, numerical and theoretical studies are performed in a quest to gain a better understanding of wall-bounded flows especially in the presence of stratification. However, there is still a lack of a clear picture on the near-wall flow properties, the onset of turbulence and the resulting mixing in wall-bounded flows.

The aim of this dissertation is to employ both theory and numerical simulations to revisit mixing in wall-bounded flows, especially in the near-wall region. The main objectives are:

- To investigate the unstratified near-wall turbulence and revisit the turbulent (eddy) viscosity (ν_t) formulation in unstratified wall-bounded flows. This will be followed by derivation of a novel proposition for the appropriate velocity, length and time scales in unstratified wall-bounded flows.
- To revisit the fundamentals of common Reynolds-averaged Navier-Stokes (RANS) closure schemes such as the standard k-ϵ model and investigate their capability to model near-wall turbulence.

- To investigate the turbulent mixing in stably stratified wall-bounded flows. The mixing of momentum, scalar and the efficiency of the mixing are evaluated.
- To study wall-bounded turbulent flows in the presence of stable stratification by performing one-dimensional RANS simulations. In particular, this includes introduction of a modified turbulent Prandtl number (Pr_t) for wall-bounded flows and calibration of the standard k-ϵ model.

In this dissertation, a novel formulation for the turbulent (eddy) viscosity given by $\nu_t = \epsilon/S^2$ is derived by assuming equilibrium between the turbulent kinetic energy production rate (P) and the dissipation rate of the turbulent kinetic energy (ϵ), where S is the mean shear rate. Also, the relevant scales of length and velocity are derived. The propositions are tested with the direct numerical simulation (DNS) data of unstratified turbulent channel flow of Hoyas & Jiménez (2006) and unstratified turbulent boundary layer flow of Sillero *et al.* (2013). The comparisons of the propositions with the exact computations from the DNS data are excellent.

Furthermore, the suitability of the equilibrium assumption (i.e. $P \approx \epsilon$) for modeling near-wall turbulence is revisited. This is important as most widely used turbulent viscosities such as the formulation of the standard k-ϵ model are developed by using the equilibrium assumption. It is analytically shown that such ν_t formulations are not suitable for modeling near-wall turbulence.

Also, the turbulent mixing in stably stratified wall-bounded flows is studied by employing analytical arguments. *'A priori'* tests are performed by using highly resolved stably stratified channel flow DNS data of García-Villalba & del Álamo (2011). It is shown that in such flows assuming $P \approx \epsilon + \epsilon_{PE}$, where ϵ_{PE} is the dissipation rate of the turbulent potential energy,

holds in a big fraction of the flow depth. Also, the results show that an irreversible flux Richardson number as $R_f^* = \epsilon_{PE}/(\epsilon + \epsilon_{PE})$ can properly predict the flux Richardson number ($R_f = -B/P$), where B is the buoyancy flux. It is also shown that neglecting the transport rate of ϵ_{PE} and assuming equilibrium as $-B \approx \epsilon_{PE}$ is not a suitable assumption.

Furthermore, the ideas discussed are utilized to perform *'a posteriori'* tests and to simulate stably stratified wall-bounded flows by using RANS numerical models. To do this, first a simple one-dimensional zero-equation as well as two-equation k-ϵ RANS models are developed. It is shown that turbulent Prandtl numbers based on the homogeneous assumption are not capable of providing a good estimation of the mixing and therefore an inhomogeneity correction must be introduced. It is analytically shown that commonly used homogeneous turbulent Prandtl numbers should be modified for a wall-bounded flow using a correction as $(1 - z/D)$, where D is the total flow depth. This work is extended by revisiting the buoyancy parameter ($C_{\epsilon 3}$) in the standard k-ϵ closure scheme. Analytical arguments are used to show that $C_{\epsilon 3} \approx 0$. RANS results show the suitability of the propositions for modeling of stably stratified turbulent channel flows.

The ultimate goal of this research is to enhance understanding of the fundamental aspects of wall-bounded environmental flows and develop appropriate turbulence models that can capture the physics of stably stratified wall-bounded turbulent flows.

Acknowledgements

I would like to sincerely thank Dr. Karan Venayagamoorthy for all his support, encouragement, imparted knowledge, his guidance during my PhD studies and also giving me the opportunity to come to CSU. Without his help, this dissertation would have never been possible. I would like to thank Dr. Brian Bledsoe for his constructive suggestions. I am also grateful to Dr. Pierre Julien for his helpful comments. Thanks, also to Dr. Thomas Birner for his guidance.

I thank my former officemate Dr. Benjamin Mater for all his help, friendship and also the scientific and philosophical discussions we had during lunch! I also thank Dr. Jordan Wilson for all the fruitful discussions we had during my PhD. I wish to thank all my friends, particularly Simon Schaad who has always kindly helped me.

Certainly, I thank my family for all their unconditional love, encouragement and support. I will be always indebted to them, particularly to my late father and my mother. Without them I would have never been the person I am today. Also, I will be always grateful to my brothers Farshid and Arash who have always selflessly supported me in all stages of my life.

Also, funding from National Science Foundation under CAREER grant OCE-1151838 is gratefully acknowledged.

Dedication

This dissertation is dedicated

to my mother, Elaheh

my brothers Farshid and Arash

and in memory of my beloved father, Faramarz Karimpour.

Table of Contents

List of Tables

List of Figures

CHAPTER 1

Introduction

1.1. Motivation

Wall-bounded turbulent flows are common phenomena in engineered flows as well as in nature such as rivers, estuaries and oceans. The existence of the solid wall has intricate effects on the turbulent flow, particularly in the vicinity of the wall which is commonly known as the near-wall region. The thin layer of the near-wall region is subtle and important to comprehend as about 50% of the maximum velocity in the free-stream occurs in this region (Hanjalić & Launder 1976) and the anisotropy of the flow is remarkable. Furthermore, many environmental flows are influenced strongly by density stratification. The simultaneous effect of the solid wall and stratification leads to presence of anisotropy and inhomogeneity in the flow causing boundary layer instability and generation of turbulence which has profound effect on momentum and scalar transport and associated mixing. Therefore, stratified wall-bounded turbulent flows are considered as one of the most complicated but interesting research topics in fluid mechanics. Although the wall effect on the flows has long been recognized, it is only fairly recently that the detailed aspects of the wall-bounded flows have become clearer mainly due to the numerical simulation studies of Kim *et al.* (1987), Durbin (1991), Armenio & Sarkar (2002), Hoyas & Jiménez (2006), Wu & Moin (2008) and García-Villalba & del Álamo (2011). However, despite such studies, there is still a lack of robust understanding of the complexity associated with wall-bounded flows, especially in the presence of density stratification. Hence, further investigation is warranted.

Unstratified wall-bounded turbulent flows widely exist such as air flow around the aerodynamic body surface of space shuttles or water flow in a shallow river. In such flows, it is essential to correctly capture the near-wall velocity profile and the transition from laminar to turbulent flow in the boundary layer. This is vital for correctly inferring the shear stress on the solid body which plays a main role for designing, sustaining and operating objects in direct contact to the turbulent fluid. The failure to do so might be fatal, such as

the disaster of Columbia space shuttle in 2003. In recent years, numerical simulations such as direct numerical simulation (DNS), large-eddy simulation (LES) and Reynolds-averaged Navier-Stokes (RANS) simulations are widely used for modeling wall-bounded flows. DNS and LES methods predict the flow with high accuracy but are prohibitively expensive and not appropriate for modeling complex flows. On the other hand, while RANS models are much faster, they suffer from lack of accuracy. Hence, in spite of great strides made to introduce robust RANS models for simulating near-wall turbulence, there is still uncertainty about the performance of such models for simulating flows with high Reynolds numbers and complex geometries. Hence, further research is required to investigate RANS closure schemes for modeling unstratified wall-bounded turbulent flows.

Besides unstratified flows, stratified wall-bounded turbulent flows are quite common especially in nature. Oceanic flows are a good example of such flows. Stable stratification is ubiquitous in the ocean and its effect on the turbulence and mixing has long been recognized. Stable stratification can be due to vertical temperature and/or salinity gradients (Staquet & Sommeria 2002) leading to qualitative and quantitative changes in the small-scale mixing of momentum and scalars, ultimately influencing large-scale processes (Armenio & Sarkar 2002). On the other hand, the presence of stable stratification resulting in buoyancy forces along with existence of a perturbation smaller than buoyancy frequency are prerequisites for internal waves generation (Aguilar & Sutherland 2006). Therefore, the ocean as a stably stratified environment which is constantly under the influence of external forces such as tidal waves and wind stress fluctuations at the free-surface is a suitable environment for the excitement, propagation and dissipation of internal waves. A major source of internal waves generation in the ocean is through stratified fluid flow over bottom topographies such as submarine ridges and seamounts (Legg & Adcroft 2003, Legg 2004). This interaction with bottom features not only can result in generation of internal waves, but is also a major cause of internal waves instability and breaking and hence generation of turbulence. The breaking of the internal waves resulting from interaction with the bottom boundary is usually considered as a major source of energy required for turbulence and enhanced mixing in the

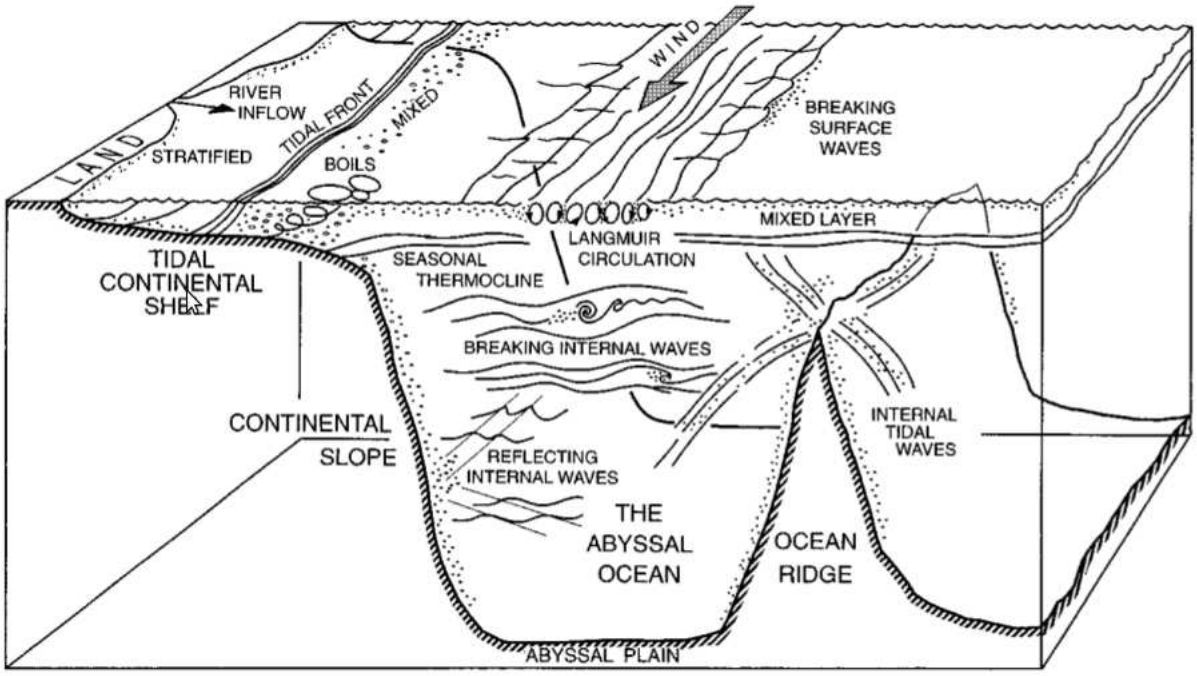

FIGURE 1.1. Sketch (not to scale) showing some of the processes related to ocean turbulence. (from Thorpe 2004).

ocean. A major hypothesis is that high turbulent (eddy) diffusivity (κ_t) in localized turbulent patches is caused by breaking of internal waves due to their interaction with bottom boundary (Gregg 1987, Munk & Wunsch 1998). Therefore, having a tangible understanding of the bottom boundary layer in the presence of stratification, substantially improves the comprehension of oceanic mixing processes.

Mixing is usually envisioned as a cascade that begins with energy transfer from surface tides to internal tides and subsequent breaking internal waves resulting in turbulence (Rudnick *et al.* 2003). This has accentuated the study of the stratified bottom boundary layer in order to better understand the turbulent mixing and transport processes of nutrients, pollutants and salinity in the ocean. Figure (1.1) schematically depicts the small-scale oceanic processes.

1.2. Background and Objectives

In this research, fundamental aspects of smooth wall-bounded flows and ensuing mixing will be studied using theoretical analysis, *'a priori'* testing by using published DNS data and

numerical simulations. Studies on both unstratified and stratified wall-bounded turbulent flows are carried out. The main objectives of this research are as follows

(1) To attain a detailed comprehension of wall effect on the mixing of momentum and scalar in the near-wall region in fully developed unstratified and stratified wall-bounded turbulent flows. In particular, fundamental characteristic scales of the turbulence in the context of the turbulent-viscosity hypothesis (TVH) will be determined in the near-wall region, where mean shear rate is dominant.

(2) To investigate the effect of the equilibrium assumption by considering formulations of the turbulent viscosity (ν_t) developed based on the equilibrium assumption and further study their capability for modeling near-wall turbulence.

(3) To develop an appropriate turbulent Prandtl number for modeling stably stratified wall-bounded flows using Reynolds-averaged Navier-Stokes (RANS) schemes and assess the efficacy of the standard k-ϵ closure scheme for modeling stably stratified wall-bounded flows.

1.3. Dissertation Layout

The remainder of this dissertation is composed of four further chapters. The contents of chapters 3, 4 and 5 have been written up as journal manuscripts, hence they are relatively self-contained and as such some redundancy exists, especially with regard to the literature.

Chapter 2 consists of a literature review on the turbulence schemes, unstratified and stratified wall-bounded flows and mixing. It expands on some of the issues mentioned in section 1.1. Governing equations of flow dynamics and different turbulence schemes are also discussed.

Chapter 3 presents the work done in this study to understand unstratified wall-bounded flows from a fundamental point of view. In this chapter, the relevant characteristic scales are derived by using the equilibrium assumption. Also, *'a priori'* tests are performed to examine their suitability for describing the turbulence, using DNS data of wall-bounded

turbulent flows. Furthermore, shortcomings of turbulent viscosity formulations based on the equilibrium assumption are elucidated.

In chapter 4, the turbulent mixing in stably stratified wall-bounded flows is studied. The equilibrium assumption is made and the mixing of momentum, scalar and the efficiency of the turbulent mixing are evaluated.

In chapter 5, the efficacy of present models for simulating stably stratified wall-bounded turbulent flows is examined. Also, an appropriate Pr_t formulation for modeling such flows is introduced. The proposed formulation is developed by using analytical discussions and its efficacy is tested by performing numerical simulations. The performance of the standard k-ϵ closure scheme and especially the buoyancy parameter ($C_{\epsilon 3}$) is investigated, as well. To do this, analytical arguments are presented and modeling of a stably stratified channel flow is implemented.

1.4. Summary

This dissertation presents an investigation of wall-bounded turbulent flows with an eye toward developing appropriate RANS models for simulating wall-bounded flows. This is done by revisiting fundamental concepts of both unstratified and stratified near-wall turbulence to predict momentum and active scalar mixing followed by implementation and testing of proposed formulations in RANS simulations.

CHAPTER 2

Literature Review

2.1. Introduction

The interaction of fluid flow with solid walls is common in nature and engineered flows. The nonlinear behavior of turbulent flows, the inhomogeneity arising from the wall combined with the anisotropy effects of stratification as well as the possible presence of internal waves, have made wall-bounded flows one of the most complex but interesting problems to study. Numerous studies using field experiments, laboratory experiments and numerical simulations have focused on understanding this problem.

In this chapter, a review of the governing equations of fluid flows is provided first, followed by an overview of the significant properties and modeling methods of wall-bounded turbulent flows. Further, the effect of stratification on wall-bounded turbulence and turbulent mixing are discussed.

More comprehensive reviews on the unstratified and/or stratified wall-bounded flows can be found in the works of Kim *et al.* (1987), Durbin (1991), Pope (2000), Armenio & Sarkar (2002), George (2007), Jones *et al.* (2008), Marusic *et al.* (2010) and García-Villalba & del Álamo (2011). Detailed discussions on the turbulent mixing are provided in works of Linden (1980), Barrett & Van Atta (1991), Smyth *et al.* (2001), Staquet & Bouruet-Aubertot (2001), Venayagamoorthy & Stretch (2006) and Stretch *et al.* (2010).

2.2. Governing Equations

Any motion including fluid flow can be described by the principles of the momentum, mass and energy conservation. The hard to solve fluid flow governing equations are derived by using these three simple principles. In this section, the governing equations are presented for an unsteady, three-dimensional, irrotational, incompressible and stratified flow.

2.2.1. Momentum Equations. The fluid flow is controlled by Newton's second law of motion, relating the imposed force with mass and acceleration. For a three dimensional,

irrotational system with the Boussinesq approximation, the momentum equations (often known as the Navier-Stokes equations) are given by

$$\rho\frac{Du_i}{Dt} = \rho\frac{\partial u_i}{\partial t} + \rho\frac{\partial}{\partial x_j}(u_i u_j) = -\frac{\partial p}{\partial x_i} + \rho\nu\frac{\partial^2 u_i}{\partial x_j \partial x_j} - \rho g\delta_{i3}, \tag{1}$$

where ν is the molecular (kinematic) viscosity (assumed as a constant). The Einstein summation convention is used with $i, j = 1, 2, 3$ where x_3 represents the vertical coordinate. δ_{ij} is the Kronecker delta, equal to unity for $i = j$ and zero for $i \neq j$.

In geophysical flows, Coriolis force (F_f) and the gravitational force (F_g) are the external forces acting on the fluid. The Coriolis force is an apparent force in a rotating coordinate system which arises from the Earth's rotation and only changes the direction of motion, not the speed. This force is important for large scale systems, but in this study can be neglected as we just focus on small-scale events in water bodies.

The fluid density can be decomposed into a constant density (ρ_0), local mean value ($\overline{\rho}$) and fluctuation (ρ') given by

$$\rho = \rho_0 + \overline{\rho} + \rho'. \tag{2}$$

By inserting the decomposed density in equation (1) and rearranging, the momentum equation can be recast as

$$\begin{aligned}\left(1 + \frac{\rho'}{\rho_0 + \overline{\rho}}\right)\left(\frac{Du_i}{Dt}\right) \;=\; & -\left(\frac{1}{\rho_0 + \overline{\rho}}\right)\frac{\partial p}{\partial x_i} \\ & + \left(1 + \frac{\rho'}{\rho_0 + \overline{\rho}}\right)\nu\frac{\partial^2 u_i}{\partial x_j \partial x_j} \\ & - \left(\frac{\rho_0 + \overline{\rho} + \rho'}{\rho_0 + \overline{\rho}}\right) g\delta_{i3}.\end{aligned} \tag{3}$$

In stratified water bodies the ratio $\left(\frac{\rho'}{\rho_0+\overline{\rho}}\right) \ll 1$ and can be neglected in the acceleration (inertial) and viscosity terms, but should be retained in the gravity term as it is the primary contributor to buoyancy. This assumption is known as the Boussinesq approximation. Moreover, as $\overline{\rho} \ll \rho_0$ then the mean density is negligible compared with the background density.

In addition, if $\rho_r = \rho_0 + \overline{\rho}$ and $p_r = p_0 + \overline{p}$ are considered as reference density and pressure, and the hydrostatic relation holds, then the reference pressure and density are related as $\partial p_r/\partial x_3 = -\rho_r g$. This assumption helps in numerical simulations when starting from the rest, as the pressure field is taken as the initial hydrostatic pressure field. However, for an irrotational, incompressible and stratified fluid the Navier-Stokes equation (equation 3) can be rewritten as

$$\frac{\partial u_i}{\partial t} + \frac{\partial}{\partial x_j}(u_i u_j) = -\frac{1}{\rho_0}\frac{\partial p}{\partial x_i} + \nu\frac{\partial^2 u_i}{\partial x_j \partial x_j} - \left(\frac{\rho}{\rho_0}\right) g\delta_{i3}. \tag{4}$$

2.2.2. Continuity Equation. In fluid mechanics, mass is absolutely conserved and can be described by a mass conservation equation. The continuity equation using an Eulerian point of view is given by

$$\frac{\partial \rho}{\partial t} + \frac{\partial(\rho u_i)}{\partial x_i} = 0, \tag{5}$$

or from a Lagrangian point of view is as

$$\frac{D\rho}{Dt} + \rho\frac{\partial u_i}{\partial x_i} = 0, \tag{6}$$

where $D/Dt = \partial/\partial t + u_i(\partial/\partial x_i)$ is the total or material derivative. For the flows under Boussinesq approximation, $\rho^{-1}(D\rho)/(Dt)$ is negligible compared to $\partial u_i/\partial x_i$, therefore the continuity equation reduces to

$$\frac{\partial u_i}{\partial x_i} = 0. \tag{7}$$

This implies that the flow field is divergence free.

2.2.3. Density Transport Equation. In unstratified flows, the density is constant and acts as a 'passive' quantity in the momentum equation, but in stratified flows the density field evolves with the flow and is coupled with the momentum equation through the buoyancy term in the vertical momentum equation. This highlights the importance of considering the evolution of density transport as one of the flow governing equations. The density transport

is depicted through an advection-diffusion equation based on the energy equation as

$$\frac{D\rho}{Dt} = \frac{\partial \rho}{\partial t} + \frac{\partial}{\partial x_j}(\rho u_j) = \kappa_m \frac{\partial^2 \rho}{\partial x_j \partial x_j}, \tag{8}$$

where κ_m is the molecular diffusivity.

2.3. Turbulence Schemes

The highly nonlinear Navier-Stokes equations are hard to solve analytically even for the simplest turbulent flows. The mathematical solution of Navier-Stokes equations describing the complete spatial and temporal behavior of turbulent flows can be obtained by solving the fluid governing equations numerically. In general, there are three main approaches for solving these equations numerically, namely: Direct Numerical Simulations (DNS), Large-Eddy Simulations (LES) and Reynolds-averaged Navier-Stokes (RANS) simulations. DNS resolves the whole spatial and temporal scales of the flow without employing any 'turbulence model', while LES uses a spatial filter to simulate large scales explicitly and uses a turbulence model for small scales. RANS simulations just model the mean field of the flow by using turbulence closure schemes. Figure (2.1) compares these simulation models. Brief details of these models will be provided later.

2.3.1. Reynolds-Averaged Navier-Stokes Simulations.

Reynolds-averaged Navier-Stokes (RANS) equations are derived by applying Reynolds decomposition and averaging to the Navier-Stokes equations. Reynolds decomposition involves splitting any instantaneous quantity into mean and fluctuating components by time-averaging, e.g. the velocity field can be represented as

$$u_i = \overline{U_i} + u_i', \tag{9}$$

where $\overline{()}$ and $(')$ show the mean and fluctuation, respectively. Therefore, the momentum equation in the RANS framework can be written as

$$\frac{\partial \overline{U_i}}{\partial t} + \frac{\partial}{\partial x_j}(\overline{U_i U_j}) = -\frac{1}{\rho_0}\frac{\partial \overline{p}}{\partial x_i} + \nu \frac{\partial^2 \overline{U_i}}{\partial x_j \partial x_j} - \frac{\overline{\rho}}{\rho_0} g \delta_{i3} - \frac{\partial}{\partial x_j}(\overline{u_i' u_j'}), \tag{10}$$

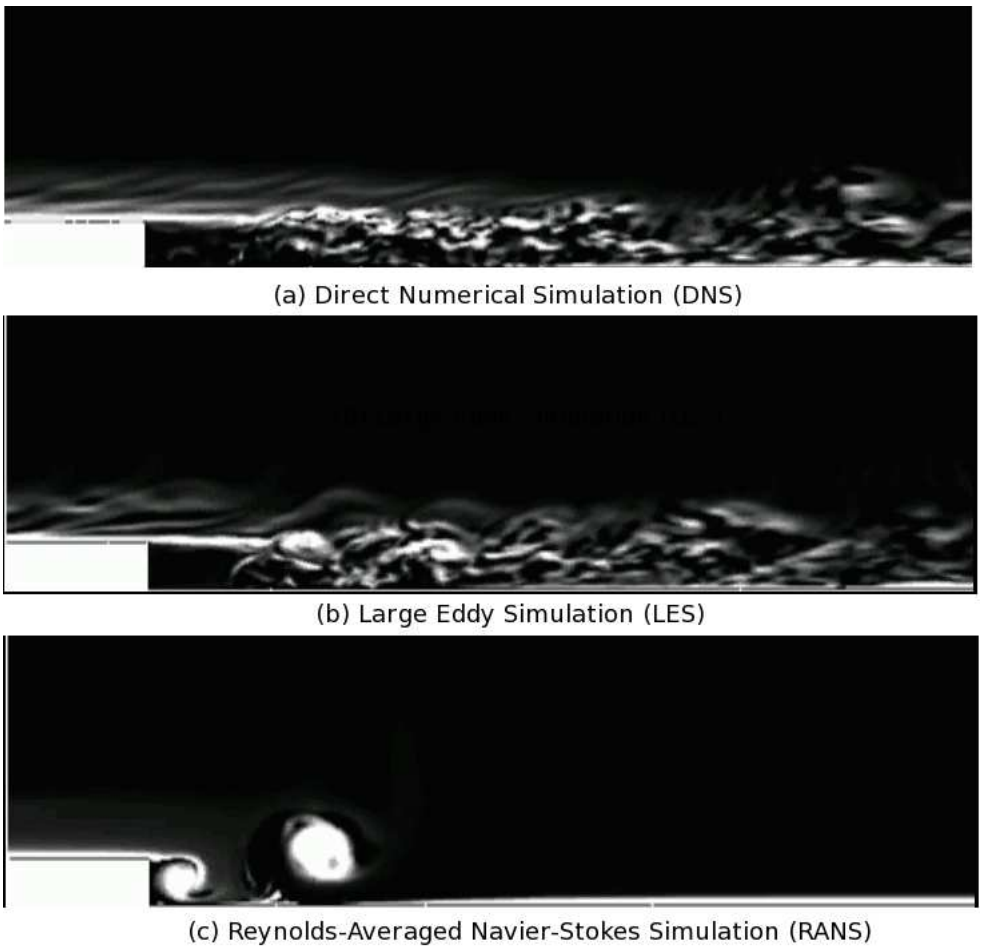

FIGURE 2.1. Flow over a back-ward facing step (spanwise vorticity) obtained from: (a) Direct Numerical Simulations (DNS), (b) Large-Eddy Simulations (LES), and (c) Reynolds-averaged Navier-Stokes (RANS) Simulations (Wu, Homsy & Moin; Gallery of Turbulent Flows, Center for Turbulence Research)

where $\overline{u_i' u_j'}$ is called the Reynolds stress or the turbulent momentum flux. The mean continuity equation is similar to its instantaneous counterpart (i.e. divergence free) and is given by

$$\frac{\partial \overline{U_i}}{\partial x_i} = 0. \tag{11}$$

The mean density transport evolves as

$$\frac{\partial \overline{\rho}}{\partial t} + \frac{\partial}{\partial x_j}(\overline{\rho U_j}) = \kappa_m \frac{\partial^2 \overline{\rho}}{\partial x_j \partial x_j} - \frac{\partial}{\partial x_j}(\overline{\rho' u_j'}), \tag{12}$$

where $\overline{\rho' u_j'}$ is the turbulent density flux. As shown in equations (10)-(12), the RANS equations resemble the basic governing equations, except for the turbulent momentum and density

fluxes which resulted from the Reynolds decomposition and averaging. Six unknown terms of the Reynolds stress tensor and three unknown terms of the density flux term imply that the number of unknowns exceeds the number of available equations. This leads to an undetermined system of equations commonly referred to as the 'closure problem'. To resolve this severe shortcoming, a number of hypotheses and methods are prescribed. The turbulent-viscosity and gradient-diffusion hypotheses are the most widely used concepts to deal with the closure problem. The turbulent-viscosity hypothesis (TVH) assumes that the deviatoric Reynolds stress is proportional to the mean shear strain rate as

$$-(\overline{u_i' u_j'}) + \frac{2}{3} k \delta_{ij} = -\nu_t (\frac{\partial \overline{U_i}}{\partial x_j} + \frac{\partial \overline{U_j}}{\partial x_i}) = 2\nu_t \overline{S_{ij}}, \tag{13}$$

where $k = (1/2)u_i'^2 = 0.5(u'^2 + v'^2 + w'^2)$ is the turbulent kinetic energy and ν_t is the turbulent (eddy) viscosity. The gradient-diffusion hypothesis (GDH) assumes that the turbulent density (scalar) flux is aligned with the mean density (scalar) gradient as

$$-(\overline{\rho' u_j'}) = \kappa_t \frac{\partial \overline{\rho}}{\partial x_j}, \tag{14}$$

where κ_t is a positive scalar, named turbulent (eddy) diffusivity. Although these hypotheses have known restrictions and shortcomings (e.g. see Pope 2000), they are widely accepted and implemented in RANS turbulence simulations. These hypotheses resolve the closure problem by decreasing the number of unknowns, but still require a correct proposition for the turbulent viscosity and diffusivity. In spite of great efforts, suitable formulations for the turbulent viscosity and diffusivity are still sought-after goals.

Different closure schemes are introduced widely to define the turbulent viscosity (ν_t). Depending on the number of additional transport equations that are used to solve for ν_t, these closure schemes are classified as zero-equation, one-equation or two-equation models. Zero-equation or algebraic models do not require additional transport equations (PDE's) and provide a prediction of the turbulent viscosity (ν_t) directly from the mean flow variables. One-equation models involve the use of one additional transport equation (usually turbulent kinetic energy) and assess the turbulent viscosity (ν_t) based on the estimated turbulent

quantity. Two-equation RANS closure schemes such as the standard k-ϵ model make use of two additional transport equations for turbulence quantities to define the turbulent viscosity (ν_t). On the other hand, in order to provide closure for the turbulent flux term in the density transport equation, most turbulence schemes make use of a turbulent Prandtl number (Pr_t) instead of defining the turbulent diffusivity (κ_t) explicitly. The turbulent Prandtl number is defined as

$$Pr_t = \frac{\nu_t}{\kappa_t}. \tag{15}$$

A general parameterization for Pr_t is widely sought and over the last few decades, many researchers have proposed formulations for Pr_t (e.g. Kays 1994, Schumann & Gerz 1995 and Venayagamoorthy & Stretch 2010). However, the efficacy of these propositions for modeling stratified flows has been a matter of doubt.

Extending the Reynolds decomposition and averaging process to the energy equations results in the introduction of new turbulent quantities known as the turbulent kinetic energy (k) and the turbulent potential energy (E_p'). In what follows, these concepts are briefly discussed.

• **Turbulent kinetic energy**

The turbulent kinetic energy is half the sum of the isotropic Reynolds stresses given by

$$k = \frac{1}{2}(u_i' u_i') = \frac{1}{2}(u'^2 + v'^2 + w'^2). \tag{16}$$

The evolution equation for the turbulent kinetic energy can be derived by splitting the total kinetic energy equation into the mean and fluctuating (turbulent) components (see Pope 2000 for a detailed discussion). For an incompressible, stratified flow the turbulent kinetic

energy is given by

$$\frac{\partial k}{\partial t}+\overline{U_j}\frac{\partial k}{\partial x_j} = \underbrace{-(\overline{u_i'u_j'})\frac{\partial \overline{U_i}}{\partial x_j}}_{I}\underbrace{-\nu\left(\overline{\frac{\partial u_i'}{\partial x_j}\frac{\partial u_i'}{\partial x_j}}+\overline{\frac{\partial u_i'}{\partial x_j}\frac{\partial u_j'}{\partial x_i}}\right)}_{II}\underbrace{-\frac{g}{\rho_0}\overline{\rho' u_j'}\delta_{i3}}_{III}$$
$$\underbrace{+\nu\frac{\partial^2 k}{\partial x_j^2}}_{IV}\underbrace{-\frac{1}{2}\frac{\partial(\overline{u_i'u_i'u_j'})}{\partial x_j}}_{V}\underbrace{-\frac{1}{\rho_0}\frac{\partial(\overline{u_i'p'})}{\partial x_j}}_{VI}, \tag{17}$$

To summarize, the terms in equation (17) are as follows:

I) Production rate of the turbulent kinetic energy (P).

II) Dissipation rate of the turbulent kinetic energy (ϵ).

III) Buoyancy flux (B).

IV) Viscous transport of the turbulent kinetic energy (D_ν).

V) Turbulent velocity transport of the turbulent kinetic energy (T).

VI) Pressure transport of the turbulent kinetic energy (Π).

The exact value for the dissipation rate of the turbulent kinetic energy is

$$\epsilon=\nu\overline{\frac{\partial u_i'}{\partial x_j}\frac{\partial u_i'}{\partial x_j}}+\nu\frac{\partial^2(\overline{u_i'u_j'})}{\partial x_i x_j}. \tag{18}$$

The last term in equation (18) is very small compared to other terms (Pope 2000) and is usually neglected.

•Turbulent potential energy

The turbulent potential energy is defined as

$$E_p'=-\frac{g}{\rho_0}\int\overline{\rho' dz}. \tag{19}$$

By assuming that $\rho'/z'=\partial\overline{\rho}/\partial z$, where z' is the displacement from a stable position along the background density gradient and replacing $dz=dz'=(\partial\overline{\rho}/\partial z)^{-1}d\rho'$, equation (19) can be rewritten as

$$E_p'=-\frac{g}{\rho_0}\left(\frac{\partial\overline{\rho}}{\partial z}\right)^{-1}\int\overline{\rho' d\rho'}=N^2\left(\frac{\partial\overline{\rho}}{\partial z}\right)^{-2}\left(\frac{1}{2}\overline{\rho'^2}\right), \tag{20}$$

where the transport equation for the scalar (density) variance ($(1/2)\overline{\rho'^2}$) is

$$\frac{\partial(\frac{1}{2}\overline{\rho'^2})}{\partial t}+\overline{U_j}\frac{\partial(\frac{1}{2}\overline{\rho'^2})}{\partial x_j} = \underbrace{-(\overline{\rho' u_j'})\frac{\partial\overline{\rho}}{\partial x_j}}_{I}\underbrace{-\kappa_m\overline{\rho'\frac{\partial^2\rho'}{\partial x_j\partial x_j}}}_{II}\underbrace{+\frac{\partial\left(\overline{\frac{1}{2}\rho'^2 u_j'}\right)}{\partial x_j}}_{III}. \quad (21)$$

The terms in equation (21) are

I) Production rate of density variance (P_ρ).

II) Dissipation rate of density variance (ϵ_ρ).

III) Transport rate of density variance (T_ρ).

The transport equation of the turbulent potential energy can be simply obtained by multiplying both sides of equation (21) by $N^2\left(\partial\overline{\rho}/\partial z\right)^{-2}$.

As previously discussed, RANS modeling relies on employment of turbulence closure schemes to model turbulent flows. The k-ϵ closure scheme is the most widely used scheme for modeling turbulence (Durbin & Pettersson Reif 2011). Hence, in the following we introduce and revisit the k-ϵ model.

2.3.1.1. *The k-ϵ Model.* The k-ϵ model is a two-equation complete turbulence model which is widely used in engineering and incorporated in commercial CFD codes. Launder & Spalding (1972) and Jones & Launder (1973) are widely credited as the developers of the standard k-ϵ model. This turbulence closure scheme solves two transport equations to obtain the turbulent kinetic energy (k) and its dissipation rate (ϵ). In the standard k-ϵ model, the turbulent viscosity (ν_t) for regions away from the wall is derived assuming equilibrium between the turbulent kinetic energy production rate (P) and the dissipation rate of the turbulent kinetic energy (ϵ) for an unstratified flow (i.e. $P\approx\epsilon$). Hence, we can write $\nu_t P=(-\overline{u'w'})^2\approx\nu_t\epsilon$. Using the proposition of Kolmogorov (1942) as $-\overline{u'w'}=ck^{1/2}$, the turbulent viscosity (ν_t) for an unstratified flow is given by

$$\nu_t=c^4\frac{k^2}{\epsilon}=C_\mu\frac{k^2}{\epsilon}, \quad (22)$$

where $C_\mu=(|\overline{u'w'}|/k)^2$ is the turbulent viscosity parameter, shown by experiments and DNS data (e.g. Kim *et al.* 1987) to be approximately equal to 0.09 in the log-law region (i.e.

away from the near-wall region). It is well known that the standard k-ϵ model is not suitable for modeling the near-wall turbulence, as the formulation for the turbulent viscosity (ν_t) overpredicts the exact ν_t in this region. An in-depth study of near-wall modeling using the k-ϵ model will be presented in chapter 3.

In order to calculate the turbulent viscosity (ν_t), the standard k-ϵ model requires solutions for k and ϵ. To do this, the k-ϵ model uses an almost exact equation to solve for the turbulent kinetic energy as

$$\frac{\partial k}{\partial t} + \overline{U_j}\frac{\partial k}{\partial x_j} = P - \epsilon + B + \frac{\partial}{\partial x_j}\left(\frac{\nu_t}{\sigma_k}\frac{\partial k}{\partial x_j}\right). \tag{23}$$

The last term is the only empirical term and is the modeled transport of the turbulent kinetic energy by using the gradient-diffusion hypothesis.

It is hard to define ϵ explicitly as the velocity fluctuations are required. Therefore, the k-ϵ model solves an empirical transport equation for ϵ that is analogous to the transport equation of k (equation 23) given by

$$\frac{\partial \epsilon}{\partial t} + \overline{U_j}\frac{\partial \epsilon}{\partial x_j} = C_{\epsilon 1}\frac{P\epsilon}{k} - C_{\epsilon 2}\frac{\epsilon^2}{k} + C_{\epsilon 3}\frac{B\epsilon}{k} + \frac{\partial}{\partial x_j}\left(\frac{\nu_t}{\sigma_\epsilon}\frac{\partial k}{\partial x_j}\right). \tag{24}$$

In this equation, $C_{\epsilon 1}$, $C_{\epsilon 2}$ and $C_{\epsilon 3}$ are empirical constants for production, dissipation and buoyancy terms. The last term in equation (24) is a modeled transport term by using the gradient-diffusion hypothesis. The empirical coefficients are given in table (2.1).

C_μ	$C_{\epsilon 1}$	$C_{\epsilon 2}$	σ_k	σ_ϵ
0.09	1.44	1.92	1.0	1.3

TABLE 2.1. Values of constants in the standard k-ϵ model

There is no consensus on the value of $C_{\epsilon 3}$ and is still a source of controversy in stratified turbulence modeling. Durbin & Pettersson Reif (2011) assumed $C_{\epsilon 3} = C_{\epsilon 1} = 1.44$ as this results in $-B \leq P$, Baum & Caponi (1992) suggested $C_{\epsilon 3} = 1.14$ while Burchard & Baumert (1995) proposed negative values for $C_{\epsilon 3}$.

2.3.2. LARGE-EDDY SIMULATION. The accuracy of RANS models is always a matter of discussion in turbulence modeling, therefore numerical methods with better accuracy, but

still feasible for industrial applications are desired. Large-eddy simulation (LES) has gained attention in the past few decades especially with increase of the computational power. At present, LES is widely used as a powerful tool in research and industry with reasonable computational cost and accuracy. LES captures the unsteady and energy-containing motions of large eddies, but still relies on turbulence models to model the effect of small scales. A spatial decomposition called 'filtering' is applied to the governing equations, splitting the velocity field into a filtered or mean value ($\langle U \rangle$) and a residual or a sub-grid scale ($\langle u' \rangle$). The filter size can either be determined implicitly by the numerical domain grid size or by introducing filter functions (Gullbrand & Chow 2003). The filtered governing equations for unsteady, three-dimensional, stratified flows with Boussinesq approximation in LES are

$$\frac{\partial \langle U_i \rangle}{\partial t} + \frac{\partial \langle U_i U_j \rangle}{\partial x_j} = -\frac{1}{\rho_0}\frac{\partial \langle p \rangle}{\partial x_i} + \nu \frac{\partial^2 \langle U_i \rangle}{\partial x_j \partial x_j} - g\frac{\langle \rho \rangle}{\rho_0}\delta_{i3} - \frac{\partial \tau_{ij}^{SGS}}{\partial x_j}, \tag{25}$$

subject to continuity equation as

$$\frac{\partial \langle U_i \rangle}{\partial x_i} = 0. \tag{26}$$

Also, the filtered density transport equation is

$$\frac{\partial \langle \rho \rangle}{\partial t} + \frac{\partial \langle \rho U_j \rangle}{\partial x_j} = \kappa_m \frac{\partial^2 \langle \rho \rangle}{\partial x_j \partial x_j} - \frac{\partial \chi_j^{SGS}}{\partial x_j}. \tag{27}$$

In equations (26) and (27), τ_{ij}^{SGS} and χ_j^{SGS} are the sub-grid scale (SGS) tensor and sub-grid scale flux vector respectively and are defined as

$$\tau_{ij}^{SGS} = \langle U_i U_j \rangle - \langle U_i \rangle \langle U_j \rangle, \tag{28}$$

$$\chi_j^{SGS} = \langle \rho U_j \rangle - \langle \rho \rangle \langle U_j \rangle. \tag{29}$$

With the existence of residuals, like RANS models, LES suffers from the closure problem, and requires SGS models to resolve closure. The accuracy of LES highly depends on the efficiency of SGS models used to define the sub-grid scale (SGS) motions. The simplest and most well-known closure method is introduced by Smagorinsky (1963). This model uses a

linear turbulent viscosity (ν_t) to model the residual motions as

$$\tau_{ij}^{SGS} = -2\nu_t \langle S_{ij} \rangle, \tag{30}$$

where the turbulent (eddy) viscosity is defined as

$$\nu_t = l_s^2 \langle S \rangle = (C_S \Delta)^2 \langle S \rangle. \tag{31}$$

In this equation, Δ is usually taken as the grid size, C_S is the Smagorinsky constant and $\langle S \rangle = \sqrt{2\langle S_{ij} \rangle \langle S_{ij} \rangle}$ is the characteristic rate of strain. The main drawback of Smagorinsky's model is that it uses a predetermined empirical constant, which is not universal and shows large variations depending on the flow type, geometry, domain resolution and the local characteristics of the flow (Germano *et al.* 1991, Park *et al.* 2006). Lilly (1966) defined $C_S \simeq 0.23$ for a homogeneous isotropic turbulence. Deardorff (1970) ran a three-dimensional turbulent channel flow and observed that a large value of C_S results in damping of large-scale fluctuations and proposed $C_S = 0.1$. However, the commonly used value is $C_S \simeq 0.1 - 0.2$. Germano *et al.* (1991) introduced a modification to Smagorinsky's model by using a dynamic sub-grid scale model which allows Smagorinsky constant (C_S) to change with time and space. The proposed method employs a two-level filtering of the flow variables to establish an algebraic relation between the resolved turbulent stresses and the sub-grid scale stresses. On the other hand, the other deficiency of Smagorinsky's model is that the SGS turbulent viscosity does not vanish at regions where the sub-grid scale dissipation is expected to be zero and therefore even the dynamic sub-grid scale models show large variations in time and space (Park *et al.* 2006). Vreman (2004) has proposed a model based on the mean shear rate and grid size that ensures the SGS turbulent viscosity goes to zero when SGS dissipation vanishes. The model is tested for channel flows and transitional flows and showed good agreement with experiments and DNS data. Park *et al.* (2006) proposed modification to Vreman's model and introduced a dynamic coefficient by assuming general equilibrium between the sub-grid scale dissipation and viscous dissipation through a two-level filtering. You & Moin (2007)

further modified Vreman's model and simplified Park *et al.* (2006) model by introducing a single-level filtering model.

2.3.3. Direct Numerical Simulation. Direct numerical simulation (DNS) is used to solve for the velocity and scalar field of turbulent flows without resort to a 'turbulence model'. DNS fully resolves the temporal and spatial scales of the flow from the Kolmogorov length scale (η), asserted to be the smallest scale in the turbulent flow where the molecular viscosity (ν) dominates, to the largest energy-containing length scales. Solving a very finely resolved flow domain is an extremely hard task that was not possible until only a few decades ago. Despite the increase in computational power, DNS is still restricted to simple flows with regular geometries. Furthermore, at higher Reynolds numbers, the number of the grid points required to resolve the flow field down to the Kolmogorov length scale increases exponentially, therefore DNS is also limited to low to moderate Reynolds number flows. These shortcomings have made DNS to be more of a valuable technique employed to understand the fundamental physics of turbulent flows rather than a tool for industrial applications.

2.4. Wall-Bounded Turbulence Basics

Wall-bounded turbulent flows are ubiquitous in most natural and engineered flows. The presence of the solid wall has profound effects on the transport of momentum, mass and heat. As such, it is not surprising that the subject of wall-bounded flows has received much attention in the last few decades. Wall-bounded flows can be generally classified into three canonical categories of channel flow, pipe flow and boundary layer flow. Fully developed channel flow with simple geometry has been the subject of research with the goal of understanding the complex structure of turbulent wall-bounded flows. Nikuradse (1929) and Reichardt (1938) are among the first investigators to study fully developed channel flows, while Laufer (1948) has provided the first details of the fully developed channel flow statistics. Eckelmann (1974) performed experiments to investigate the turbulence statistics in the near-wall region by using an oil channel with a thick viscous sublayer in order to measure very close to the wall. These early experiments provided valuable insights on the complex

turbulence interactions in wall-bounded flows, but there was still poor agreement in the reported measurements (Kim *et al.* 1987). This accentuated the need for performing highly resolved numerical simulations for a detailed investigation of wall-bounded flows. Deardorff (1970) and Schumann (1973) are among the first to perform three-dimensional simulations to study wall-bounded flows. However, they did not resolve the near-wall region due to computational costs. Kim *et al.* (1987) performed the first (seminal) DNS of fully developed channel flow. Emergence of DNS opened a new path in turbulence studies, enabling researchers to measure exact turbulence statistics such as Reynolds stresses. The early numerical works were restricted to low-Reynolds-number flows due to limited computational facilities, but over the years a number of DNS works with higher Reynolds numbers have been implemented such as works of Moser *et al.* (1999), del Álamo *et al.* (2004), Hoyas & Jiménez (2006). Higher Reynolds numbers simulations enable researchers to have a better understanding of wall-bounded flows especially in the near-wall region.

Experimental and DNS observations have shown that wall-bounded turbulent flows can usually be subdivided into two-main regions: an inner region for $z/D < 0.1$ and an outer region for $z/D > 0.1$, where z is the local flow depth from the wall and D is the total depth. The inner region can be further subdivided into three different layers namely: viscous sublayer for $z^+ < 5$, buffer layer for $5 < z^+ < 30$ and log-law region which overlaps both the inner region and outer region with $z^+ > 30$ and $z/D < 0.3$. The wall unit (z^+) is defined as

$$z^+ = u_\tau z/\nu, \tag{32}$$

where u_τ is the friction velocity and ν is the molecular (kinematic) viscosity. The viscous sublayer and the buffer layer together are defined as the near-wall region or viscous region since the viscosity is important and the energetic and the dissipative scales overlap (Jiménez & Moser 2007). Although the thickness of the near-wall region is two or more orders of magnitude smaller than the total flow depth, its effect extends throughout all the flow region as almost 50% of the flow velocity from the wall to the free-surface occurs in this thin region (Hanjalić & Launder 1976). The remaining velocity difference is mostly obtained in

the logarithmic layer. Near the wall the mean shear rate is high with the highest mean shear rate occurring right at the wall leading to considerable inhomogeneity and the viscosity effect is noticeable resulting in low-Reynolds-number flow. However, Durbin (1991) has discussed that it is the inviscid wall blocking effect resulting from the impermeability condition at solid boundary (i.e. zero normal velocity) that suppresses the turbulent transport in the wall region, not the viscous effects.

It is widely shown that in the near-wall region there is an imbalance between the production rate of the turbulent kinetic energy (P) and the dissipation rate of the turbulent kinetic energy (ϵ), which leads to a noticeable transport of k in this region. However, observations show that in the log-law region which starts at $z^+ \approx 30$, the transport of k becomes negligible and it is legitimate to assume equilibrium between P and ϵ (i.e. $P/\epsilon \approx 1$). Hence, the logarithmic region is also named as the equilibrium layer (Townsend 1961). Due to the non-linear behavior of the near-wall region which can also be physically attributed to the rapid decrease of the turbulent eddy sizes as approaching the wall, most turbulence models have difficulties modeling this region. Therefore, most of the existing formulations for the turbulent viscosity such as the formulation of ν_t in the standard k-ϵ model are developed assuming the existence of a logarithmic layer and hence the balance between the production and the dissipation rates of k. Such turbulence closure schemes avoid modeling the near-wall region turbulence by employing wall-functions. A wall-function helps model the wall-bounded flows from the logarithmic layer by assuming the existence of a logarithmic velocity profile and constant stress region. However, the DNS data show that these models are qualitatively wrong to be used for modeling the near-wall region, requiring new developments (Pope 2000). For example, Durbin (1991) has discussed that the standard k-ϵ model overpredicts the near-wall turbulent viscosity (ν_t). To handle this drawback, special treatment called damping functions (f_μ) are introduced to reduce the turbulent viscosity in the near-wall region. A damping function is the ratio of the exact turbulent viscosity to the

predicted turbulent viscosity given by

$$f_\mu = \frac{\nu_t}{C_\mu k^2/\epsilon}. \tag{33}$$

Such ideas were first introduced by van Driest (1956). Other popular damping functions have been introduced by Jones & Launder (1973), Launder & Sharma (1974), Lam & Bremhorst (1981), Patel *et al.* (1985) and Rodi & Mansour (1993). Most of these models fall back on the employment of the friction velocity (u_τ) and/or the wall unit (z^+). The major drawback of these models is that they are mostly tuned for low-Reynolds-number DNS data and are not universal. To resolve this shortcoming, Durbin (1991) has introduced a more universal model that avoids the use of a damping function. He concludes that the vertical (cross-stream) velocity fluctuation is responsible for the transport of the turbulence in a wall-bounded flow and introduces a fourth-order turbulence scheme called k-ϵ-$\overline{v^2}$ as

$$\nu_t = c'_\mu \overline{w'^2} \frac{k}{\epsilon}, \tag{34}$$

where $c'_\mu \simeq 0.2$ is a constant and w' is the cross-stream velocity fluctuation. Although this model performs well near the wall, it is a more sophisticated model compared to the standard k-ϵ model, solving for two extra transport terms. Also, it still employs a constant (c'_μ) which is sensitive to the Reynolds number. Hence, a simpler model is still a sought-after goal.

2.5. Stratification in Wall-Bounded Flows

Stably stratified channel flows are inevitable in nature such as in the atmosphere, estuaries and oceans, where temperature and/or salinity gradients are large enough that buoyancy effects become dynamically important. The atmospheric boundary layer is typically stable at nights due to stable temperature gradients, while oceanic flows are often stable. Buoyancy effects arising from the density stratification add another term of complexity to any turbulent flow through coupling of the momentum and the density transport equations. The buoyancy force arising from the stable stratification impedes turbulent motions converting a portion of the turbulent kinetic energy into turbulent potential energy through mixing (Briggs *et*

al. 1998). To date there has been a great deal of work on homogeneous stratified flows and unstratified inhomogeneous flows but it is only recently that research works on inhomogeneous stratified flows are emerging. Most experiments on wall-bounded flows are performed on open-channel flows or boundary layers. Webster (1964) studied grid-generated turbulent flows with vertical temperature and velocity gradients in outer layers in wind tunnels. One of the first experiments on stratified wall-bounded flows was done by Arya (1975) on a flat plate. He made observations in a well-developed, thermally stratified, horizontal, flat-plate boundary layer and the effects of buoyancy on the mean flow and turbulence structure are studied. He observed that the mean velocity and temperature profiles are dependent on the thermal stratification in both the inner and outer layers. Komori *et al.* (1983) experimentally studied stably stratified open-channel flow. They investigated the outer layer, where the wall effect is small and observed that the turbulence quantities are correlated with the local gradient Richardson number (Ri_g). The gradient Richardson number (Ri_g) is a relative measure of the strength of the buoyancy and mechanical forces in a fluid flow and is defined as

$$Ri_g = \frac{N^2}{S^2}. \tag{35}$$

Here, $N = -\sqrt{g/\rho_0(\partial\overline{\rho}/\partial z)}$ is the buoyancy or Brunt-Väisälä frequency and $S = d\overline{U}/dz$ is the mean shear rate with z defined as the vertical distance from the wall. N shows the oscillating frequency of a fluid particle when displaced from its stable position in a stratified fluid and is a measure of the strength of the density stratification. Ohya *et al.* (1997) studied the turbulence structure in a thermally stratified wind tunnel and observed suppression of velocity fluctuations in both streamwise and vertical directions. However, stratified channel flows are hard to realize in laboratory experiments because of technical difficulties to keep the walls at constant temperature, the influence of the side walls, etc. As a result, the existing laboratory experiments are few and at fairly low Reynolds numbers. These experiments mostly show the final fate of the mean flow profiles and the suppression of turbulent statistics due to stable stratification, without providing the small-scale turbulence statistics in stably stratified wall-bounded flows.

On the other hand, with the emergence of highly resolved numerical simulations, the numerical study of wall-bounded flows are becoming feasible and is fairly straightforward compared to laboratory experiments. Garg *et al.* (2000) performed numerical simulation of stably stratified channel flows. They used LES and DNS to delineate the stratified flow regimes and transition between them based on the gradient Richardson and Reynolds numbers. For a better understanding of the buoyancy effect, a Dirichlet boundary condition was used and the density was kept constant at both upper and lower boundaries. They also studied mean flow quantities and observed the suppression of the log-law region. Armenio & Sarkar (2002) studied stably stratified channel flows behavior for various stratifications with the same density boundary condition as Garg *et al.* (2000). They used LES technique for very low friction Reynolds number of $Re_\tau \approx 180$ and with friction Richardson numbers up to $Ri_\tau = 480$. The friction Richardson number is defined as

$$Ri_\tau = \frac{g/\rho_0 \frac{|\Delta\rho|}{D}}{(u_\tau/D)^2} = \frac{|\Delta\rho| g D}{\rho_0 u_\tau^2}, \tag{36}$$

where $\Delta\rho$ is the maximum density difference in the channel at the initialization of the simulation. They concluded that the gradient Richardson number (Ri_g) is a very good local buoyancy determinant. The turbulent motion was observed to be two-dimensional with increasing stratification, while for the highest stratification the buoyancy-affected region encroaches into the inner layer, suppressing the low speed streaks in the near-wall region. Also, in the core of the channel where the mean shear rate (S) relaxes, internal wave motions were seen. Taylor *et al.* (2005) employed LES to investigate stably stratified open channel flow. They imposed a constant heat flux at the top and an adiabatic bottom wall (i.e. no heat transfer at the wall), different from previous works. They showed that this different boundary condition leads to an untouched near-wall turbulence production and consequently the buoyancy flux, the turbulent Prandtl number (Pr_t) and a generalized flux Richardson number ($R_f = -B/(-B+\epsilon)$) are seen to be different from free shear layers and channels with constant temperature walls, highlighting the major effect of the near-wall on the entire behavior of the stratified channel flow. Interestingly, unlike Armenio & Sarkar (2002), they

did not see the collapse of quantities as a function of the gradient Richardson number (Ri_g). They observed that the vertical turbulent Froude number (Fr_v) defined in equation (37) is a better measure of the turbulence in the upper portion of the channel where buoyancy is dominant and affects the turbulent patches generated at the bottom wall. The vertical turbulent Froude number is

$$Fr_v = \frac{\left(\overline{w'^2}\right)^{1/2}}{NL_E}, \tag{37}$$

where L_E is the Ellison length scale introduced by Ellison (1957) which provides a measure of the vertical distance traveled by particles before either returning to their equilibrium position or mixing in the density field (Venayagamoorthy & Stretch 2010). L_E is defined as

$$L_E = \frac{\left(\overline{\rho'^2}\right)^{1/2}}{|\,(d\overline{\rho}/dz)\,|}, \tag{38}$$

where ρ' denotes the density fluctuation. The latest work is the DNS by García-Villalba & del Álamo (2011) which has so far the highest Reynolds number with $Re_\tau = 550$. They have used similar configuration as Armenio & Sarkar (2002) and arrived at almost similar conclusions to those suggested by them.

It should be noted that although these numerical simulations have provided valuable information about turbulence quantities that are not easy to obtain from field or laboratory experiments, they suffer from the low-Reynolds-number issue. This shortcoming causes the flow not to be sufficiently turbulent especially for higher stratifications.

However, like unstratified flows, DNS and LES methods are not appropriate for modeling large-scale stratified wall-bounded flows and RANS turbulence models remain popular. For such flows, it is required to capture buoyancy fluxes (or the turbulent diffusivity) additional to momentum fluxes. The standard k-ϵ model remains a popular method for modeling stratified flows, commonly using a turbulent Prandtl number (Pr_t) to link the momentum and density (scalar) fluxes. This highlights the importance of revisiting this model as well as Pr_t for modeling stably stratified wall-bounded flows. A complete discussion will be provided in chapter 5.

2.6. Instabilities and Breaking

Most of the studied processes in geophysical fluid dynamics have been for cases where the rotation is dominant, implying small Rossby numbers defined as

$$R_o = U/fL, \tag{39}$$

where f is the Coriolis frequency and U and L are characteristic velocity and length scales, respectively. These large-scale phenomena depend on and lead to very small-scale processes and finally turbulent motions, where rotation is not important. The chaotic and churning nature of turbulent flows usually arise from onset of instabilities in the fluid. Therefore, in the context of geophysical systems it is essential to fully comprehend the small-scale phenomena, such as instability and breaking processes in order to investigate and model geophysical flows.

Instabilities and breaking are in general defined and regarded as a short-term, transient and active process ensuing irreversible dissipation of the fluid flow energy (Imberger 1998, Michallet & Ivey 1999) which lead to turbulent motions with small length scales. The complex instability and consequently breaking result in distortion of isopycnals leading to 'irreversible' transfer of turbulent kinetic energy into potential energy through rearrangement of the density profile. This process is known as 'turbulent mixing'. The turbulent mixing is at the bottom end of a set of obscure and intricate processes leading to very small-scale motions in the ocean and plays an important role in determining distribution of stratification and biogeochemical matter in water columns (Wüest *et al.* 2000).

However, there are various types of instabilities with distinct mechanisms occurring in stratified flows (Sonmor & Klaassen 1997). These instabilities are usually a function of the flow characteristics such as the amplitude of the internal wave and the interaction with the surrounding. Primarily breaking is considered to occur from two types of instabilities: 'static (convective) instability' and 'dynamic (shear) instability'. These are discussed in more detail next.

2.6.1. Static Instability or Convective Overturn. In general, a convective instability is considered to occur when a heavier fluid is superposed over a lighter fluid (i.e. $\frac{\partial \rho}{\partial z} > 0$ or $N^2 < 0$) in a gravitational field (Daly 1967). Any perturbation of this interface tends to grow with time, resulting in the well-known Rayleigh-Taylor instability. Rayleigh-Taylor instability is driven by the conversion of the potential energy in the originally inverted stratification to kinetic energy (Sharp 1984). Rayleigh (1894) and Taylor (1950) are the first who have analytically predicted the rate of growth of such an instability. Their prediction is extensively confirmed by different researchers such as Lewis (1950) who experimentally showed that for an air-liquid interface, the theoretical prediction agrees well with experiments in the initial phase of the instability.

Atmospheric instabilities are usually associated with density overturns and convective instabilities. In the atmosphere, as the wave propagates upward, the amplitude increases as the ambient density is decreasing. If this propagation continues, the amplitude becomes large enough for overturning to occur and the heavier fluid is lifted over the lighter fluid, resulting in a convective instability. However, it is not straightforward to discern internal waves breaking in the ocean.

Such an instability is common in the ocean too especially when internal wave field interacts with the bottom topography. Kao *et al.* (1985), Helfrich (1992), Michallet & Ivey (1999) are among the first researchers to study progressive shoaling waves of large amplitudes interacting with slopes. They have visualized the breaking process in their experiments and have found that convective instabilities are initial instabilities leading to the breaking of internal solitary waves on slopes. Hult *et al.* (2009) experimentally investigated periodic progressive two-layer interfacial waves interaction with a submerged ridge. They concluded from their results that a noticeable portion of the breaking on a ridge in a two-layer system is convective.

Numerical simulations are also used to study convective instabilities (e.g. Bouruet-Aubertot *et al.* 2001, Sutherland 2001, Koudella & Staquet 2006, Fritts *et al.* 2009a,b).

Venayagamoorthy & Fringer (2012) discussed the breaking of progressive internal waves, interacting with a shelf break in a linearly stratified fluid by employing highly resolved LES. They observed significant overturning and distortion of isopycnals leading to convective instabilities in the slope region highlighting the importance of convective instabilities in shallow regions.

2.6.2. Dynamic or Shear Instability. Dynamic or shear instabilities occur due to the high mean shear rate of the flow relative to the buoyancy frequency, where small-scale instabilities draw energy from the mean flow. Kelvin-Helmholtz billows are a classical example of shear instabilities introduced by Helmholtz (1868) and Kelvin (1871). They devised a theory to describe the stability of infinitesimal, spatially periodic disturbances to the interface between two layers of differing density in relative motion. However, in literature the term is used for a growing instability in any stably stratified shear flow, with density and velocity varying in depth. The most accessible example of a Kelvin-Helmholtz instability is the surface gravity waves, where at the air-water interface the density difference is about three orders of magnitude. As Smyth & Moum (2012) have pointed out, the Kelvin-Helmholtz instability is a critical link in the chain of the oceanic events leading to mixing from internal waves. Defining useful parameterization and prevalence conditions of the Kelvin-Helmholtz instability and its contribution to mixing is a first-order priority. Reynolds (1883) made the first experiments on the shear instabilities in a two-layer flow composed of two immiscible fluids, which was part of his attempt to study the onset of turbulence in a pipe. The most important results on the Kelvin-Helmholtz instability are attributed to the seminal works of Miles (1961), Howard (1961), Klebanoff *et al.* (1962) and Thorpe (1971). Miles (1961) and Howard (1961) have provided a theoretical stability criterion for a parallel shear flow in an inviscid, incompressible fluid with variable density $\rho(z)$ under static stability (i.e. $\partial\rho(z)/\partial z < 0$). By employing theoretical arguments they showed that in a heterogeneous (stratified) shear flow the sufficient conditions for stability are a non-zero mean shear rate ($S = d\overline{U}/dz \neq 0$) and $Ri_g > 0.25$. Klebanoff *et al.* (1962) ran experiments to reveal the nature of motions in the non-linear range of boundary layer instability and the onset of

turbulence. They have shown that the three-dimensional effect should be taken into account while investigating the non-linear wave motions and the instability phenomenon in a shear boundary layer flow. Thorpe (1971) used miscible two-layer fluid of water and brine to experimentally investigate the instability for small-amplitude disturbances in an accelerating stratified shear layer and characterized the instability and transition to turbulence. Also, numerous examinations are performed to classify the breaking events as a result of internal waves interacting with bottom topographic features. Eriksen (1985) and Garrett & Gilbert (1988) studied the internal wave reflection from sloping boundaries and discussed that this reflection can cause the enhancement of the mean shear leading to shear instabilities.

One of the first published works discussing observed values for critical gradient Richardson number (Ri_{gc}) in oceanic flows appears to be that of Woods (1968). Eriksen (1978) used the critical gradient Richardson number as a local indicator of fine structure instabilities in the ocean. His measurements of mooring off a sloping bed in Bermuda showed a reduction of density below lines of $N^2 = 0.25S^2$. However, whether a flow will transition into turbulence and the shear instability will occur or not, when the wave breaking criterion ($Ri_{gc} = 0.25$) is satisfied for development of a Kelvin-Helmholtz instability, does not only depend on the value of the gradient Richardson number being below the critical value, but is also a function of time. There are circumstances when Ri_g is trespassing the critical value, but before overturning can occur, the mean shear relaxes. Fringer & Street (2003) numerically studied a progressive wave. For some flow regimes, they have observed a much lower critical Richardson number as $Ri_{gc} = 0.13$ compared with 0.25, indicating that waves might still travel without breaking with gradient Richardson numbers less than the critical value 0.25. Sveen *et al.* (2002) studied an internal wave interacting with a submerged ridge and showed that as long as $Ri_g \geq 0.25$ no shear instability occurs, however in the strong breaking or the initial phase of wave-ridge encounter, shear instabilities were created. Also the numerical work of Barad & Fringer (2010) which simulated shear instabilities in internal solitary-like waves showed that a much lower critical value of $Ri_g = 0.1$ is required for the onset of shear instabilities.

Shear instabilities are not easy to observe in field since fine-scale turbulent structure is difficult to measure. Sandstrom & Oakey (1995) associated high turbulence with a highly sheared subsurface interface, although the details of the gradient Richardson number were not clear. Several researchers such as Woods (1968), Armi & Farmer (1988), Gossard (1990) have measured field shear instabilities but it was Moum *et al.* (2003) that clearly measured Kelvin-Helmholtz instabilities. They studied the structure within the shear-induced decaying solitary waves propagating over Oregon's continental shelf. The measurements depict trains of near-surface, solitary-like waves of depression that propagate in the absence of significant shoaling effects, with clear signatures of shear instabilities that are the primary source of turbulence and dissipation. Their observations show that the shear is sufficiently high to create explosively growing, small wavelength shear instabilities and have conjectured that they are the possible source of Kelvin-Helmholtz billows.

The aim of understanding the breaking and instability event in stratified flows is to be able to infer turbulent mixing. In the next section, a review of the turbulent mixing is discussed.

2.7. Turbulent Mixing

The ability of turbulent flows to effectively mix mass and momentum in the environment is vital to the dynamics of such flows with wide-span consequences in nature and engineered applications. Eckart (1948) considered turbulent mixing to be a three-stage process of entrainment, dispersion (stirring) and diffusion. Three levels of turbulent mixing are known to occur in nature namely: passive mixing, mixing coupled with the dynamics of the fluid and mixing that causes changes to the fluid (Dimotakis 2005). For the first and simplest case, mixing is passive as is the case between passive scalars. Mixing of matched-density gases, ink or low-concentration dyes in a liquid, small particle smoke/clouds are examples of this type of mixing. Such a simple mixing does not feed back on the flow dynamics, therefore a correct prediction of the mixing is not required to describe flow dynamics, although the mixing is driven by the turbulent flow. The second level of mixing is coupled with the flow

dynamics, such as mixing between fluids of different densities, mixing of temperature and density fields in large oceanic currents (Adkins *et al.* 2002, Wunsch & Ferrari 2004). Hence, prediction of flow dynamics and mixing are coupled. The third and most complex mixing is also coupled to the fluid dynamics and happens when as a result of mixing of fluids, changes are produced to fluids properties such as in density, composition, etc. Examples are most of combustion phenomena or processes taking place in stellar bodies resulting to the production of light elements from heavy ones.

The second level mixing can be regarded as the most important one influencing the life and climate on the Earth. A great example of this type of mixing is mixing in stratified flows (stable or unstable). Due to misalignment between the density and pressure gradients, a baroclinic vorticity field is generated and represented as an independent term in the vorticity equation (Petersen *et al.* 2007). The baroclinic vorticity drives internal instability that can increase scalar- or density-isosurfaces (surfaces of constant density) generation which ensues mixing. The mixing along isopycnals can be approximated by using two-dimensional turbulence models (Pasquero *et al.* 2001), but mixing across the isopycnals (i.e. diapycnal or vertical mixing) presents a special modeling challenge and requires additional time and space scales introduction (Riley & Lelong 2000).

In the ocean, the turbulent mixing is a ubiquitous phenomenon and is commonly conjectured as a direct consequence of internal waves breaking. Without turbulent mixing, in a few thousand years the ocean would be a cold, salty pool (Munk & Wunsch 1998). The average turbulent diffusivity (κ_t) based on the balance between mixing and the deep-water upwelling is predicted to be roughly $10^{-4}m^2s^{-1}$, but Munk & Wunsch (1998) showed that the turbulent diffusivity (κ_t) in the ocean far from the boundaries is about $10^{-5}m^2s^{-1}$. A plausible source for the mixing energy required to maintain the oceanic structure could be from internal waves interacting with undersea topography (Munk & Wunsch 1998). Therefore a great deal of work focuses on induced mixing by internal waves such as Ivey & Nokes (1989), Helfrich (1992), Michallet & Ivey (1999), Slinn & Riley (1996), Wunsch & Ferrari (2004), Chen (2008) and Hult *et al.* (2011).

It is essential to quantify the absolute amount of mixing but its efficiency is of more importance, which is usually quantified by using the definition of the flux Richardson number (R_f) or mixing efficiency. The mixing efficiency is defined as the ratio of the increase in the potential energy due to mixing to the loss of the kinetic energy as

$$R_f = \frac{\Delta PE}{\Delta KE}. \tag{40}$$

The common formulation for the flux Richardson number (R_f) is defined as the ratio of the buoyancy flux $B = -g/\rho_0(\overline{\rho' w'})$ and the turbulent kinetic energy production rate $P = -\overline{u'w'}(d\overline{U}/dz)$ as

$$R_f = \frac{-B}{P}. \tag{41}$$

The major drawback is that this definition of R_f can be negative in non-stationary flows (Venayagamoorthy & Stretch 2010) or highly stratified channel flows where countergradient buoyancy fluxes are observed (Armenio & Sarkar 2002) and exceed 1 for high gradient Richardson numbers (e.g. García-Villalba & del Álamo 2011). Peltier & Caulfield (2003) discussed that the mixing efficiency should be calculated based on irreversible mixing and viscous dissipation of the turbulent kinetic energy (ϵ) as

$$R_f^* = \frac{\epsilon_{PE}}{\epsilon + \epsilon_{PE}}, \tag{42}$$

where $\epsilon_{PE} = N^2 \epsilon_\rho (d\overline{\rho}/dz)^{-2}$ is the dissipation rate of the turbulent potential energy, with $\epsilon_\rho = \kappa \overline{\nabla \rho' . \nabla \rho'}$ defined as the scalar variance dissipation rate. As the dissipation rate of the turbulent kinetic energy (ϵ) and the turbulent potential energy dissipation rate (ϵ_{PE}) are positive-definite, then the irreversible definition requires that $0 \leq R_f^* \leq 1$.

The correct prediction of R_f is a sought-after demand and still an open question. In numerical modeling of stratified flows, R_f is directly required for proper calculation of the turbulent (eddy) viscosity and diffusivity. Hence, it is a key parameter for modeling geophysical flows (Pardyjak *et al.* 2002). Experimental and numerical works are carried out to infer R_f. For example, Ivey & Nokes (1989) used laboratory experiments to examine the mixing due to the breaking of internal waves in a continuously stratified fluid on a sloping

boundary by confining the attention to critical waves when the slope of the group velocity of incident waves is equal to the bottom slope. They measured the mixing efficiency in the breaking process with the upper limit of approximately 20%. Linden & Redondo (1991) created a pure Rayleigh-Taylor instability by overlying brine over fresh water, which resulted in overturning. This method could provide a convenient way to see how much of the initial potential energy was used to mix the fluid and what portion was dissipated by viscosity. The mixing efficiency for such an experiment can be $0 \leq R_f \leq 0.5$. Surprisingly, the results show that for different Atwood numbers ($A_t = (\rho_2 - \rho_1)/(\rho_2 + \rho_1)$, where ρ_2 is the density of the heavier fluid) even the maximum value is attainable. Also, for high Atwood numbers it was observed that $R_f \simeq 0.35$. Helfrich (1992) ran experiments on the solitary depression wave interacting with a uniform slope in a two-layer system and observed breaking and production of turbulent surges traveling upslope. His measurements revealed that about $15 \pm 5\%$ of the first mode wave breaking energy goes into irreversible vertical mixing. Stretch *et al.* (2010) used data from towed grid experiments and DNS data of decaying turbulence for different stratifications. Both experimental and DNS results showed an increasing trend for low stratifications and constant values for high stratifications. However, while the DNS data suggest a maximum flux Richardson number of 30%, the experimental results give about 6%.

As it is evident from different investigations, to date there is no general consensus on a universal parameterization for R_f. This is due to lack of evidence on what the behavior of R_f should be under very strong stratifications in high Reynolds number flows (Karimpour & Venayagamoorthy 2014). Laboratory experiments and direct numerical simulations remain inconclusive about this issue due to Reynolds number limitations. Field experiments tend to show quite a bit of scatter due to difficulties to measure R_f as well as contamination from other processes such as internal waves. It is typical to use a constant flux Richardson number to infer mixing, but there is a lack of consensus on its value, e.g. $R_f \leq 0.17$ is introduced by Osborn (1980) or Oakey (1982) introduced a highly variable value of $R_f \simeq 0.206 \pm 0.174$ and Lilly *et al.* (1974) estimated $R_f \simeq 0.25$.

On the other hand, evidences suggest that the flux Richardson number (R_f) has to be a function of forcing and stratification (Ivey *et al.* 2008). Therefore a dynamic expression for R_f is required. Mellor & Yamada (1982) proposed a flux Richardson number (R_f) as a function of the gradient Richardson number (Ri_g) as

$$R_f = 0.725[Ri_g + 0.186 - (Ri_g^2 - 0.316Ri_g + 0.0346)^{0.5}], \tag{43}$$

which suggests $R_f \lesssim 0.25$. Nakanishi (2001) has used LES simulations to slightly improve Mellor & Yamada (1982) formulation with a maximum flux Richardson number of 0.3.

2.8. Summary

This chapter has provided a brief overview on some fundamental aspects of turbulence modeling methods, wall-bounded flows, the breaking and mixing. Also, a brief review of investigations (field, laboratory experiments and numerical simulation results) focusing on these subjects was provided. In the next chapter, we focus on unstratified near-wall turbulence by using analytical arguments.

CHAPTER 3

Equilibrium Assumption for Unstratified Wall-Bounded Turbulence

In this chapter a discussion and description of near-wall turbulence is presented. In section 3.1 the near-wall turbulence in an unstratified turbulent channel flow is revisited using the equilibrium assumption and the relevant length, velocity and time scales are derived. The propositions are examined using DNS data of unstratified channel and boundary layer flows. In section 3.2, the proposition of the standard k-ϵ model for the turbulent viscosity which is developed based on the equilibrium assumption is analytically revisited and its suitability for modeling near-wall turbulence is investigated.

3.1. Unstratified Channel Flow[1]

3.1.1. Introduction. Unstratified wall-bounded turbulent flows are prevalent in many engineered and natural flows such as turbulent flow in channels, pipelines and rivers. The presence of the solid wall has profound effects on the transport of momentum, mass and heat. As such, it is not surprising that the subject of near-wall modeling has received much attention in the last few decades. However, modeling the near-wall effects is not trivial due to the highly inhomogeneous and anisotropic nature of the flow in the 'near-wall' region, which can be considered to be the most volatile region of the turbulent boundary layer where most of the turbulence is produced. Turbulence closure schemes such as the k-ϵ model (Launder & Spalding 1972) are often used in Reynolds-averaged Navier-Stokes (RANS) numerical simulations to model turbulence in wall-bounded flows. Such models use the turbulent-viscosity hypothesis to link the turbulent momentum flux (Reynolds stresses) with the mean shear rate (S) through a turbulent (eddy) viscosity (ν_t). For example, in a uni-directional shear flow (such as in a turbulent channel flow) with a mean streamwise velocity $\left(\overline{U}\right)$, and

[1]The results presented in this section have been published in substantial part as "Some insights for the prediction of near-wall turbulence" by F. Karimpour and S. K. Venayagamoorthy, in the *Journal of Fluid Mechanics*, Vol. 723, pp 126-139, 2013. This chapter is written in a collective "we" tense to acknowledge collaborative work with the co-author.

taking z as the wall-normal coordinate, the turbulent momentum flux is given by

$$\overline{u'w'} = -\nu_t \frac{d\overline{U}}{dz} = -\nu_t S, \tag{44}$$

where the mean shear rate $S = d\overline{U}/dz$. There are a number of different closure schemes that have been developed to model ν_t, but two-equation models such as the k-ϵ model, have emerged to be the most widely used complete closure schemes (Pope 2000, Durbin & Pettersson Reif 2011).

Wall-bounded flow (specifically channel flow) can be categorized into two main regions: an inner region and an outer region. The inner region can be further subdivided into three different layers namely: the viscous sublayer for $z^+ < 5$, buffer layer for $5 < z^+ < 30$ and the log-law region (constant-stress region that overlaps the inner and outer regions) for $z^+ > 30$, where z^+ is the wall unit defined as $z^+ = u_\tau z/\nu$ with u_τ, z and ν defined as the friction velocity, distance from the wall and the molecular (kinematic) viscosity, respectively (Pope 2000). The viscous sublayer and buffer layer together are classified as the near-wall (or viscous wall) region since viscosity is important and the energetic and dissipative scales overlap (Jiménez & Moser 2007). There have been numerous discussions on the appropriate velocity scale for both the inner and outer flow regions. The velocity scale that is assumed to be common to both regions of the flow is the friction velocity (u_τ). However, the length scales are different; in the inner region, it is the viscous length scale (ν/u_τ) that is relevant while in the outer region, the boundary layer thickness is considered to be the appropriate length scale. Such arguments (in the limit of infinite Reynolds number) give rise to the logarithmic law for the mean velocity profile and are now commonly referred to as the "classical" scaling (Jones *et al.* 2008). Some recent review papers by Marusic *et al.* (2010), Smits *et al.* (2011), George (2007) and Gad-el-Hak & Bandyopadhyay (1994) provide comprehensive reviews on wall-bounded turbulent flows that highlight the issue of inner and outer scales of the flow and their universality.

In this study, the focus is on the near-wall predictability of turbulence. Although the thickness of the near-wall region is two or more orders of magnitude smaller than the total

flow depth, its effect extends throughout the whole flow as almost 50% of the total flow velocity from the wall to the free surface occurs in this thin region (Hanjalić & Launder 1976). The remaining velocity differences mostly occur in the logarithmic layer. Therefore understanding the flow behavior in the near-wall region is essential for modeling the turbulence. To this end, direct numerical simulations (DNS) have been used extensively to study the kinematics and dynamics of wall-bounded flows (for a recent in-depth review, see Jiménez 2012). Near the wall, the mean shear rate is very high and the local Reynolds number is low due to viscous effects. However, Durbin (1991) argued that the low-Reynolds-number effect is not as important as the wall blocking effect which results from the impermeability condition at the wall (i.e. zero normal velocity). All of the above conditions make this thin layer very interesting to study and highlight the complexity involved in modeling the flow in the near-wall region compared to free shear flows.

The difficult and costly problem of resolving the very thin near-wall layer at high Reynolds number can be avoided by using wall functions which requires the existence of a log-law region where production and dissipation of turbulence are nearly in balance. For example, in the standard k-ϵ model, ν_t is then calculated as

$$\nu_t = C_\mu \frac{k^2}{\epsilon}, \tag{45}$$

where k is the turbulent kinetic energy, ϵ is the dissipation rate of the turbulent kinetic energy, and $C_\mu = (|\overline{u'w'}|/k)^2$ is the turbulent viscosity parameter (constant) and usually assumed to be 0.09 in the constant-stress (log-law) region. This result for the turbulent viscosity can be derived through a number of ways but it can be simply inferred from dimensional analysis by assuming that the characteristic velocity scale is $k^{1/2}$ and the characteristic time scale is $T_L = k/\epsilon$. The turbulent viscosity formulation with a constant C_μ works well above the near-wall region, but as discussed by Durbin (1991) and indicated in Figure (3.1), it overpredicts the turbulent viscosity (ν_t) in the near-wall region even when C_μ is almost half of the commonly assumed value of 0.09. The results shown in Figure (3.1) are computed from the channel flow DNS data of Hoyas & Jiménez (2006) at a friction Reynolds number

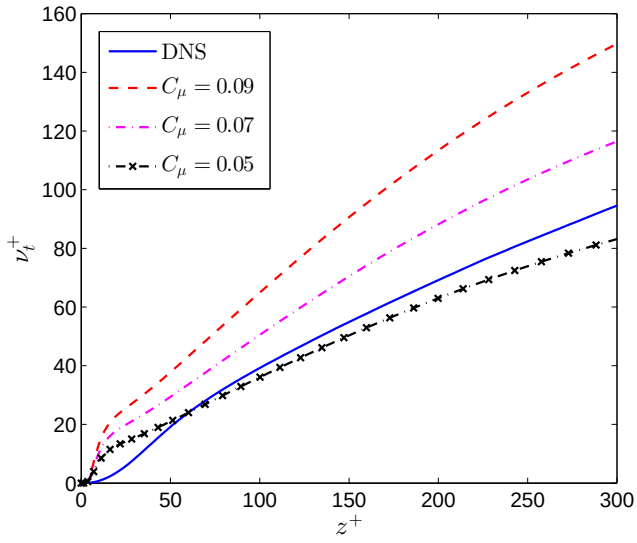

FIGURE 3.1. Comparison of the exact turbulent viscosity and the k-ϵ prediction in a turbulent channel flow at Re_τ=2003, computed from the DNS data of Hoyas & Jiménez (2006).

Re_τ=2003. The turbulent viscosities have been computed using both the exact definition obtained from equation (44) and the k-ϵ formulation given in equation (45) with the exact k and ϵ values from the DNS. Durbin & Pettersson Reif (2011) denote such comparisons as *'a priori'* tests.

This severe shortcoming has made it essential to make modifications to the k-ϵ model to correctly capture the near-wall behavior. Attempts to model the near-wall effects date back to van Driest (1956) who used a damping function to reduce the turbulent viscosity near the wall. A damping function is the ratio of the exact turbulent viscosity to the turbulent viscosity predicted by the turbulence model given by

$$f_\mu = \frac{\nu_t}{C_\mu \frac{k^2}{\epsilon}}. \tag{46}$$

Since then numerous proposals have been made to reduce the turbulent viscosity in the near-wall region. Some of the commonly cited formulations include those by Jones & Launder (1973), Lam & Bremhorst (1981), Patel *et al.* (1985), and Rodi & Mansour (1993). Most of these formulations use damping functions (sometimes loosely referred to as low-Reynolds-number models) that are based on z^+ and/or u_τ, and tend to be generally ineffective. Durbin

(1991) rejected the notion of using arbitrary damping functions to overcome the deficiency of the k-ϵ model. He pointed out that the k-ϵ formulation is isotropic while the near-wall turbulence is anisotropic, and argued that it is the wall-normal turbulent velocity which is responsible for transport. He proposed the so-called k-ϵ-$\overline{v^2}$ model which is essentially an elliptic relaxation model that allows for a representation of the wall blocking effect. It involves the solution of a fourth-order (i.e. a four-equation model) coupled system of differential equations in order to calculate the turbulent viscosity as

$$\nu_t = c'_\mu \overline{w'^2} \frac{k}{\epsilon}, \tag{47}$$

where c'_μ is a constant with a suggested value of 0.20 (Durbin 1991). It is important to note that in the k-ϵ-$\overline{v^2}$ model, the velocity scale is chosen as $\overline{v^2}$ (a model for the variance of the wall-normal component of turbulent velocity $\overline{w'^2}$), while the time scale is still chosen to be T_L, like in the standard k-ϵ formulations given in equation (45) or equation (46) with a lower bound set by the Kolomogorov time scale ($T_\eta = (\nu/\epsilon)^{1/2}$). This model agrees well with the DNS data especially in the near-wall region, but is sensitive to the choice of c'_μ away from the near-wall region as shown in Figure (3.2). It must be noted that this model has been shown to successfully predict different complex flows (for more details, see Pope 2000 and Durbin & Pettersson Reif 2011). A lot of the more recent works have focused on developing wall conditions for large-eddy simulations (LES) (see e.g. Kawai & Larsson 2012). In the RANS context, some recent work includes that of Kalitzin *et al.* (2005) where implications for the development of wall functions are discussed. Other recent RANS turbulence modeling efforts include near-wall corrections to account for low-Reynolds-number effects near the wall (Rahman & Siikonen 2005) and turbulent viscosity formulations proposed for the atmospheric boundary layer by Wilson (2012).

Our main goal is to highlight some insights that may be useful for modeling near-wall turbulence in closure schemes. We do this by revisiting the turbulent kinetic energy equation for a turbulent channel flow in order to propose a revised formulation for the turbulent viscosity, and hence derive more appropriate velocity, length and time scales. In section 3.1.2,

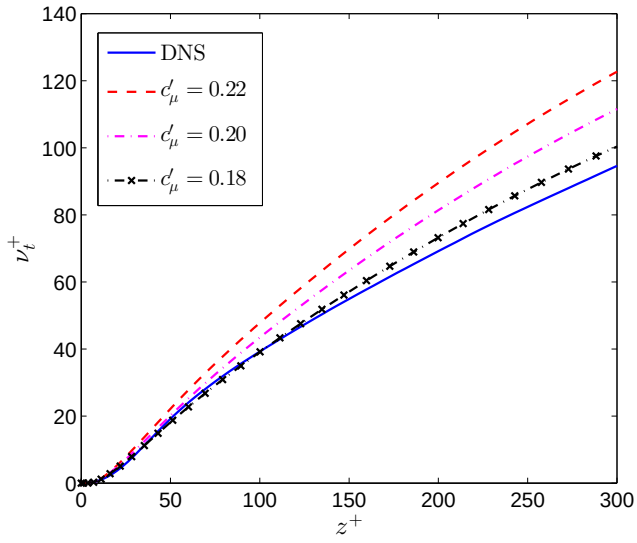

FIGURE 3.2. Comparison of the exact turbulent viscosity and the k-ϵ-$\overline{v^2}$ model prediction in a turbulent channel flow at Re_τ=2003, computed from the DNS data of Hoyas & Jiménez (2006). Curves for different c'_μ values are shown.

we present the evolution equation of the turbulent kinetic energy, followed by a proposal for the turbulent viscosity by extending the equilibrium assumption to the near-wall region. This is followed by a discussion on relevant velocity, length and time scales. In section 3.1.3, *'a priori'* tests using DNS data are presented to highlight the validity of the revised formulation. Conclusions are given in section 3.1.4.

3.1.2. Parameterization of the Turbulent Viscosity.

3.1.2.1. *Turbulent Kinetic Energy Equation.* The evolution equation for the turbulent kinetic energy (k) for an inhomogeneous constant density shear flow can be written as (using the Einstein summation convention)

$$\frac{\partial k}{\partial t} + \overline{U_j}\frac{\partial k}{\partial x_j} = P - \epsilon + D_\nu + T + \Pi, \tag{48}$$

where $P = -\overline{u'_i u'_j}\partial\overline{U_i}/\partial x_j$ is the production rate of the turbulent kinetic energy (k), $\epsilon = \nu\overline{(\partial u'_i/\partial x_j)(\partial u'_i/\partial x_j)} + \nu\partial^2(\overline{u'_i u'_j})/\partial x_j\partial x_j$ is the dissipation rate of k, $D_\nu = \nu\partial^2 k/(\partial x_j\partial x_j)$ is the viscous transport of the turbulent kinetic energy, $T = -(1/2)\partial\overline{(u'_j u'_i u'_i)}/\partial x_j$ is the turbulent velocity transport of k and $\Pi = -(1/\rho_0)\partial\overline{(p'u'_j)}/\partial x_j$ is the pressure transport

of k, respectively. It is worth noting that all the three transport terms arise due to the inhomogeneity in the flow.

3.1.2.2. *Turbulent Viscosity and Appropriate Velocity Scale.* For steady fully developed turbulent channel flow, equation (48) simplifies to

$$-\overline{u'w'}\frac{d\overline{U}}{dz} = \epsilon - D_\nu - T - \Pi, \tag{49}$$

where now the transport terms are also simpler (for details see e.g. Pope 2000). Equation (49) implies that the production of k is balanced by the dissipation and transport of k in the flow. Using the turbulent-viscosity hypothesis, P can be replaced with $\nu_t S^2$ and rearranging gives an expression for the turbulent viscosity as

$$\nu_t = (\epsilon - D_\nu - T - \Pi)/S^2. \tag{50}$$

Evidence from DNS data (dating back to the seminal DNS of channel flow by Kim *et al.* 1987) shows that in the near-wall region (especially in the buffer region), the dominant terms are P and ϵ, while the transport of k is substantially impeded. Suppose we make the assumption to neglect all the transport terms in the near-wall region (i.e. assume equilibrium in the near-wall region), then equation (50) simplifies to

$$\nu_t \approx \epsilon/S^2. \tag{51}$$

The turbulent viscosity given by equation (51) can be defined as an irreversible momentum diffusivity since it is based on ϵ, which is an irreversible quantity in the turbulent kinetic energy budget (Venayagamoorthy & Stretch 2010). Equation (51) also directly follows from the turbulent-viscosity hypothesis (equation 44), once the equilibrium assumption is made. However, let us also take a slightly long-winded path using the turbulent viscosity formulation from a dimensional point of view, to illustrate how equation (51) is also equivalent to equation (45). Dimensional reasoning suggests that the turbulent viscosity should be given by

$$\nu_t = U_{TVH}L_{TVH} = U_{TVH}^2 T_{TVH} = L_{TVH}^2/T_{TVH}, \tag{52}$$

where U_{TVH} is a characteristic velocity scale, L_{TVH} is a characteristic mixing length scale (which will be discussed later), and T_{TVH} is a characteristic time scale in the context of the turbulent-viscosity hypothesis (TVH). Pope (2000) suggested that a favorably disposed specification for the velocity scale is

$$U_{TVH} = |\overline{u'w'}|^{1/2}. \tag{53}$$

In the context of two-equation models, a good choice as also suggested by Kolmogorov (1942) is to base the velocity scale on k as

$$U_{TVH} = ck^{1/2}, \tag{54}$$

where c is usually assumed to be a constant. However, it is easy (and important) to note from equation (53) and equation (54) that c is given as the square root of the stress-intensity ratio

$$c = \left(\frac{|\overline{u'w'}|}{k}\right)^{1/2}. \tag{55}$$

In the constant-stress region (i.e. in the log-law region in wall-bounded flows), $c \approx 0.55$, based on empirical evidence that the stress intensity $-\overline{u'w'}/k \approx 0.3$ in this region. However, elsewhere it should hold as a dynamic 'constant'. Using the turbulent-viscosity hypothesis given in equation (44), c can be expressed as

$$c = \left(\frac{\nu_t S}{k}\right)^{1/2} = \left(\frac{P}{Sk}\right)^{1/2}, \tag{56}$$

where the production $P = \text{-}\overline{u'w'}S = \nu_t S^2$. The quantity $P/(Sk)$ is the ratio of the mean shear time scale $(1/S)$ to the turbulence production time scale (k/P). Hence, for equilibrium flows (when $P \approx \epsilon$), this simplifies to

$$c \approx \left(\frac{\epsilon}{Sk}\right)^{1/2} = \frac{1}{(ST_L)^{1/2}}. \tag{57}$$

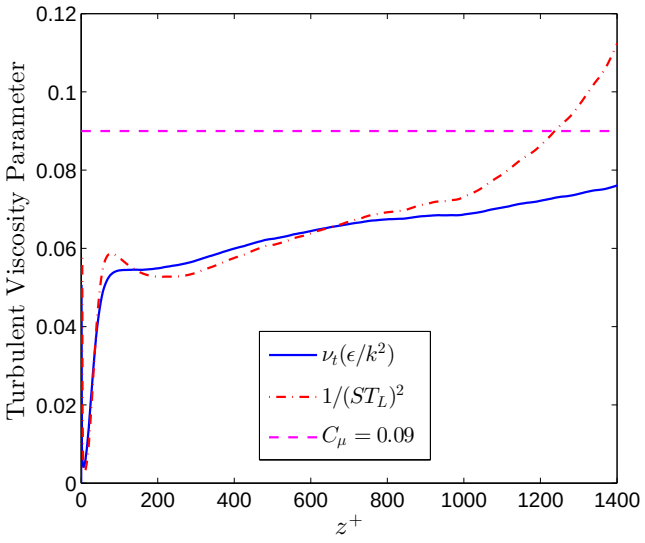

FIGURE 3.3. Profiles of $\nu_t\epsilon/k^2$ and $1/(ST_L)^2$ in a turbulent channel flow at Re_τ=2003, computed from the DNS data of Hoyas & Jiménez (2006). C_μ=0.09 is also shown for comparison.

At this point, it follows that the turbulent viscosity constant (C_μ) in equation (45) is given by

$$C_\mu = c^4 \approx \frac{1}{(ST_L)^2}. \tag{58}$$

We note that equation (45) is therefore equivalent to equation (51) if C_μ is given by equation (58). The assertion in equation (58) can be tested using DNS data. Figure (3.3) shows the behavior of $C_\mu = (1/ST_L)^2$ (computed from the DNS data) and $C_\mu = 0.09$. The exact value $\nu_t\epsilon/k^2$ computed from the DNS data is also shown. First, it is remarkable to see the excellent agreement between the curves given by equation (58) and the exact computation, especially in the near-wall region, indicating that the assumption made in neglecting the transport terms to arrive at equation (51) seems to be valid. Second, as already shown in Figure (3.1), it is not surprising that the exact quantity is very disparate from the usually assumed constant value of 0.09 for C_μ, especially close to the wall.

Furthermore, substitution of the expression for c given by equation (57) in equation (54) indicates that the appropriate velocity scale should be prescribed as

$$U_{TVH} \approx U_S = \left(\frac{1}{ST_L}k\right)^{1/2} = \left(\frac{\epsilon}{S}\right)^{1/2}, \tag{59}$$

where ST_L is the ratio of the turbulence decay time scale (T_L) to mean shear time scale ($1/S$). As a side note, it is worth noting that when $ST_L \to \infty$, the turbulence (fluctuations) in homogeneous shear flows can be described by rapid-distortion theory (see e.g. Pope 2000 for a detailed discussion), while for $ST_L \to 0$, turbulence production and turbulent viscosity vanish. This limit is nicely discussed in Pope (2000) using the so-called return-to-isotropy models. The behavior of ST_L obtained from channel flow DNS data at Re_τ=2003 (Hoyas & Jiménez 2006) is shown in Figure (3.4). It is clear that ST_L increases rapidly in the buffer layer in the near-wall region with a maximum value just greater than 18 at a distance of $z^+ \approx 8$. In essence, ST_L serves as the anisotropic correction scale in the near-wall region to the original velocity scale based on k that is used in the k-ϵ model. We also note that further away from the wall (in the far outer region, $z^+ \sim 1000$), the agreement between the exact curve and $(1/ST_L)^2$ shown in Figure (3.3) diverges. This is clearly expected as the mean shear rapidly drops to zero beyond the log-law region.

3.1.2.3. *Relevant Length and Time Scales.* Here we extend our discussion to the relevant length scale and time scale that are inherent in the turbulent viscosity formulation that was presented in the previous section. From equation (52) in section 3.1.2.2, it is clear that a number of different length, time and velocity scales can be combined to obtain a dimensionally consistent turbulent viscosity. However, the critical issue in the context of near-wall modeling is that the classical scales (i.e. $L = k^{3/2}/\epsilon$, $T_L = k/\epsilon$ and $U = k^{1/2}$) that two-equation models are based on do not seem to capture the near-wall behavior of the turbulent viscosity in a wall-bounded shear flow. Using the appropriate velocity scale obtained in equation (59), the corresponding length scale (L_{TVH}) can be back calculated

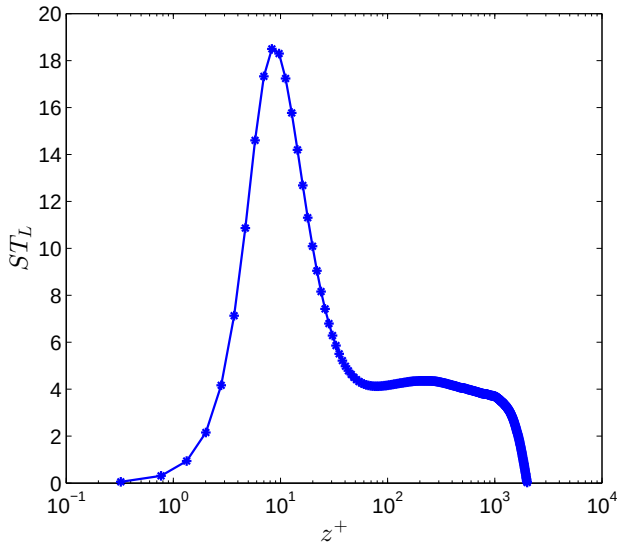

FIGURE 3.4. Profile of turbulent to mean time scales ST_L in a turbulent channel flow at Re_τ=2003, computed from the DNS data of Hoyas & Jiménez (2006).

from equation (51) as follows

$$L_{TVH} = \frac{\nu_t}{U_{TVH}} \approx \frac{\epsilon/S^2}{(k/ST_L)^{1/2}} = \left(\frac{\epsilon}{S^3}\right)^{1/2}. \tag{60}$$

This is indeed the shear length scale (L_S), sometimes referred to as the Corrsin scale as he was the first to allude to this scale in his discussion on local isotropy in turbulent shear flows (Corrsin 1958). It is considered as the relevant scale that marks the start of the inertial subrange in turbulent shear flows (e.g. see Pope 2000). Conceptually, it can be thought of as the smallest scale at which eddies are strongly deformed by mean shear. The corresponding time scale is given by

$$T_{TVH} = \frac{\nu_t}{U_{TVH}^2} = \frac{1}{S}. \tag{61}$$

We shall denote this time scale as T_S. This might perhaps appear as a surprising result since it implies that the relevant time scale is governed by the mean shear rate (S) and not T_L as used in the formulations for the models given in equation (45) and equation (47). However, it is not at all surprising once we recognize that if $k^{1/2}$ is the wrong velocity scale (as suggested

by Durbin 1991), then it must also mean that T_L will be the wrong time scale. Furthermore, this is obvious once we recall that S is implicit in the turbulent-viscosity hypothesis. In other words, T_L needs a similar anisotropic correction as the velocity scale, i.e. in this case by a factor of $(ST_L)^{-1}$.

It is constructive here to revisit the turbulent viscosity formulation proposed by Durbin (1991) as shown in equation (47). We will assume that equation (51) is valid for now and test this validity later (in section 3.1.3.1) using DNS data. Using equation (51) and assuming (for the purpose of this exercise) that T_L is the appropriate time scale (noting that this is the time scale assumed in the k-ϵ model), the corresponding velocity scale can be backed out as follows

$$\nu_t = \frac{\epsilon}{S^2} = U_M^2 T_L = U_M^2 \frac{k}{\epsilon}, \tag{62}$$

which can be rearranged to get the expression for velocity as

$$U_M = \frac{1}{ST_L} k^{1/2}. \tag{63}$$

The corresponding length scale can also be obtained in a similar manner as

$$L_M = \frac{k^{1/2}}{S} = \frac{1}{ST_L} \frac{k^{3/2}}{\epsilon}. \tag{64}$$

Venayagamoorthy & Stretch (2010) indicated that L_M can be considered as a rough measure of the active turbulent fluctuations in momentum and can be interpreted as the approximate measure of the average eddy size. Note, using L_M and T_L, equation (51) can also be expressed as $\nu_t = L_M^2/T_L$. Now if equation (51) is indeed a good approximation to the actual turbulent viscosity, then it should also be approximately equal to the turbulent viscosity obtained from equation (47). Equating these two equations reveals the following relationships

$$U_M \approx (c'_\mu \overline{w'^2})^{1/2}, \tag{65}$$

$$L_M \approx (c'_\mu \overline{w'^2} T_L^2)^{1/2}. \tag{66}$$

Essentially, the terms on the right hand side of equation (65) and equation (66) can be considered as the pertinent (effective) velocity and length scales in the k-ϵ-$\overline{v^2}$ model of Durbin (1991). We test the validity of these relationships in the next section.

3.1.3. 'A PRIORI' TESTS USING DNS DATA. In this section we test the validity of the proposed model for the turbulent viscosity given by equation (51). We then compare the velocity scale (U_S) and length scale (L_S) with the exact velocity scale (U_{TVH}), and the exact mixing length scale ($L_{TVH} = |\overline{u'w'}|^{1/2}/S$) using DNS data of turbulent channel flow. We also compare the relationships proposed in equation (65) and equation (66). Comparisons with DNS data of turbulent boundary layer flows are also presented to highlight the applicability of the proposed model to other canonical wall-bounded turbulent flows.

3.1.3.1. *Turbulent Viscosity Comparisons in Turbulent Channel Flow.* Figure (3.5) shows the *'a priori'* comparison between the exact turbulent viscosity obtained from equation (44) and the proposed approximation given in equation (51). The excellent agreement in the near-wall region is remarkable, especially given the fact that all the transport terms were neglected in arriving at equation (51). This implies that the transport terms are not as important as the production and dissipation terms in the near-wall region, at least as far as modeling the mixing in the near-wall region is concerned. We note that the turbulent viscosity given by equation (51) can be expressed in non-dimensional form as a shear Reynolds number ($Re_S = \epsilon/(\nu S^2)$). Therefore, Re_S provides a very good measure of the intensity of turbulent mixing in unstratified shear flows.

3.1.3.2. *Comparisons of Velocity and Length Scales in Turbulent Channel Flow.* Figure (3.6) shows the comparison of velocity scales and length scales discussed in section 3.1.2. First, the comparison between the exact velocity scale (U_{TVH}) and the proposed velocity scale (U_S) given by equation (59) is very good in the near-wall region (see Figure 3.6a). The corresponding comparisons between L_{TVH} and L_S given by equation (60) as shown in Figure (3.6b) is almost perfect in the near-wall region. In essence, these results clearly show that L_S, T_S and U_S are the appropriate turbulent scales that capture the behavior of the near-wall turbulence.

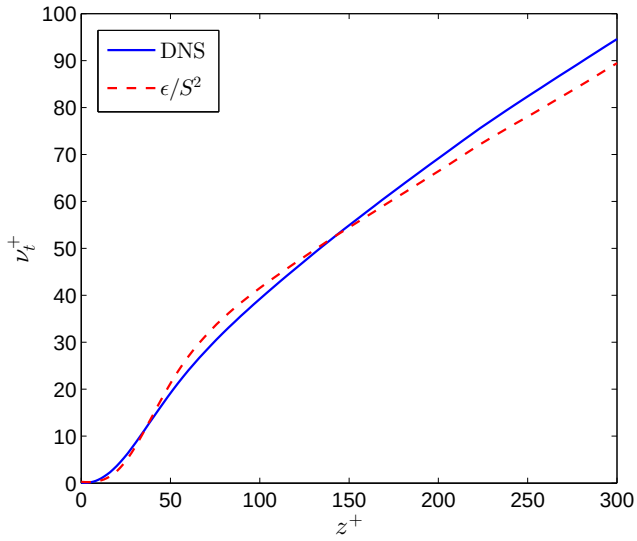

FIGURE 3.5. Comparison of the exact turbulent viscosity and the prediction given by equation (51) in a turbulent channel flow at Re_τ=2003, computed from the DNS data of Hoyas & Jiménez (2006).

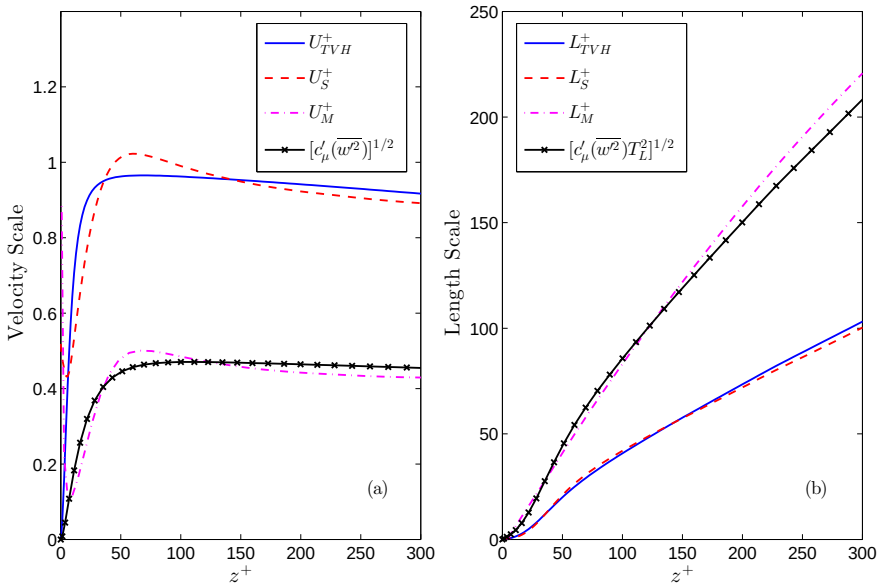

FIGURE 3.6. Comparison of (a) velocity scales; and (b) length scales in a turbulent channel flow at Re_τ=2003, computed from the DNS data of Hoyas & Jiménez (2006). Note c'_μ=0.18 was used in equation (65) & equation (66), respectively.

Figures (3.6a) and (3.6b) also show the comparisons between U_M given by equation (63) with the right hand side term in equation (65) and between L_M given by equation (64)

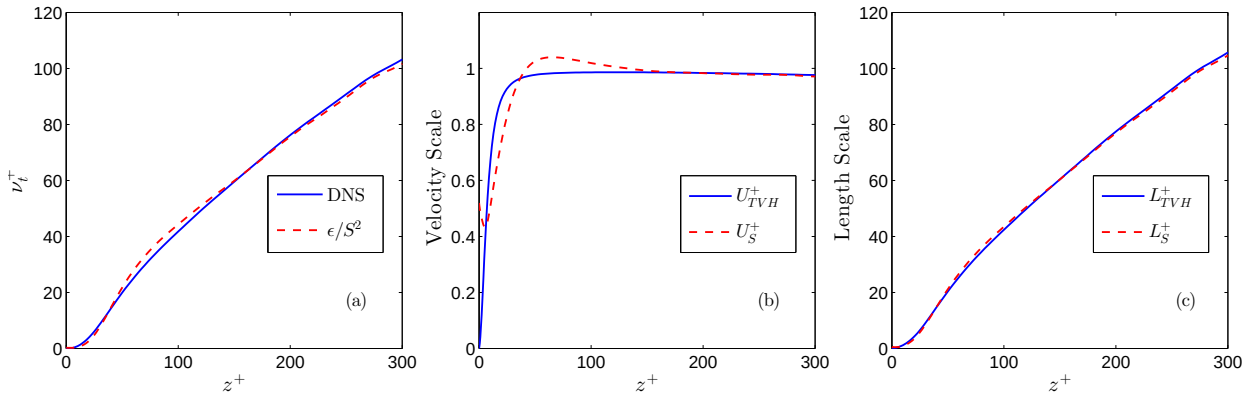

FIGURE 3.7. Comparison of (a) the exact turbulent viscosity and the prediction given by equation (51); (b) velocity scales; and (c) length scales in a turbulent boundary layer flow at $Re_\theta \approx$6500, computed from the DNS data of Sillero *et al.* (2013).

with the right hand side term in equation (66), respectively. Note, we have used c'_μ=0.18, since this value gave the best agreement with the DNS results shown in Figure (3.2). The close agreement between these scales indicate that L_M and U_M may be considered to be the pertinent length and velocity scales embedded in the k-ϵ-$\overline{v^2}$ model. However, if a comparison is done between $(\overline{w'^2})^{1/2}$ and U_{TVH} (shown in section 3.2), it becomes evident that $(\overline{w'^2})^{1/2}$ is a good choice for the velocity scale in the near-wall region but it deviates faster from U_{TVH} than U_S does. This means that the constant c'_μ in the k-ϵ-$\overline{v^2}$ model is equivalent to a time scale correction factor such that $c'_\mu T_L$ is by construction designed to mimic the behavior of the appropriate time scale $T_S = 1/S$, in order to predict the correct turbulent viscosity in the near-wall region.

3.1.3.3. *Comparisons in Turbulent Boundary Layer Flow.* Figure (3.7a) shows the *'a priori'* comparison between the exact turbulent viscosity obtained from equation (44) and the proposed approximation given in equation (51) using DNS data of turbulent boundary layer flow (Sillero *et al.* 2013) at a Reynolds number based on the momentum thickness of $Re_\theta \approx 6500$. Similar to the channel flow comparison shown in Figure (3.5), there is excellent agreement in the near-wall region. Furthermore, the agreement between the exact velocity scale (U_{TVH}) and the proposed velocity scale (U_S) is very good as shown in Figure

(3.7b). The corresponding comparisons between the length scales (L_{TVH}) and (L_S) shown in Figure (3.7c) are in excellent agreement in the near-wall region similar to the channel flow comparisons shown in Figure (3.6b). We note that comparisons (not shown) with DNS data of pipe flow at relatively low-Reynolds-number of Re_τ=190 based on the pipe radius show good agreement (Loulou *et al.* 1997). The highest Reynolds number DNS of pipe flows to date were done by Wu & Moin (2008) but unfortunately, the dissipation rate of k was not sampled and hence we were unable to verify the proposed scaling at higher Reynolds numbers that are comparable to the channel and boundary layer flows discussed in this study. Regardless, these results indicate that the proposed scaling is widely applicable to turbulent wall-bounded flows.

3.1.3.4. *Implications at Higher Reynolds Numbers.* The turbulent channel and boundary layer flow DNS data that have been used to test the proposed scaling have (to our knowledge) the highest Reynolds numbers to date. However, they are still well below the Reynolds numbers of most practical flows. There are higher Reynolds number pipe flow experiments (see e.g. the Princeton Superpipe experiments by Zagarola & Smits 1998 and McKeon *et al.* 2004) that have a significant logarithmic region but due to constraints of measurements very close to the wall do not have turbulence fluctuation statistics near the wall. However, we performed comparisons (not shown here in order to avoid repetition) of the proposed scaling with DNS of channel flow data at lower Reynolds numbers (Kim *et al.* 1987, Moser *et al.* 1999 and del Álamo *et al.* 2004). The agreement gets consistently better with increasing Re_τ, which is a promising trend, suggesting that the proposed prediction should hold true at even higher Reynolds numbers that typifies relevant practical flows.

3.1.4. Concluding Remarks. In this study, we have made the equilibrium assumption (i.e. $P \approx \epsilon$) to propose that the turbulent viscosity $\nu_t \approx \epsilon/S^2$. We have then argued by revisiting the turbulent viscosity formulation that the appropriate velocity scale is $U_S = (ST_L)^{-1/2}k^{1/2} = (\epsilon/S)^{1/2}$ as opposed to the classical scale of $k^{1/2}$. We then extended our analysis to show that the corresponding appropriate length and time scales are $L_S = (\epsilon/S^3)^{1/2}$ and $T_S = 1/S$, respectively. The comparisons between the proposed scales

and the exact scales computed from the most highly resolved turbulent channel flow DNS dataset to date show remarkable agreement. The agreement with DNS data of turbulent boundary layer flow is also very good. To our knowledge, this appears to be the first time such results have been reported for describing the behavior of near-wall turbulence. We have also provided some insights on the pertinent velocity, length and time scales that are inherent in the k-ϵ-$\overline{v^2}$ model proposed by Durbin (1991).

In essence, these results highlight how well the equilibrium assumption holds in the near-wall region. We evaluate the effect of equilibrium assumption on developing near-wall turbulence models in next section. Another obvious extension to this work is to study the effects of density stratification in wall-bounded shear flows. This adds another level of complexity through the coupling between the equations for the turbulent kinetic energy and density fluctuations via the buoyancy flux term. This aspect is what forms the subject of chapter 4 of this dissertation.

3.2. Revisit of Equilibrium Assumption[2]

3.2.1. Introduction. Reynolds-averaged Navier Stokes (RANS) turbulence models such as the k-ϵ closure scheme (Launder & Spalding 1972) commonly use the turbulent-viscosity hypothesis (hereafter TVH) to simulate wall-bounded flows. In these models, the Reynolds stresses are linked with the mean shear rate (S) through the turbulent (eddy) viscosity (ν_t). For a one-dimensional shear flow, ν_t is given by

$$\nu_t = \frac{-\overline{u'w'}}{d\overline{U}/dz}, \tag{67}$$

where $\overline{U}$ is the mean streamwise velocity and z is the vertical distance from the wall. Within the context of the TVH, dimensional reasoning can be used to recast ν_t in terms of characteristic scales of velocity (U_{TVH}), length (L_{TVH}) and time (T_{TVH}) as

$$\nu_t = U_{TVH}.L_{TVH} = U_{TVH}^2.T_{TVH} = L_{TVH}^2/T_{TVH}. \tag{68}$$

[2]The results presented in this section can be found in a paper entitled "A revisit of the equilibrium assumption for predicting near-wall turbulence" by F. Karimpour and S. K. Venayagamoorthy, that is currently in press for publication in the *Journal of Fluid Mechanics*.

Pope (2000) suggested that a favorable velocity scale for turbulent flows is $U_{TVH} = (-\overline{u'w'})^{1/2}$ which consequently results in the characteristic length scale as $L_{TVH} = (-\overline{u'w'})^{1/2}/S$ and the characteristic time scale as $T_{TVH} = T_S = 1/S$. It should be noted that these derived scales are only the relevant scales of the flow within the framework of the TVH and should not be interpreted as the scales of turbulence.

In some turbulence closure schemes such as the standard k-ϵ model which is the most commonly used two-equation closure scheme (Pope 2000, Durbin & Pettersson Reif 2011), the turbulent viscosity (ν_t) is derived by assuming local and approximate equilibrium between the production rate of the turbulent kinetic energy (P) and the dissipation rate of the turbulent kinetic energy (ϵ) in a fully developed wall-bounded turbulent flow. This assumption implies that the transport terms which result due to the presence of the solid wall are negligible and hence simplifies analysis of the wall-bounded turbulence.

In addition to assuming equilibrium (i.e. $P \approx \epsilon$), the turbulent viscosity of the k-ϵ model ($\nu_{t(k-\epsilon)}$) is developed by using the proposition of Kolmogorov (1942) to base the characteristic velocity scale on the turbulent kinetic energy (k) such that $U_{TVH} = (-\overline{u'w'})^{1/2} = ck^{1/2}$. Hence, $\nu_{t(k-\epsilon)}$ is given by

$$\nu_t \approx \nu_{t(k-\epsilon)} = c^4 \frac{k^2}{\epsilon} = C_\mu \frac{k^2}{\epsilon}. \tag{69}$$

Here, c is the square root of the stress-intensity ratio (i.e. $c = (|\overline{u'w'}|/k)^{1/2}$) and is usually assumed to be constant in the log-law region. In the standard k-ϵ model, $c \approx 0.55$ or $c^2 \approx 0.3$ is employed on the basis of empirical measurements which implies that $C_\mu \approx 0.09$.

For the k-ϵ model to work properly in the near-wall region, the turbulent (eddy) viscosity shown in equation (69) needs to be the same as the turbulent viscosity defined in equation (67). However, it is well known that this formulation (equation 69) breaks down in the near-wall region of canonical wall-bounded flows and overpredicts the exact turbulent viscosity (ν_t). This failure is normally attributed to the fact that the stress-intensity ratio (c^2) is not a constant in the near-wall region. Efforts to overcome this severe shortcoming have focused on modifications to the transport equations for k and ϵ in conjunction with empirical damping

functions to reduce $\nu_{t(k-\epsilon)}$ in the near-wall region (e.g., see Jones & Launder 1973, Launder & Sharma 1974, Lam & Bremhorst 1981 and Rodi & Mansour 1993). These functions are not universal and tend to be ineffective when tested with different sets of DNS data.

Attempts have been made to model the near-wall turbulence without employing such damping functions. Durbin (1991) proposed a model that solves for wall-bounded turbulence without recourse to a damping function. He argued that the wall-normal velocity fluctuation ($\overline{w'^2}$) is responsible for transport from the wall and not the total turbulent kinetic energy (k), as is assumed in the k-ϵ model. Hence, he developed a fourth-order turbulence closure scheme, namely k-ϵ-$\overline{v^2}$ model where $\overline{v^2}$ represents $\overline{w'^2}$. Considering the model time scale as $T_L = k/\epsilon$, the turbulent viscosity (ν_t) in Durbin's model is computed as

$$\nu_t = c'_\mu \overline{w'^2} \frac{k}{\epsilon}, \tag{70}$$

where c'_μ is a constant taken as 0.20 by Durbin (1991). Recently, Karimpour & Venayagamoorthy (2013) have shown that the ν_t formulation of Durbin's model is insensitive to c'_μ in the near-wall region. This is also in agreement with the experimental observations of Schultz & Flack (2013) where they concluded that $-\overline{u'w'}$ and $\overline{w'^2}$ are Reynolds-number-independent in the near-wall region. Durbin's model has been extensively verified with both *'a priori'* and *'a posteriori'* tests with remarkably good results.

Our main aim is to highlight the drawbacks of using the equilibrium assumption in conjunction with the use of the turbulent kinetic energy (k) to infer the pertinent velocity scale in formulating a suitable turbulent viscosity. We also derive the appropriate scales within the framework of the TVH by analyzing the turbulent viscosity formulation of Durbin (1991). In section 3.2.2, a dimensional analysis of the turbulent viscosity formulation of the standard k-ϵ model ($\nu_{t(k-\epsilon)}$) is presented to derive the relevant scales inherent in this formulation and highlight the consequence of assuming equilibrium for inferring $\nu_{t(k-\epsilon)}$. The correlation of the turbulent kinetic energy (k) with the anisotropic Reynolds stress ($\overline{u'w'}$) is revisited in section 3.2.2.2, followed by a discussion on the appropriate scales for predicting near-wall turbulence. Finally, conclusions are given in section 3.2.3. In this study, different

channel flow DNS datasets of Kim, Moin & Moser (1987) for $Re_\tau \approx 180$, Moser, Kim & Mansour (1999) for $Re_\tau \approx 395$ and 590, del Álamo *et al.* (2004) for $Re_\tau \approx 934$ and Hoyas & Jiménez (2006) for $Re_\tau \approx 2003$ are used together with the boundary layer experimental data of Marusic & Perry (1995), for performing *'a priori'* tests.

3.2.2. Assessment of the k-ϵ model turbulent viscosity. In this section, we derive the inherent scales in the turbulent viscosity formulation of the standard k-ϵ closure scheme and also discuss the possibility of introducing a universal c. We use *'a priori'* tests to reinforce our discussion.

3.2.2.1. *Revisit of relevant characteristic scales and stress intensity.* Using equation (69) and the proposition of Kolmogorov (1942) for the velocity scale (i.e. $U_{k-\epsilon} = ck^{1/2}$), the relevant length scale inherent in $\nu_{t(k-\epsilon)}$ can be derived as

$$L_{k-\epsilon} = \frac{\nu_{t(k-\epsilon)}}{U_{k-\epsilon}} = c^4 \frac{k^2/\epsilon}{ck^{1/2}} = c^3 \frac{k^{3/2}}{\epsilon}. \tag{71}$$

Using $c = (-\overline{u'w'}/k)^{1/2}$ and $P = -\overline{u'w'}S$, equation (71) can be rewritten as

$$\begin{aligned} L_{k-\epsilon} &= c^3 \frac{k^{3/2}}{\epsilon} = \left(\frac{-\overline{u'w'}}{k}\right)^{3/2} \frac{k^{3/2}}{\epsilon} = \left(\frac{-\overline{u'w'}S}{\epsilon}\right)^{3/2} \left(\frac{\epsilon}{S^3}\right)^{1/2} \\ &= \left(\frac{P}{\epsilon}\right)^{3/2} \left(\frac{\epsilon}{S^3}\right)^{1/2} = \left(\frac{P}{\epsilon}\right)^{3/2} L_c, \end{aligned} \tag{72}$$

where $L_c = (\epsilon/S^3)^{1/2}$ is the Corrsin scale, introduced for the first time by Corrsin (1958). L_c shows the smallest eddy size which is deformed by the mean shear rate. The ratio P/ϵ can be expressed in terms of length scales as

$$\frac{P}{\epsilon} = \frac{-\overline{u'w'}S}{\epsilon} = \frac{-\overline{u'w'}/S^2}{\epsilon/S^3} = \left(\frac{L_{TVH}}{L_c}\right)^2. \tag{73}$$

Using equation (73), we can rewrite equation (71) as

$$L_{k-\epsilon} = \left(\frac{P}{\epsilon}\right)^{3/2} \left(\frac{\epsilon}{S^3}\right)^{1/2} = \left(\frac{P}{\epsilon}\right) \frac{L_{TVH}}{L_c} \left(\frac{\epsilon}{S^3}\right)^{1/2} = \left(\frac{P}{\epsilon}\right) L_{TVH}. \tag{74}$$

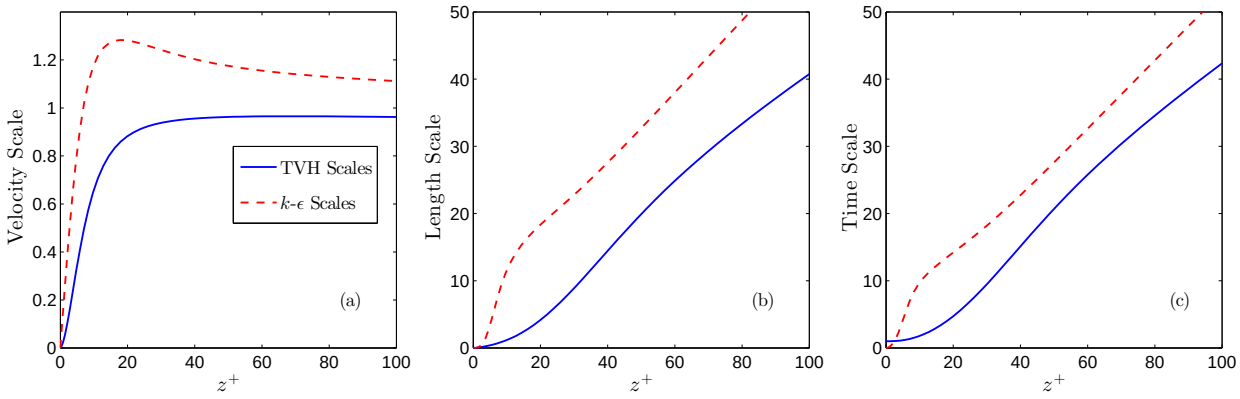

FIGURE 3.8. Comparison of a) $U_{k-\epsilon}$ with U_{TVH}; b) $L_{k-\epsilon}$ with L_{TVH} and c) $T_{k-\epsilon}$ with T_{TVH}; in a turbulent channel flow, computed from the DNS data of Hoyas & Jiménez (2006) for $Re_\tau = 2003$.

Equation (74) highlights the fact that while in the log-law region where $P \approx \epsilon$, $L_{k-\epsilon}$ is equal to L_{TVH} and consequently L_c, in the near-wall region both the length scale and therefore the turbulent viscosity ($\nu_{t(k-\epsilon)}$) are incorrect. Put another way, the turbulent viscosity from the standard k-ϵ model can be expressed in terms of the characteristic scales and the exact turbulent viscosity as

$$\nu_{t(k-\epsilon)} = c^4 \frac{k^2}{\epsilon} = \left(ck^{1/2}\right)\left(c^3 \frac{k^{3/2}}{\epsilon}\right) = \left(\frac{P}{\epsilon}\right) U_{TVH} L_{TVH} = \left(\frac{P}{\epsilon}\right) \nu_t. \tag{75}$$

Equation (75) clearly shows that in the near-wall region this formulation breaks down as it is a function of P/ϵ. This implies that the failure of $\nu_{t(k-\epsilon)}$ is independent of the fact that the exact value of c is ambiguous and hence damping c is not sufficient to make $\nu_{t(k-\epsilon)}$ suitable for modeling the near-wall turbulence.

Furthermore, using $U_{k-\epsilon} = ck^{1/2}$ and $L_{k-\epsilon}$ the relevant time scale can be deduced as

$$T_{k-\epsilon} = \frac{L_{k-\epsilon}}{U_{k-\epsilon}} = c^2 \frac{k}{\epsilon}, \tag{76}$$

which can also be rewritten as

$$T_{k-\epsilon} = c^2 \frac{k}{\epsilon} = \frac{-\overline{u'w'}}{k} \frac{k}{\epsilon} = \left(\frac{-\overline{u'w'}S}{\epsilon}\right) \frac{1}{S} = \left(\frac{P}{\epsilon}\right) \frac{1}{S}, \tag{77}$$

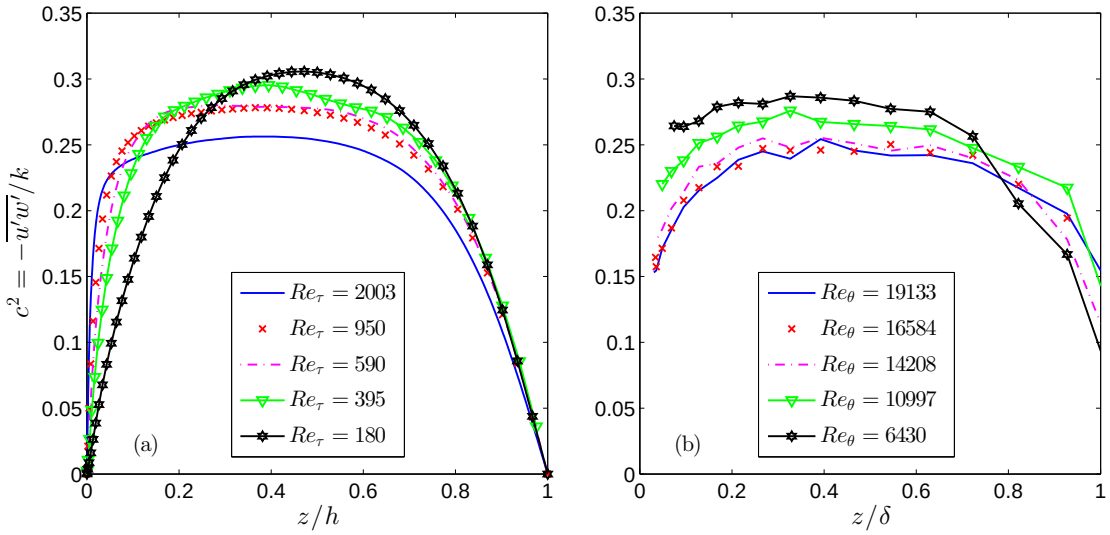

FIGURE 3.9. Comparison of $c^2 = -\overline{u'w'}/k$ for different Reynolds numbers using (a) the DNS data of turbulent channel flows for $Re_\tau = 2003, 934, 590, 395$ and 180; and (b) the experimental data of boundary layer flow of Marusic & Perry (1995).

which again shows that the time scale is only correct where equilibrium holds. This finding also shows that the traditionally assumed time scale $T_L = k/\epsilon$ in the standard k-ϵ model should be modified with c^2.

The comparisons of the standard k-ϵ model scales with the TVH scales are shown in Figure (3.8) using $c \approx 0.55$. It is obvious that (even in the log-law region) the standard k-ϵ model scales highly overpredict the corresponding characteristic scales which raises the doubt about the suitability of assuming a constant $c \approx 0.55$ in the log-law region. To assess this issue further, Figure (3.9) shows profiles of $c^2 = -\overline{u'w'}/k$ obtained from direct numerical simulations (DNS) data of channel flows as well as high-Reynolds-number experimental boundary layer data. In Figure (3.9), $Re_\tau = u_\tau h/\nu$ is the friction Reynolds number where h is half of the channel depth. Also, $Re_\theta = U_e\theta/\nu$ is the momentum thickness Reynolds number with θ defined as the momentum thickness, U_e as 99% of the maximum velocity and δ is the boundary layer thickness. The profiles clearly show that assuming $c \approx 0.55$ or $c^2 \approx 0.3$ is wrong. In fact, the profiles suggest that c decreases with increasing Reynolds number in the log-law region at least for this range of Reynolds numbers.

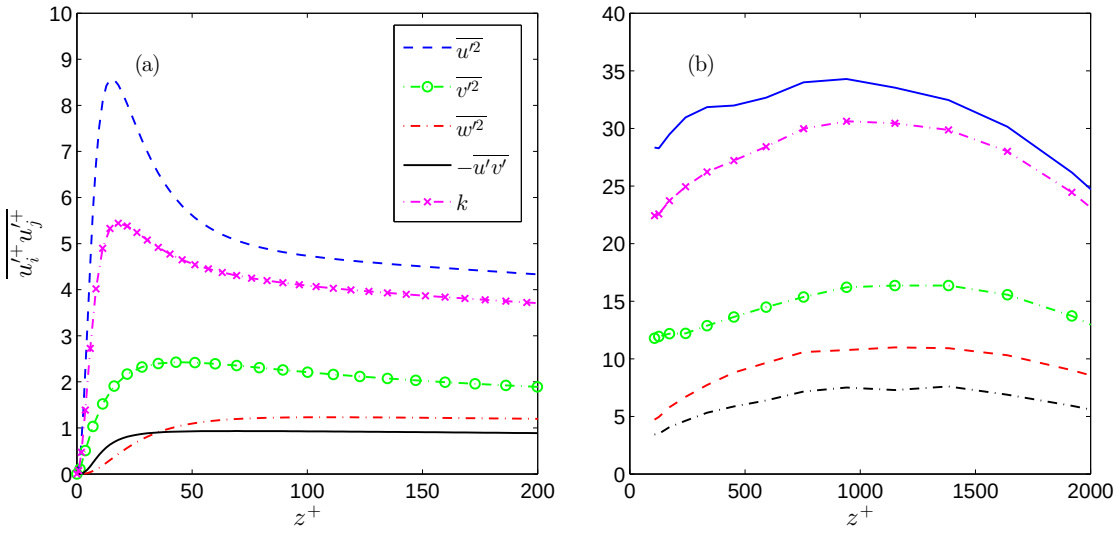

FIGURE 3.10. Comparison of Reynolds stresses and the turbulent kinetic energy (k) computed from (a) the DNS data of Hoyas & Jiménez (2006) for $Re_\tau = 2003$; and (b) the experimental boundary layer data of Marusic & Perry (1995) for $Re_\theta = 19133$.

Now, we revisit the behavior of c. In a preliminary attempt, Karimpour & Venayagamoorthy (2013) have shown that by using the equilibrium assumption all the way to the wall, a turbulent viscosity formulation can be derived as $\nu_t \approx \epsilon/S^2$ which implies that $c \approx 1/(ST_L)^{1/2}$. The comparison of their propositions with exact DNS computations showed small differences. However, it is clear that their formulation is not appropriate for modeling.

Here, we reassess the possibility of independently describing c by relaxing the equilibrium assumption that Karimpour & Venayagamoorthy (2013) made. The square root of the stress-intensity ratio ($c = (-\overline{u'w'}/k)^{1/2}$) can be recast as follows

$$c = \left(\frac{-\overline{u'w'}}{k}\right)^{1/2} = \left(\frac{-\overline{u'w'}S/\epsilon}{Sk/\epsilon}\right)^{1/2} = \left(\frac{P}{\epsilon}\right)^{1/2}\left(\frac{1}{ST_L}\right)^{1/2} = \frac{L_{TVH}}{L_c}\left(\frac{1}{ST_L}\right)^{1/2}. \qquad (78)$$

ST_L is the ratio of the turbulence (decay) time scale (T_L) to the mean shear time scale ($1/S$) and can be considered to be a measure of the linearization of the turbulent flow (Jiménez 2013). Equation (78) clearly shows that c and therefore the proposed velocity scale of Kolmogorov (1942) inherently depend on the behavior of P/ϵ and hence L_{TVH}. It can be inferred from Figure (3.9) and equation (78) that k cannot be an appropriate parameter of

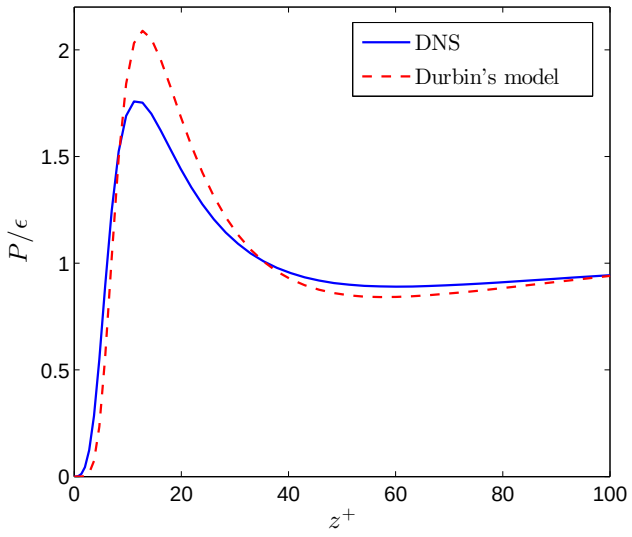

FIGURE 3.11. Comparison of Durbin's model P/ϵ and exact value computed from the DNS data of Hoyas & Jiménez (2006) for $Re_\tau = 2003$.

choice to describe $\overline{u'w'}$. This highlights the reason for the lack of success in formulating a universal damping function to appropriately decrease c in the near-wall region.

3.2.2.2. *Correlation of the Reynolds stresses.* In this section, we assess the correlation of the anisotropic Reynolds stress ($\overline{u'w'}$) with isotropic Reynolds stresses. In his valuable work, Lumley (1978) has discussed that the wall-normal velocity fluctuation ($\overline{w'^2}$) is a more appropriate velocity scale since it mimics the behavior of ($-\overline{u'w'}$) better compared to k. Figure (3.10) confirms his assertion, and it can be seen that k behaves similarly to the streamwise velocity fluctuation ($\overline{u'^2}$) while $\overline{w'^2}$ closely matches $-\overline{u'w'}$. As discussed in §1, Durbin (1991) made a similar argument and introduced the turbulent viscosity as $\nu_t = c'_\mu \overline{w'^2}(k/\epsilon)$.

Durbin's proposition for ν_t is widely used and its good comparison with exact ν_t is already shown in several works. Here, we test its efficacy for predicting P/ϵ in the near-wall region. Figure (3.11) presents the comparison of P/ϵ using Durbin's formulation with the exact value from DNS data. While there is a slight mismatch, the comparison is still favorable and confirms the suitability of the turbulent viscosity formulation proposed by Durbin (1991) for predicting the near-wall turbulence. This implies that the appropriate relevant scales in the

context of the TVH are inherent in Durbin's model. Therefore, it is instructive to derive the scales inherent in his model within the context of the TVH framework.

Durbin (1991) considered $T_L = k/\epsilon$ as the relevant time scale for his model with a lower bound set by a factor of the Kolmogorov time scale $(\nu/\epsilon)^{1/2}$ where ν is the kinematic viscosity, but as discussed earlier, the characteristic time scale in the context of the turbulent-viscosity hypothesis is $T_{TVH} = T_S = 1/S$. Using $-\overline{u'w'} = \nu_t S$, the relevant velocity and length scales inherent in his model can be derived respectively, as follows

$$U_{TVH} = \left(-\overline{u'w'}\right)^{1/2} \approx U_{k-\epsilon-v^2} = c_\mu'^{1/2} (ST_L)^{1/2} \left(\overline{w'^2}\right)^{1/2}, \tag{79}$$

$$L_{TVH} = \frac{\left(-\overline{u'w'}\right)^{1/2}}{S} \approx L_{k-\epsilon-v^2} = \left(\frac{c'_\mu}{ST_L}\right)^{1/2} \left(\overline{w'^2}\right)^{1/2} \frac{k}{\epsilon}. \tag{80}$$

Comparisons of these scales with the corresponding characteristic scales of length (L_{TVH}) and velocity (U_{TVH}) are excellent as shown in Figure (3.12). Also, in this figure, $\overline{w'^2}$ is shown for comparison. Moreover, it is clear that $T_{k-\epsilon-v^2} = L_{k-\epsilon-v^2}/U_{k-\epsilon-v^2} = 1/S$ which is equal to $T_{TVH} = 1/S$ and hence no comparison between the time scales is required. In Figures (3.11) and (3.12), $c'_\mu \approx 0.18$ is used since it provides a better prediction of the overall turbulent viscosity across the channel depth for this set of DNS data.

In equations (79) and (80), ST_L serves as an anisotropic correction to $\overline{w'^2}$ (which can also be considered to be a non-equilibrium correction in the near-wall region), while it is absent in the ν_t formulation given in equation (70). The reason for this is simply because $\overline{w'^2}$ is less than $-\overline{u'w'}$ in the near-wall region (see Figure 3.10) while $T_L = k/\epsilon$ is greater than $1/S$ in the near wall regions (see Figure 3.8c). These effects cancel out identically when computing the turbulent viscosity (i.e. $\nu_t = U_{k-\epsilon-v^2} \times L_{k-\epsilon-v^2}$).

3.2.3. Concluding Remarks. In this study, the validity of the equilibrium assumption in the near-wall region was revisited. Using dimensional reasoning, we have shown that the equilibrium assumption leads to incorrect prediction of the characteristic scales in the near-wall region and highlighted some of the shortcomings of using damping functions to model

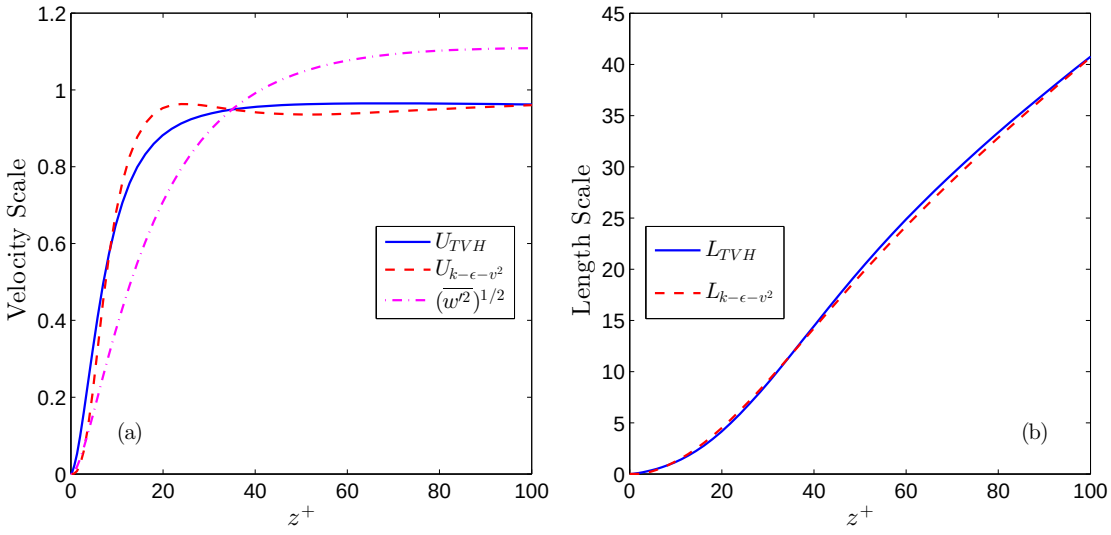

FIGURE 3.12. Comparison of (a) $U_{k-\epsilon-v^2}$ and $\overline{w'^2}$ with U_{TVH}; and (b) $L_{k-\epsilon-v^2}$ with L_{TVH} computed from the DNS data of Hoyas & Jiménez (2006) for $Re_\tau = 2003$.

the near-wall turbulence. This is followed by a detailed discussion on the importance of introducing an appropriate velocity scale than the traditionally assumed scale $ck^{1/2}$. To this end, the successful model of Durbin (1991) which makes use of $\overline{w'^2}$ instead of k is analyzed and the relevant length and velocity scales are derived. Our analysis shows that inherently there is an anisotropic correction of ST_L to Durbin's model constant (c'_μ) which is not explicit in the original turbulent viscosity formulation in his model. *'A priori'* comparisons of these relevant scales using DNS data are excellent and indicate their relevance in capturing the characteristic scales. Furthermore, the predicted behavior of P/ϵ using Durbin's turbulent viscosity formulation shows favorable comparison with the exact profile obtained from DNS data. Overall, this study highlights the fidelity of Durbin's model in capturing the characteristic scales of turbulence (within the framework of the turbulent-viscosity hypothesis) in the near-wall region.

3.3. SUMMARY

In this chapter, a study of turbulent wall-bounded flows was provided. The equilibrium assumption was used to study the turbulent quantities of inhomogeneous flows. The results

show that the irreversibility assumption can be used for predicting turbulence for unstratified flows. However, assuming equilibrium between P and ϵ is not appropriate for employment in RANS closure schemes. We have further analyzed the turbulent viscosity introduced by Durbin (1991) developed for unstratified wall-bounded flows without assuming equilibrium. Our analyses show that $(\overline{w'^2})^{1/2}$ is a suitable quantity to model $\overline{u'w'}$. Chapter 4 presents the work to further understand turbulent mixing in a stably stratified wall-bounded turbulent flow.

CHAPTER 4

Tubulent Mixing in Wall-Bounded Flows[1]

In this chapter, we provide an analysis of turbulent mixing in stably stratified wall-bounded flows. For a fully developed stratified channel flow, we invoke the equilibrium assumption between the production rate of the turbulent kinetic energy (P), the dissipation rate of the turbulent kinetic energy (ϵ) and the dissipation rate of the turbulent potential energy (ϵ_{PE}) to highlight a number of pertinent issues that have implications for predicting the turbulent mixing. DNS data of stably stratified channel flow is used to test the propositions.

4.1. Introduction

Most geophysical flows such as those in estuaries, lakes, oceans and the atmosphere are influenced by both the density stratification and the bottom boundary. In such flows, the simultaneous existence of the density stratification and the solid wall results in anomalous mixing of momentum and active scalar (density) compared to other turbulent flows. Hence, it is not surprising that stratified wall-bounded flows are usually considered as one of the most complex turbulent flows and have been the subject of several studies such as the works of Arya (1975), Komori *et al.* (1983), Garg *et al.* (2000), Armenio & Sarkar (2002), Nieuwstadt (2005), Taylor, Sarkar & Armenio (2005) and García-Villalba & del Álamo (2011).

Quantifying the mixing of the momentum as well as the diapycnal mixing of density is imperative as they directly impact the state of the geophysical flows in both the ocean and the atmosphere. The turbulent (eddy) viscosity (ν_t) and the turbulent (eddy) diffusivity are the two parameters which are widely used for assessment of the state of the flow (such as turbulent mixing) in physical oceanography or atmospheric sciences and are also employed for simulating stratified turbulent flows in numerical models. For a uni-directional shear

[1]The results presented in this chapter is submitted in substantial part as a paper entitled "On turbulent mixing in stably stratified wall-bounded flows" by F. Karimpour and S. K. Venayagamoorthy, to *Physics of Fluids*. This chapter is written in a collective "we" tense to acknowledge collaborative work with the co-author.

flow, using the turbulent-viscosity hypothesis, the turbulent viscosity (ν_t) is defined as

$$\nu_t = \frac{-\overline{u'w'}}{d\overline{U}/dz}, \tag{81}$$

and using the gradient-diffusion hypothesis, the turbulent diffusivity (κ_t) is given by

$$\kappa_t = \frac{-\overline{\rho'w'}}{d\overline{\rho}/dz}, \tag{82}$$

where $\overline{U}$ is the mean streamwise velocity, z is the normal distance from the wall and $\overline{\rho}$ is the fluid mean density.

The turbulent viscosity and diffusivity have to be specified (computed) using turbulence closure schemes. As a result, several parameterizations have been proposed that make use of mean and/or other turbulent quantities. A common approach for parameterization of ν_t and κ_t is to assume stationarity (i.e. statistics are invariant due to change in time) and homogeneity (i.e. statistics are invariant under translations) in the flow. For example, the formulation of ν_t in the k-ϵ model is developed by assuming the equilibrium between the production rate of the turbulent kinetic energy (P), the dissipation rate of the turbulent kinetic energy (ϵ) and the buoyancy flux (B) which is given by (Rodi 1993)

$$\nu_t = (1 - R_f)C_\mu \frac{k^2}{\epsilon}. \tag{83}$$

Here, $k = \frac{1}{2}(\overline{u'^2} + \overline{v'^2} + \overline{w'^2})$ is the turbulent kinetic energy, ϵ is the dissipation rate of the turbulent kinetic energy, $C_\mu = (-\overline{u'w'}/k)^2$ is the turbulent viscosity parameter usually taken as $C_\mu \approx 0.09$. R_f is the flux Richardson number that for a shear flow is usually defined as (Peltier & Caulfield 2003)

$$R_f = \frac{-B}{P}, \tag{84}$$

where $B = -g/\rho_0(\overline{\rho'w'})$ is the buoyancy flux and $P = -\overline{u'w'}(d\overline{U}/dz)$ is the rate of production of k. Similarly, a formulation for κ_t was proposed by Osborn (1980) by assuming equilibrium between the buoyancy flux (B) and the dissipation rate of the turbulent potential energy

(ϵ_{PE}) and is given by $\kappa_t = \epsilon_{PE}/N^2$. Here, $N = \sqrt{(-g/\rho_0)(d\overline{\rho}/dz)}$ is the Brunt-Väisälä or buoyancy frequency.

Besides ν_t and κ_t, the efficiency of mixing is another key parameter in geophysical flows. The flux Richardson number R_f given by equation (84), is commonly used to characterize the efficiency of mixing in stably stratified turbulent flows. A drawback of this formulation is that it is defined in flux form and could therefore be negative for non-stationary strongly stable flows where countergradient fluxes are noticeable (Venayagamoorthy & Stretch 2010, Armenio & Sarkar 2002).

Peltier & Caulfield (2003) discussed that R_f may be taken to be a cumulative mixing efficiency that is calculated by integrating the instantaneous mixing efficiency over a sufficient time interval. They have defined the instantaneous mixing efficiency (i.e. an irreversible flux Richardson number R_f^*) based on the irreversible transfer of the turbulent kinetic energy (k) into the turbulent potential energy (E'_{PE}) given by

$$R_f^* = \frac{\epsilon_{PE}}{\epsilon + \epsilon_{PE}}, \tag{85}$$

where ϵ_{PE} is the dissipation rate of the turbulent potential energy which is defined as

$$\epsilon_{PE} = N^2 \left(\frac{\partial \overline{\rho}}{\partial z}\right)^{-2} \epsilon_\rho. \tag{86}$$

Here, $\epsilon_\rho = \kappa_m \overline{\nabla\rho' . \nabla\rho'}$ is the scalar variance dissipation rate with κ_m defined as the molecular diffusivity. Both ϵ and ϵ_{PE} are positive-definite quantities, ensuring that R_f^* will be limited to $0 \leq R_f^* \leq 1$. Their proposed definition for R_f which is the time-integration of R_f^*, eliminates the stirring effects (reversible contributions). However, the common definition of $R_f = -B/P$ incorporates the stirring effects as both B and P inherently consist of the reversible fluxes. Therefore, sometimes the instantaneous mixing efficiency (R_f^*) is used instead of $R_f = -B/P$ due to its bounded nature. This substitution is still a matter of doubt and needs more investigation in order to ascertain the conditions under which these two quantities may be used interchangeably.

In this chapter, we evaluate the suitability of assuming equilibrium for inference of R_f, ν_t and κ_t in stably stratified wall-bounded flows. In section 4.2, we present the evolution equations of the turbulent kinetic energy and scalar variance. We derive a revised formulation for the turbulent viscosity (ν_t) for a stably stratified turbulent channel flow by using the equilibrium assumption (i.e. $P \approx \epsilon + \epsilon_{PE}$) all the way to the wall. Dimensional arguments are then used to propose appropriate (relevant) velocity and length scales. In section 4.3, the validity of the propositions are evaluated by performing *'a priori'* tests using channel flow DNS data. First, the behavior of R_f is compared with R_f^*. Second, the validity of the proposed ν_t and relevant scales are evaluated. In section 4.4, the equilibrium between the buoyancy flux and the dissipation rate of the turbulent potential energy is invoked (i.e. $-B \approx \epsilon_{PE}$) which leads to Osborn's (1980) formulation for κ_t. The suitability of this formulation for estimating κ_t in stably stratified wall-bounded flows is evaluated by performing *'a priori'* tests. Conclusions are given in section 4.5. In this study, we use the stably stratified turbulent channel flow DNS dataset of García-Villalba & del Álamo (2011) with a friction Reynolds number of $Re_\tau = u_\tau \delta/\nu = 550$ for different initial stratifications given by friction Richardson numbers of $Ri_\tau = |\Delta\rho| g\delta/\rho_0 u_\tau^2 = 0,\ 60$ & 120 to perform *'a priori'* tests. Here, u_τ is the friction velocity, δ is half of the channel depth and ν is the kinematic (molecular) viscosity and $|\Delta\rho|$ is the initial density difference between the bottom of the channel ($z = 0$) and the free-stream ($z = \delta$).

4.2. Prediction of the Turbulent Viscosity

4.2.1. Evolution Equations. The evolution equations for the turbulent kinetic energy (k) and the density (scalar) variance ($\overline{\rho'^2}$) for an inhomogeneous stratified shear flow with the Boussinesq approximation can be respectively written as

$$\frac{\partial k}{\partial t} + \overline{U_j}\frac{\partial k}{\partial x_j} = P - \epsilon + B + D_\nu + T + \Pi, \tag{87}$$

$$\frac{\partial \left(\frac{1}{2}\overline{\rho'^2}\right)}{\partial t} + \overline{U_j}\frac{\partial \left(\frac{1}{2}\overline{\rho'^2}\right)}{\partial x_j} = P_\rho - \epsilon_\rho + T_\rho, \tag{88}$$

where $P = (-\overline{u_i' u_j'})\partial\overline{U_i}/\partial x_j$ is the production rate of the turbulent kinetic energy (k), $\epsilon = \nu(\overline{\partial u_i'/\partial x_j)(\partial u_i'/\partial x_j)} + \nu(\overline{\partial u_i'/\partial x_j)(\partial u_j'/\partial x_i)}$ is the dissipation rate of k, $B = (-g/\rho_0)(\overline{\rho' u_i'})\delta_{i3}$ is the buoyancy flux with δ_{ij} as the Kronecker delta, $D_\nu = \nu(\partial^2 k/\partial x_j^2)$ is the viscous transport of k, $T = -(1/2)\partial(\overline{u_j' u_i' u_i'})/\partial x_j$ is the turbulent velocity transport of k and $\Pi = -(1/\rho_0)\partial(\overline{p' u_j'})/\partial x_j$ is the pressure transport of k, respectively. $P_\rho = (-\overline{\rho' u_j'})\partial\overline{\rho}/\partial x_j$ is the production rate of the density variance, $\epsilon_\rho = \kappa_m(\overline{\partial\rho'/\partial x_j)(\partial\rho'/\partial x_j})$ is the dissipation rate of the density variance and $T_\rho = -(1/2)\partial(\overline{\rho'^2 u_j'})/\partial x_j$ is the transport term of the density variance. The transport terms in the turbulent kinetic energy and density variance equations arise due to the inhomogeneity in the flow.

4.2.2. Equilibrium assumption. For steady, fully developed stratified wall-bounded turbulent flows, equations (87) and (88) simplify to

$$-\overline{u'w'}\frac{d\overline{U}}{dz} = \epsilon - B - D_\nu - T - \Pi, \tag{89}$$

$$-\overline{\rho' w'}\frac{d\overline{\rho}}{dz} = \epsilon_\rho - T_\rho. \tag{90}$$

Equations (89) and (90) imply that the production of k is balanced by the buoyancy flux, the dissipation and transport rates of k. Similarly, the production of $\overline{\rho'^2}$ is balanced by the dissipation and transport rates of the density variance, when the flow is stationary. Using the turbulent-viscosity hypothesis (TVH), equation (89) can be rewritten as

$$\nu_t = \frac{\epsilon - B - D_\nu - T - \Pi}{S^2}, \tag{91}$$

which (by using $B = -PR_f$) can be recast as

$$\nu_t = \left(\frac{1}{1 - R_f}\right)\frac{\epsilon - D_\nu - T - \Pi}{S^2}. \tag{92}$$

Similarly, using the gradient-diffusion hypothesis (GDH), equation (90) can be recast in terms of the turbulent diffusivity (κ_t) as follows

$$\kappa_t = \frac{\epsilon_\rho - T_\rho}{(d\overline{\rho}/dz)^2}. \tag{93}$$

It also follows from the GDH that the buoyancy flux $B = -\kappa_t N^2$. Hence, using κ_t introduced in equation (93), (B) can be rewritten as

$$B = -\kappa_t N^2 = -\frac{\epsilon_\rho - T_\rho}{(d\overline{\rho}/dz)^2} N^2 = T_{PE} - \epsilon_{PE}, \tag{94}$$

where $\epsilon_{PE} = N^2(d\overline{\rho}/dz)^{-2}\epsilon_\rho$ is the dissipation rate of the turbulent potential energy and $T_{PE} = N^2(d\overline{\rho}/dz)^{-2}T_\rho$ is the transport rate of the turbulent potential energy. We can now express the flux Richardson number (R_f) as

$$R_f = \frac{-B}{P} = \frac{\epsilon_{PE} - T_{PE}}{\epsilon + \epsilon_{PE} - D_\nu - T - \Pi - T_{PE}}. \tag{95}$$

By subtituting R_f given by equation (95) into equation (92), ν_t can be rewritten as

$$\nu_t = \frac{(\epsilon + \epsilon_{PE}) - (D_\nu + T + \Pi + T_{PE})}{S^2}, \tag{96}$$

which can be further simplified to yield

$$\begin{aligned} \nu_t &= \left(\frac{1}{1 - \frac{\epsilon_{PE}}{\epsilon + \epsilon_{PE}}}\right)\frac{\epsilon}{S^2} - \frac{D_\nu + T + \Pi + T_{PE}}{S^2} \\ &= \left(\frac{1}{1 - R_f^*}\right)\frac{\epsilon}{S^2} - \frac{D_\nu + T + \Pi + T_{PE}}{S^2}. \end{aligned} \tag{97}$$

Here, $R_f^* = \epsilon_{PE}/(\epsilon + \epsilon_{PE})$ is the irreversible flux Richardson number discussed earlier.

Using the equilibrium assumption (i.e. assuming $P \approx \epsilon + \epsilon_{PE}$), R_f can be approximated with R_f^* as shown in equation (98).

$$R_f = \frac{-B}{P} \approx R_f^* = \frac{\epsilon_{PE}}{\epsilon + \epsilon_{PE}}, \tag{98}$$

which consequently implies that ν_t given in equations (92) and (97) simplifies to

$$\nu_t \approx \frac{\epsilon + \epsilon_{PE}}{S^2} = \left(\frac{1}{1 - R_f^*}\right) \frac{\epsilon}{S^2}. \tag{99}$$

The implication of the equilibrium assumption is that the flux Richardson number (R_f) and the irreversible flux Richardson number (R_f^*) should be approximately equal (i.e. $R_f \approx R_f^*$). We test the validity of these propositions in section 4.3.

4.2.3. Relevant Velocity and Length Scales. Here, we discuss the relevant velocity and length scales in the context of the turbulent-viscosity hypothesis (TVH) that define the turbulent viscosity (ν_t) in stably stratified wall-bounded turbulent flows. Using dimensional analysis, the turbulent viscosity (ν_t) can be recast in terms of velocity, length and time scales as

$$\nu_t = U_{TVH} L_{TVH} = U_{TVH}^2 T_{TVH} = L_{TVH}^2 / T_{TVH}, \tag{100}$$

where U_{TVH} is the characteristic velocity scale proposed by Pope (2000) as $(-\overline{u'w'})^{1/2}$, L_{TVH} is the characteristic length scale, and T_{TVH} is the characteristic time scale. From the TVH, it is clear that

$$-\overline{u'w'} = U_{TVH}^2 = \nu_t S. \tag{101}$$

Now, by invoking the equilibrium assumption (i.e. $P \approx \epsilon + \epsilon_{PE}$) and therefore using $\nu_t \approx 1/(1 - R_f^*)\epsilon/S^2$, equation (101) can be rewritten as

$$U_{TVH}^2 \approx U_S^2 = \left(\frac{1}{1 - R_f^*}\right) \left(\frac{\epsilon}{S^2}\right) S, \tag{102}$$

where U_S is an approximation for U_{TVH}. Hence, the velocity scale (U_S) can be defined as

$$U_{TVH} \approx U_S = \left(\frac{\epsilon + \epsilon_{PE}}{S}\right)^{1/2} = \left(\frac{1}{1 - R_f^*}\right)^{1/2} \left(\frac{\epsilon}{S}\right)^{1/2}. \tag{103}$$

Now, using equations (99), (100) and (103), the length scale (L_{TVH}) can be approximated as

$$\begin{aligned} L_{TVH} &= \frac{\nu_t}{U_{TVH}} = \frac{\left(-\overline{u'w'}\right)^{1/2}}{S} \\ &\approx L_S = \frac{\nu_t}{U_s} = \frac{\left(\epsilon + \epsilon_{PE}\right)/S^2}{\left(\left(\epsilon + \epsilon_{PE}\right)/S\right)^{1/2}} \\ &= \left(\frac{\epsilon + \epsilon_{PE}}{S^3}\right)^{1/2} = \left(\frac{1}{1 - R_f^*}\right)^{1/2} \left(\frac{\epsilon}{S^3}\right)^{1/2}, \end{aligned} \tag{104}$$

where L_S is an approximation for L_{TVH}. It should be noted that for an unstratified flow (i.e. $R_f = 0$), $L_S = (\epsilon/S^3)^{1/2}$ is the classical Corrsin length scale, L_c introduced by Corrsin (1958). The Corrsin length scale is usually taken to denote the upper limit of the inertial subrange and is the smallest eddy size which is deformed by the mean shear rate (S). Thus, in unstratified flows, L_c may be interpreted as an equilibrium length scale where $P \approx \epsilon$. Extending this argument to the present context, L_S can be considered as a modified Corrsin length scale for stably stratified flows, which implies that it is the pertinent length scale of the flow when equilibrium holds (i.e. $P \approx \epsilon + \epsilon_{PE}$).

4.3. 'A priori' Tests Using DNS Data

In this section, we first compare the behavior of R_f with R_f^* in order to evaluate the conditions and extent of the flow regime where $R_f \approx R_f^*$ holds. We also assess the validity of the proposed formulation for ν_t shown in equation (99). This is followed by an assessment of the validity of the proposed velocity and length scales.

4.3.1. Prediction of the Flux Richardson Number. In section 4.2.2, we have analytically shown that in a stratified channel flow $R_f = -B/P$ could be approximated with an irreversible form given by $R_f^* = \epsilon_{PE}/(\epsilon + \epsilon_{PE})$, if the reversible transport terms could be assumed negligible. The comparison between these two quantities are shown as a function of Ri_g in Figure (4.1). Interestingly, for $Ri_g \lesssim 0.25$, both quantities closely follow each other and grow almost linearly with Ri_g. For stably stratified flows, it is common to consider $Ri_g = 0.25$ as a critical Richardson number for the onset of instabilities. The critical gradient

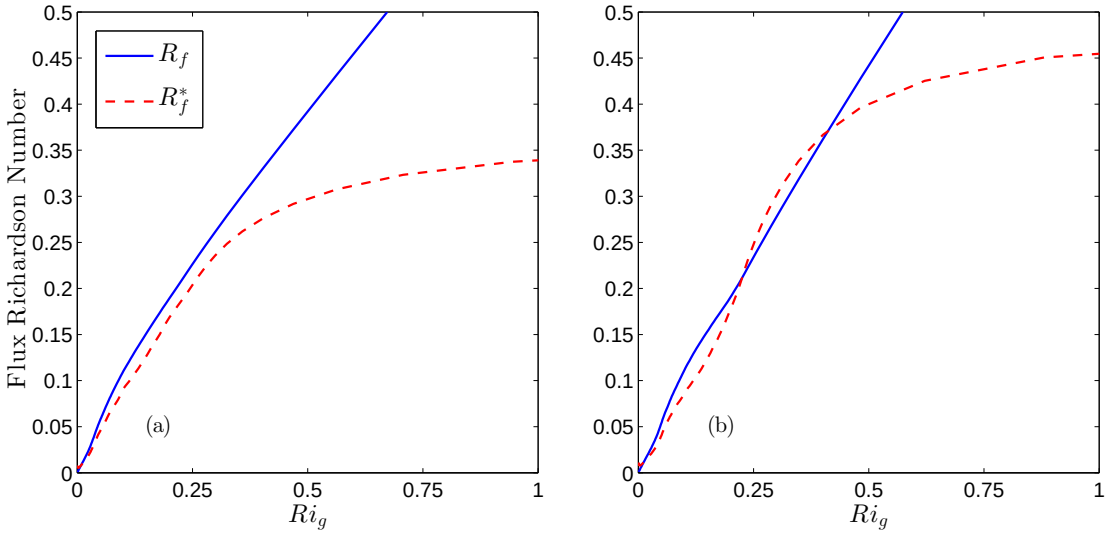

FIGURE 4.1. Profiles of the reversible and the irreversible flux Richardson number versus Ri_g for a turbulent channel flow at $Re_\tau = 550$ and (a) $Ri_\tau = 60$; and (b) $Ri_\tau = 120$ computed from the DNS data of García-Villalba & del Álamo (2011).

Richardson number of $Ri_{gc} = 0.25$ was derived for the first time by Miles (1961) and Howard (1961) and denotes the threshold of linear stability for a stably, stratified, two-dimensional flow. While there is still no consensus on the exact value of Ri_{gc} for high Reynolds number stably stratified flows, values in the range of 0.1-1 have been proposed (Galperin, Sukoriansky & Anderson 2007). It is commonly hypothesized that for $Ri_g < Ri_{gc}$ the mean shear rate dominates the restoring buoyancy forces due to density stratification, triggering the onset of Kelvin-Helmholtz instabilities and consequently generation of turbulence. In regions of low Ri_g, irreversible turbulent mixing results in an increase of the background potential energy. For $Ri_g > Ri_{gc}$, linear internal waves and countergradient fluxes persist causing reversible exchanges between turbulent kinetic energy (k) and available potential energy.

It is clear from Figure (4.1) that $R_f \approx R_f^*$ for $Ri_g \lesssim 0.25$. However, an important follow-up question is to determine for what fraction of the flow depth does this approximation hold? To answer this question, Ri_g is plotted as function of flow depth in Figure (4.2). It is clear that for the bulk of the flow depth (almost 85%), the gradient Richardson number falls below the critical value of 0.25. This implies that the irreversible flux Richardson number

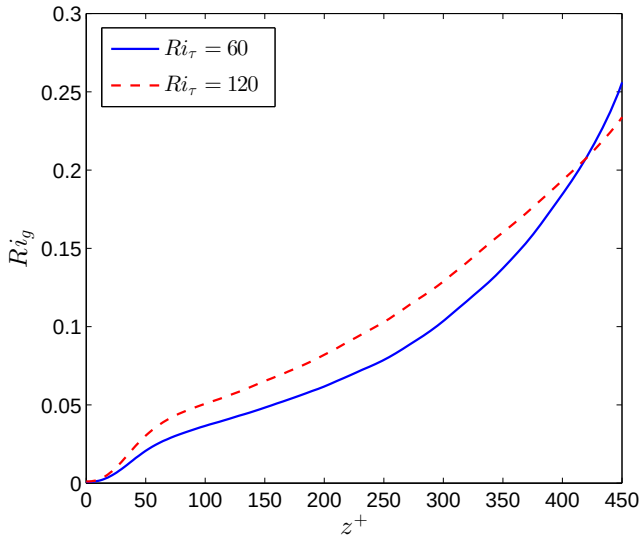

FIGURE 4.2. Profiles of Ri_g in depth for a turbulent channel flow at $Re_\tau = 550$ & $Ri_\tau = 60, 120$ computed from the DNS data of García-Villalba & del Álamo (2011).

(R_f^*) mimics the behavior of R_f in stably stratified turbulent channel flows. It is only in the outer (wake) region that Ri_g increases without bound as a result of the relaxation of the mean shear rate. This stably stratified region supports the presence of linear internal wave motions leading to the generation of strong countergradient fluxes. Furthermore, it should be noted that the production and dissipation terms are very small in this far-wall region. As a result, the transport terms become relatively dominant causing R_f to deviate from R_f^* as shown in Figure (4.1).

In Figure (4.3), the behavior of exact R_f versus Ri_g for two different initial stratifications is shown. It is interesting to observe from Figure (4.3) that the exact flux Richardson number (R_f) shows a universal behavior for $Ri_g \lesssim 0.25$ for different stratifications. This is in contrast to the behavior of R_f and R_f^* for high gradient Richardson numbers which indicate dependence on the strength of the density stratification. The key insight from this observation is that R_f may have a universal behavior as long as turbulence is sustained in stably stratified flows.

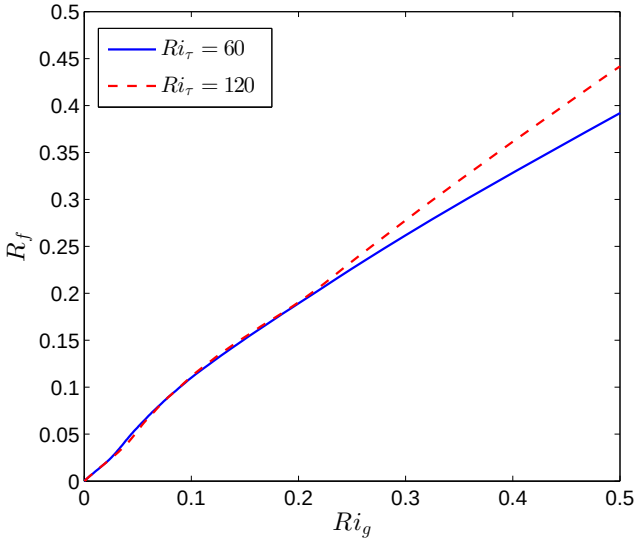

FIGURE 4.3. Profiles of R_f versus Ri_g for a turbulent channel flow at $Re_\tau = 550$ & $Ri_\tau = 60, 120$ computed from the DNS data of García-Villalba & del Álamo (2011).

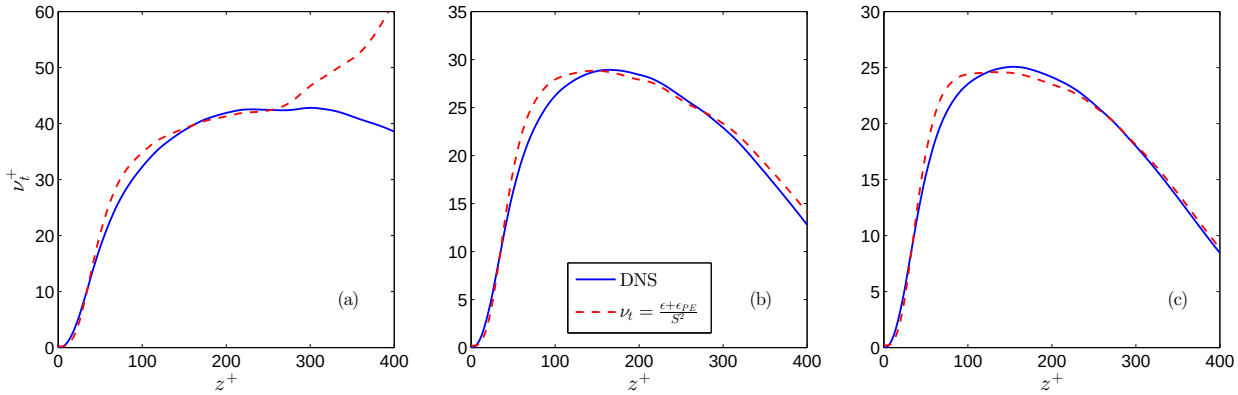

FIGURE 4.4. Comparison of the exact turbulent viscosity and the prediction given by equation (99) in a turbulent channel flow at $Re_\tau = 550$ and (a) $Ri_\tau = 0$; (b) $Ri_\tau = 60$; and c) $Ri_\tau = 120$ computed from the DNS data of García-Villalba & del Álamo (2011).

4.3.2. TURBULENT VISCOSITY COMPARISONS. The comparison between the proposed turbulent viscosity from equation (99) and the exact turbulent viscosity given by equation (81) is shown in Figure (4.4) for initial stratifications of $Ri_\tau = 0,\ 60$ & 120. There is an excellent agreement in the near-wall region and beyond. This is a remarkably interesting result, especially given the fact that all the transport terms are neglected in deriving equation

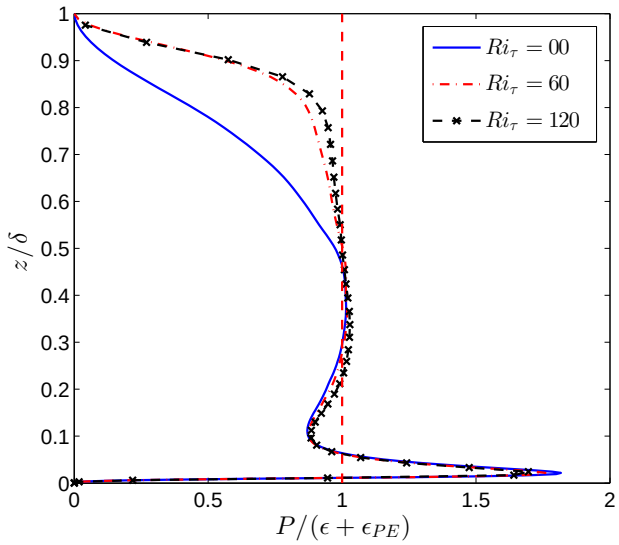

FIGURE 4.5. Comparison of $P/(\epsilon + \epsilon_{PE})$ for different initial stratifications with $Ri_\tau = 0,\ 60\ \&\ 120$ in a turbulent channel flow at $Re_\tau = 550$, computed from the DNS data of García-Villalba & del Álamo (2011).

(99). This result highlights the suitability of neglecting the reversible transport terms in the transport equation of k in wall-bounded flows. Moreover, it is interesting to note that while the turbulent viscosity (ν_t) of unstratified flow is predicted well for up to almost half of the flow depth (here up to $z^+ \approx 275$), the prediction substantially improves for most of the channel depth for the stably stratified cases. This implies that the presence of the buoyancy fluxes in stably stratified flows appears to keep the flow in equilibrium over a greater portion of the flow depth. This can be readily seen by comparing $P/(\epsilon+\epsilon_{PE})$ for the unstratified and stratified cases as shown in Figure (4.5) for $Ri_\tau = 0,\ 60\ \&\ 120$. This confirms the assertion that $P \approx \epsilon + \epsilon_{PE}$ holds over a larger fraction of the flow depth compared to unstratified channel flow.

4.3.3. COMPARISONS OF VELOCITY AND LENGTH SCALES. Figure (4.6) shows the comparison of velocity scales and length scales discussed in section 4.2.3. First, the comparison between the exact velocity scale (U_{TVH}) and the proposed velocity scale (U_S) given by equation (103) is very good (Figure 4.6a-c). The corresponding comparison between L_{TVH} and

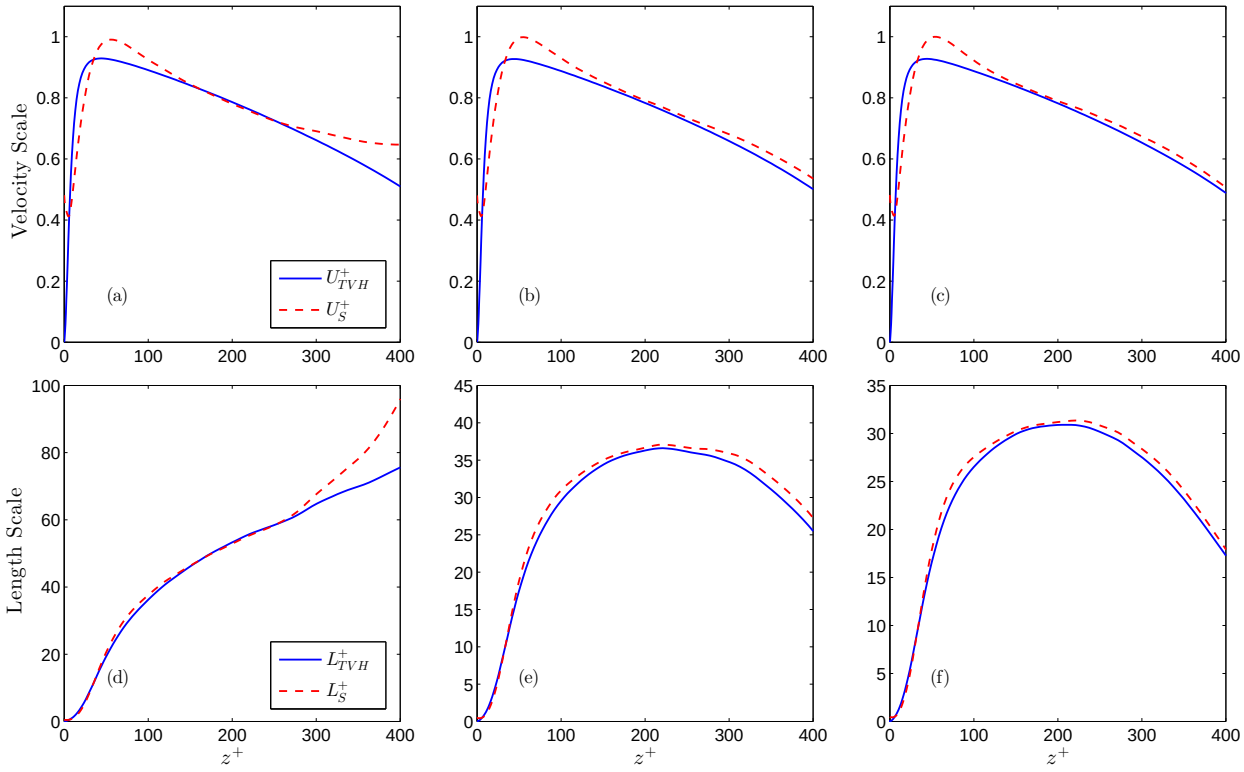

FIGURE 4.6. Comparison of velocity scales (upper panel) and length scales (lower panel) in a turbulent channel flow at $Re_\tau = 550$ and (a,d) $Ri_\tau = 0$; (b,e) $Ri_\tau = 60$; and (c,f) $Ri_\tau = 120$ computed from the DNS data of García-Villalba & del Álamo (2011).

L_S given by equation (104) is almost perfect in the near-wall region and beyond (Figure 4.6d-f). Similar to the ν_t comparison, the agreement improves with increase in stratification.

4.4. Prediction of Turbulent Diffusivity

The correct prediction of the turbulent diffusivity (κ_t) is important for quantifying scalar mixing and consequently the flow dynamics. As shown in section 4.3.2, the equilibrium assumption results in a good estimation for ν_t. Here, we test the suitability of employing the equilibrium assumption for predicting the turbulent diffusivity in a stably stratified channel flow.

4.4.1. Equilibrium assumption. Using the transport equation of the scalar variance introduced in equation (88), the evolution equation of the turbulent potential energy (E'_{PE})

can be derived as

$$\frac{\partial E'_{PE}}{\partial t} + \overline{U_j}\frac{\partial E'_{PE}}{\partial x_j} = -B - \epsilon_{PE} + T_{PE}. \tag{105}$$

As it can be seen in this equation and equation (87), the buoyancy flux is present in both the turbulent kinetic energy and the turbulent potential energy evolution equations with opposite signs. This indicates that for stable density gradients, turbulent kinetic energy is transferred via buoyancy flux into available potential energy. For unstable (convective) density gradients, available potential energy can be transferred as buoyancy flux into turbulent kinetic energy. It must be noted that the presence of internal wave motions can cause countergradient fluxes that transfer energy back and forth between turbulent kinetic energy and available potential energy.

As shown in equation (94), for a fully developed flow equation (105) can be rearranged as

$$-B = \epsilon_{PE} - T_{PE}. \tag{106}$$

By replacing $-B = \kappa_t N^2$, the turbulent diffusivity can be derived as

$$\kappa_t = \frac{\epsilon_{PE} - T_{PE}}{N^2}. \tag{107}$$

Now, by assuming the equilibrium between the buoyancy flux (B) and the dissipation rate of the turbulent potential energy (ϵ_{PE}) as $-B \approx \epsilon_{PE}$, κ_t simplifies to

$$\kappa_t \approx \frac{\epsilon_{PE}}{N^2}. \tag{108}$$

This is the well-known formulation of Osborn (1980) which is widely used to infer κ_t in geophysical flows.

4.4.2. 'A PRIORI' TESTING OF DERIVED FORMULATIONS USING DNS DATA. Figure (4.7) shows the comparison between the equilibrium based formulation for κ_t given by equation (108) and the exact κ_t given by equation (82). The overall prediction of the turbulent

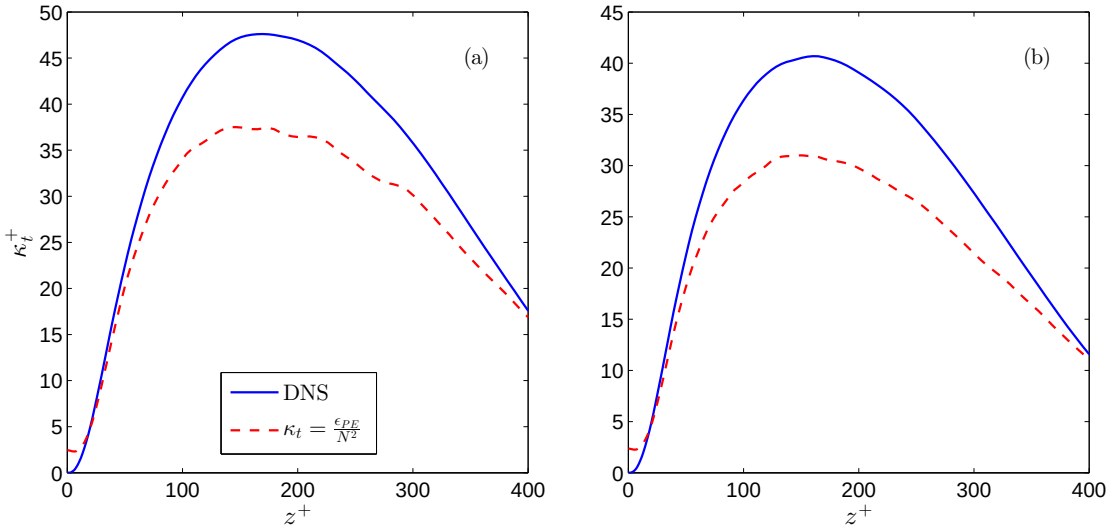

FIGURE 4.7. Comparison of the exact turbulent diffusivity and the prediction given in equation (108) in a turbulent channel flow with a) $Ri_\tau = 60$ and b) $Ri_\tau = 120$ & at $Re_\tau = 550$, computed from the DNS data of García-Villaba & del Álamo (2011).

diffusivity based on equilibrium between $-B$ and ϵ_{PE} is good in the near-wall region. In this region the mean shear rate is strong and thus turbulence is vigorously sustained which results in irreversible transfer of kinetic energy to background potential energy. However, this agreement starts to break down away from the wall. This is in contrast to the predictions shown earlier for the turbulent viscosity where remarkable agreement was seen even in the far-wall region. This breakdown can be mainly attributed to the presence of linear internal waves in the far-wall region of the channel flow. This result highlights the complexity associated with the co-existence of internal waves and turbulence in stably stratified flows. Separating wave and turbulence in such flows remains an important challenge.

In order to better investigate the validity of assuming equilibrium between ϵ_{PE} and $-B$, it will be instructive to revisit $-B/\epsilon_{PE}$ which shows the ratio of the production to dissipation rates of the turbulent potential energy. This ratio can be considered to be equivalent to $P/(\epsilon + \epsilon_{PE})$ in the evolution equation of k. $-B/\epsilon_{PE}$ behavior is shown in Figure (4.8) which clearly shows that unlike $P/(\epsilon + \epsilon_{PE}) \approx 1$ which holds over a big fraction of the flow

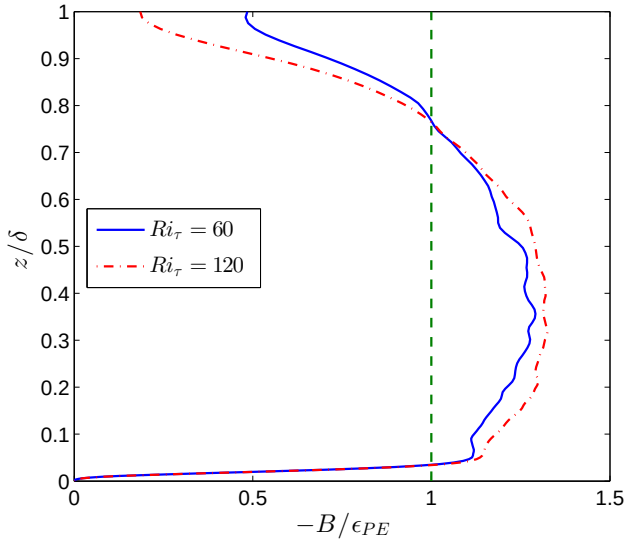

FIGURE 4.8. Comparison of $-B/\epsilon_{PE}$ for different initial stratifications with $Ri_\tau =$ 60 & 120 in a turbulent channel flow at $Re_\tau = 550$, computed from the DNS data of García-Villaba & del Álamo (2011).

depth (Figure 4.5), an equilibrium region where $-B \approx \epsilon_{PE}$, can be barely observed in stably stratified wall-bounded flows.

4.5. Concluding Remarks

In this study, we have revisited the suitability of the equilibrium (irreversibility) assumption (i.e. $P \approx \epsilon + \epsilon_{PE}$ and $-B \approx \epsilon_{PE}$) for estimating the flux Richardson number (R_f), turbulent viscosity (ν_t) and turbulent diffusivity (κ_t) in a stably stratified channel flow. We have first shown by using DNS data that the flux Richardson number defined as $R_f = -B/P$ and the irreversible flux Richardson number $R_f^* = \epsilon_{PE}/(\epsilon + \epsilon_{PE})$ which is derived from R_f by assuming equilibrium, show excellent comparison for $Ri_g \lesssim 0.25$,

We then invoked the equilibrium assumption between P, ϵ and ϵ_{PE} to propose that $\nu_t \approx 1/(1 - R_f^*)(\epsilon/S^2)$. We then used dimensional arguments to show that the appropriate velocity scale is $U_S = (1 - R_f^*)^{-1/2}(\epsilon/S)^{1/2}$ and the appropriate length scale is $L_S = (1 - R_f^*)^{-1/2}(\epsilon/S^3)^{1/2}$, respectively. The comparisons of the proposed turbulent viscosity and the relevant scales with the exact turbulent viscosity and scales computed from the DNS data of stably stratified turbulent channel flow are remarkably good. Interestingly, it is observed

that the comparisons become better when the stratification strength increases which implies that in stratified wall-bounded flows, equilibrium ($P \approx \epsilon + \epsilon_{PE}$) holds for a bigger fraction of the flow depth compared to the unstratified counterpart.

Finally, we have tested the suitability of assuming equilibrium for predicting κ_t. This is done by invoking the equilibrium assumption between the buoyancy flux (B) and the dissipation rate of the turbulent potential energy (ϵ_{PE}) (i.e. $-B \approx \epsilon_{PE}$) to propose that $\kappa_t \approx \epsilon_{PE}/N^2$. The comparison of the proposed turbulent diffusivity with the exact turbulent diffusivity computed form the DNS data is good in the near-wall region. However, unlike the prediction of the turbulent viscosity, the results show that the agreement deteriorates far from the wall. This can be attributed to the presence of linear internal waves in the far-wall region that cause advective fluxes that do not contribute to irreversible turbulent mixing. Future DNS studies of stably stratified channel flows at higher Reynolds numbers are required in order to test the sensitivity of the predictions presented in this study. It is expected that the predictions should improve at higher Reynolds numbers based on trends observed with increasing Reynolds numbers for unstratified channel flow.

The next chapter presents numerical modeling of stably stratified wall-bounded flows. One-dimensional RANS codes are developed in the context of zero-equation and k-ϵ turbulence closure schemes to model stably stratified channel flows.

CHAPTER 5

Stratified Channel Flow Modeling

In this chapter, we investigate modeling of stably stratified wall-bounded turbulent flows using RANS turbulence closure schemes. In section 5.1, we propose a parameterization for the turbulent Prandtl number (Pr_t) for stably stratified flows under the influence of a smooth solid wall. The turbulent Prandtl number is the linking bridge between the turbulent momentum and scalar fluxes in the context of Reynolds-averaged Navier-Stokes (RANS) simulations. Therefore, it is important to use appropriate parameterizations for (Pr_t) in order to define the right level of momentum and scalar mixing in stably stratified flows. In section 5.2, we revisit the capability of the standard k-ϵ model for simulating stratified flows. We use analytical arguments to assess the buoyancy parameter ($C_{\epsilon 3}$). In this chapter, RANS simulations are performed to model a one-dimensional stably stratified channel flow and the results are compared with channel flow DNS data.

5.1. Revisit of the Turbulent Prandtl Number[1]

5.1.1. Introduction. The majority of geophysical flows (e.g. in the oceans, lakes, estuaries and the atmosphere) are substantially influenced by stable density stratification. The density stratification causes buoyancy forces that can significantly influence the mixing of both momentum and scalars (Rodi 1987). Hence, it is important to develop turbulence models with the ability to predict mixing in such flows. However, many geophysical flows are also influenced by wall (solid) boundaries such as in the coastal ocean, lakes and the atmospheric boundary layer (ABL). The presence of the wall introduces inhomogeneities in the flow which causes complex turbulent structures close to the wall (i.e. in the so-called inner wall region, see for example Pope (2000) for more details). This is in contrast to free-shear flows which are able to develop without the confining influence of the wall. Hence, it is

[1]The results presented in this section are published in substantial part as a paper entitled "A simple turbulence model for stably stratified wall-bounded flows" by F. Karimpour and S. K. Venayagamoorthy, in the *Journal of Geophysical Research: Oceans*, Vol. 119, pp 870-880, 2014. This section is written in a collective "we" tense to acknowledge collaborative work with the co-author.

expected that the mixing dynamics in a stably stratified wall-bounded flow should be different than the simpler homogeneous stably stratified flow, where the fluctuating quantities (such as the velocity and density fluctuations) are statistically homogeneous. Statistical homogeneity implies that the statistics are invariant under translation (Pope 2000).

Numerical simulations of turbulent flows range from direct numerical simulations (DNS) where the highly nonlinear Navier-Stokes equations together with the continuity and density transport equations are solved directly to yield the instantaneous flow fields without recourse to a turbulence model; to Reynolds-averaged Navier-Stokes (RANS) simulations where an averaged (statistical) flow solution is obtained. DNS is one of the commonly used simulation techniques to gain better fundamental understanding of turbulence. On the other hand, RANS simulations are used for practical applications where the emphasis is on better understanding of complex phenomena such as bottom boundary layer mixing in the coastal ocean and internal wave-driven mixing in the ocean (Burchard 2002). It is important to note that DNS is prohibitively expensive for most practical flow problems and therefore only suitable to very idealized flows (Pope 2000). However, there have been a number of DNS and large-eddy simulation (LES) studies that have focused on stably stratified wall-bounded flows (see e.g. Armenio and Sarkar 2002, Nieuwstadt 2005 and García-Villalba & del Álamo 2011). In the RANS formulation, the averaging process (using Reynolds decomposition) results in additional terms known as the Reynolds stresses (turbulent momentum fluxes) and turbulent scalar fluxes in the mean momentum and scalar transport equations, respectively. These extra terms imply that the number of unknowns is greater than the number of available (mean flow) equations leading to an undetermined system commonly referred to as the turbulence closure problem.

A common and widely employed approach to close the RANS equations is through the use of the turbulent-viscosity hypothesis together with the gradient-diffusion hypothesis. The turbulent-viscosity hypothesis is analogous to the stress-rate-of-strain relation for a Newtonian fluid. Similarly, the gradient-diffusion hypothesis is analogous to Fourier's law of heat conduction and Fick's law of molecular diffusion (Pope 2000). The basic assumption

in these hypotheses is that the turbulent momentum flux (or turbulent scalar flux) is transported down (i.e. aligned with) the mean gradient of the respective averaged flow variable. Essentially, using these hypotheses, the turbulence closure problem reduces to the prediction of a turbulent (eddy) viscosity (ν_t) and a corresponding turbulent (eddy) diffusivity (κ_t). Although the assumptions in these hypotheses are seldom valid in many flows, they are nevertheless widely used to close the RANS equations due to their simplicity. There are numerous approaches for modeling ν_t and κ_t ranging from simple zero-equation (algebraic) models to more sophisticated two-equation turbulence models (e.g. the k-ϵ model by Jones & Launder 1972). For stably stratified flows, parameterizing both ν_t and κ_t in such a way as to yield the right levels of both momentum and scalar (density) mixing has proved to be challenging. Therefore, it is essential to develop robust RANS models that have the benefit of fast calculation speeds along with accuracy. This continues to remain an open research problem for the turbulence modeling community.

Many RANS models use the turbulent Prandtl (or Schmidt) number ($Pr_t = \nu_t/\kappa_t$) to link the turbulent momentum and scalar fluxes (Venayagamoorthy & Stretch 2010). In a uni-directional planar shear flow (e.g. a turbulent channel flow), ν_t is defined as

$$\nu_t = \frac{-\overline{u'w'}}{d\overline{U}/dz}, \tag{109}$$

and κ_t is given by

$$\kappa_t = \frac{-\overline{\rho'w'}}{d\overline{\rho}/dz}, \tag{110}$$

where $\overline{u'w'}$ is the Reynolds stress (turbulent momentum flux), $\overline{\rho'w'}$ is the turbulent density flux, z is the normal distance from the wall, $d\overline{U}/dz$ is the mean shear rate (often denoted as S) and $d\overline{\rho}/dz$ is the vertical mean density gradient. It is easy to see from the definition of the turbulent Prandtl number, the importance of parameterizing it to correctly capture the turbulent momentum and scalar fluxes. This is even more important when the scalar is active such as in stably stratified flows. There are a number of parameterizations for Pr_t for stably stratified flows such as those proposed many decades ago by Munk & Anderson

(1948) (hereafter MA) and more recently by Venayagamoorthy & Stretch (2010) (hereafter VS), to mention a couple. The two main factors that tend to influence the turbulent mixing in stably stratified wall-bounded flows are the density stratification and the solid boundary (MA). However, in many flow conditions such as in the mixed layer, the effect of the boundary is very limited and can thus be neglected. Based on such arguments, most turbulent Prandtl number parameterizations only consider the effect of the density stratification and hence by default are only applicable to homogeneous (free) shear flows. But in a wall-bounded flow, the presence of the solid wall introduces inhomogeneities in the flow that causes anomalous transport of momentum and scalar close to the wall (Launder & Spalding 1972, Crimaldi *et al.* 2006).

In this study, we discuss the behavior of the turbulent Prandtl number in the presence of a solid wall and introduce a new parameterization for Pr_t that accounts for the presence of the wall along with stratification. In order to test the new parameterization for Pr_t, a zero-equation (algebraic) RANS model that makes use of the modified turbulent viscosity (ν_t) proposed by MA as well as the two-equation standard k-ϵ turbulence closure scheme, are developed in MATLAB and the results are compared with the DNS data of stably stratified channel flow of García-Villalba & del Álamo (2011). We also compare the Pr_t parameterization of MA for homogeneous flows to highlight the shortcomings of homogeneous formulation for Pr_t in predicting both momentum and scalar mixing correctly in wall-bounded flows.

5.1.2. Parameterization of the Turbulent Prandtl Number. It has been shown (e.g. Schumann & Gerz 1995, VS) that in a stably stratified homogeneous flow, Pr_t can be defined as

$$Pr_t = \frac{Ri_g}{R_f} + Pr_{t0}, \tag{111}$$

where Pr_{t0} is the neutral Prandtl number in the limit of zero stratification in a homogeneous shear flow. Pr_{t0} has been shown to be close to unity (Kays *et al.* 1993, Kays 1994). In equation (111), Ri_g is the gradient Richardson number and is defined as

$$Ri_g = \frac{N^2}{S^2}, \tag{112}$$

where $N = \sqrt{-(g/\rho_0)(d\overline{\rho}/dz)}$ is the Brunt-Väisälä or buoyancy frequency, g is the gravitational acceleration and ρ_0 is the background density of the fluid. N represents the frequency of a fluid particle oscillating in a flow when displaced from its stable position and provides a measure of the strength of the density stratification. R_f is the flux Richardson number which in shear flows is conventionally defined as (Peltier & Caulfield 2003)

$$R_f = \frac{-B}{P}, \tag{113}$$

where $B = -g/\rho_0(\overline{\rho' w'})$ is the buoyancy flux and $P = -\overline{u'w'}(d\overline{U}/dz)$ is the rate of production of the turbulent kinetic energy ($k = 0.5u_i'^2$, using Einstein summation). Direct measurement of the buoyancy flux in stratified flows is not trivial due to technical difficulties as well as complex physical processes such as contamination from internal waves. To circumvent this problem, indirect approaches are used to infer B from the scalar dissipation rate (χ), the turbulent kinetic energy dissipation rate (ϵ), N and the Thorpe overturning length scale (L_T). Osborn & Cox (1972) have defined the buoyancy flux indirectly by assuming that the advective terms are negligible. To date, there is no general consensus on a universal parameterization for R_f even though a number of parameterizations exist for R_f. This is mainly due to the lack of evidence on what the behavior of R_f should be under very strong stable stratification in high-Reynolds-number flows. Laboratory experiments and direct numerical simulations remain inconclusive about this issue due to Reynolds number limitations. Field experiments tend to show quite a bit of scatter. However, recent DNS studies, in particular those of Mashayek & Peltier (2013) and Mashayek *et al.* (2013), have sought to increase the Reynolds number limit of numerical simulations to realistic geophysical flows. These recent results indicate that R_f might be highly variable and difficult to parameterize in free shear layers, especially at strong stratification. Regardless, there have been some formulations that have gained acceptance. For example, Osborn (1980) has proposed that $R_f \leq 0.17$ based on a few laboratory experiments of shear flows. It should be noted however, that there is growing evidence that the assumptions of fully developed turbulence, stationarity and homogeneity, inherent in Osborn's formulation as well as a

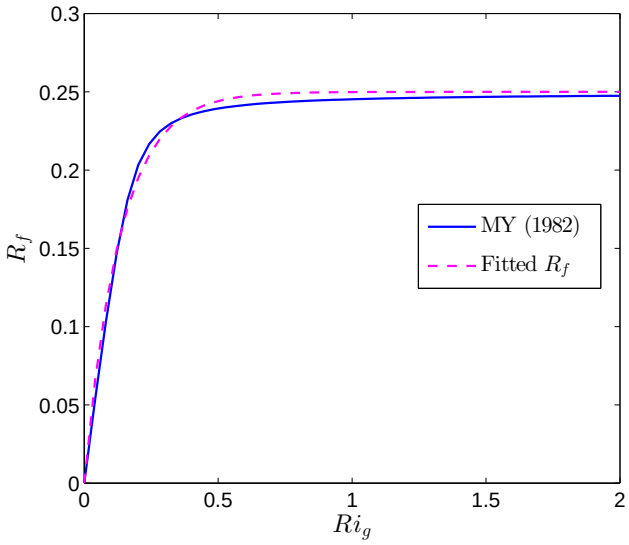

FIGURE 5.1. The flux Richardson number (R_f) as a function of the gradient Richardson number (Ri_g).

constant value of R_f are highly debatable (see e.g. Mashayek & Peltier 2013, Mashayek *et al.* 2013 and Ivey *et al.* 2008). Mellor & Yamada (1982) (hereafter MY) have proposed a parameterization where $R_f \leq 0.25$, given by

$$R_f = 0.725 \left[Ri_g + 0.186 - \left(Ri_g^2 - 0.316 Ri_g + 0.0346 \right)^{1/2} \right]. \tag{114}$$

Recently, Canuto *et al.* (2001) using the dataset of Maderich *et al.* (1995), have shown that the flux Richardson number is directly related to Ri_g. They showed that R_f increases with Ri_g from zero for neutral (zero) stratification and asymptotes to a value $R_{f\infty} \approx 0.25$ around $Ri_g \approx 1$. The measured flux Richardson numbers show an exponential behavior as a function of the gradient Richardson number. Here, we propose a simple exponential relationship for R_f as a function of Ri_g

$$R_f = R_{f\infty} \left[1 - exp\left(-\gamma Ri_g \right) \right], \tag{115}$$

where $R_{f\infty} = 0.25$ and γ is a constant that is set equal to 7.5. The behavior of R_f as a function of Ri_g given by equations (114) and (115) are shown in Figure (5.1). It is clear that the proposed formulation is very similar to the formulation of MY given in equation (114). As shown in equation (111), the homogeneous Pr_t increases linearly without bound with the

gradient Richardson number (Ri_g). Some studies have been carried out to highlight the effect of the wall on Pr_t such as Kawamura *et al.* (1998), Crimaldi *et al.* (2006) and Srinivasan & Papavassiliou (2010). Crimaldi *et al.* (2006) have measured Pr_t in an unstratified boundary layer flow in the laboratory. They have observed that Pr_t is much higher than unity near the bed (i.e. for $z^+ = zu_\tau/\nu < 30$, where z^+ is the wall unit, u_τ is the friction or turbulent velocity and ν is the kinematic or molecular viscosity) and decreases almost linearly to about unity in the free-stream. This implies that at the wall, Pr_t is a maximum and decreases to the value of the homogeneous shear flow case in the outer flow region. Coincidentally, this behavior is in agreement with the linear shear stress distribution in a channel flow given by

$$\tau = \tau_w \left(1 - \frac{z}{D}\right), \tag{116}$$

where τ is the shear stress at a level z from the wall, τ_w is the (maximum) shear stress at the wall, D is the flow depth and z is bounded in the range $0 \leq z \leq D$. We note that the linear shear stress distribution given in equation (116) holds strictly only for channel and pipe flows. However, the shear stress distribution from DNS of boundary-layer flow (Jiménez *et al.* 2010) indicates that assuming a linear distribution is reasonable in the logarithmic region. Kawamura *et al.* (1998) performed a DNS study of heat transfer in a channel flow. Their results show that beginning in the log-law region where $z^+ \approx 30$, Pr_t starts to decrease to about unity in the outer free-stream. Srinivasan & Papavassiliou (2010) showed that for an unstratified wall-bounded flow for fluids with molecular Prandtl number of $Pr = \nu/\kappa_m > 0.7$ with κ_m defined as the molecular diffusivity, the neutral turbulent Prandtl number starts from values above unity at the wall and decreases to almost the molecular Prandtl number (Pr) at the free-surface. It is also worth noting in passing that Launder & Spalding (1972) indicate that Pr_t ought to follow a linear distribution with a higher value at the wall that decreases as the free-stream is approached. Therefore, the following formulation for the unstratified (neutral) Pr_t in a wall-bounded flow can be proposed

$$Pr_{tw0} = \left(1 - \frac{z}{D}\right) Pr_{twd0} + Pr_{t0}, \tag{117}$$

where Pr_{twd0} is the difference between the neutral turbulent Prandtl number at the wall (Pr_{tw0}) and the neutral turbulent Prandtl number for a homogeneous shear flow (Pr_{t0}). DNS data in the near-wall region ($z^+ \approx 30$) indicate that Pr_{tw0} varies in the range 1–1.5 for different molecular Prandtl numbers (Pr) (e.g. see the discussion in McEligot & Taylor 1996). Crimaldi *et al.* (2006) showed that Pr_{tw0} is around 2 in the log-law region and tapers off almost linearly to close to unity as the free-stream is approached. Most RANS simulations make use of the logarithmic law of the wall to model wall-bounded flows, therefore here, we use $Pr_{tw0} \approx 1.1$. Different values for the neutral turbulent Prandtl number (Pr_{t0}) in homogeneous shear flows have been suggested but there is consensus that its value is very close to unity (VS). However, VS have argued that $Pr_{t0} = 0.7$ using DNS data of homogeneous shear flows, in agreement with several other studies (e.g. Schumann & Gerz 1995). We use this value for the purpose of this study. For the unstratified case, equation (117) provides a linear correction to the Pr_{t0}, with the value at the beginning of logarithmic region equal to Pr_{tw0}. This linear formulation is in agreement with the observed DNS data, experiment of Crimaldi *et al.* (2006) and also proposition of Launder & Spalding (1972). It is also worth noting that if the wall effect is removed, the formulation given by equation (117) reverts back to neutral value in homogeneous unstratified shear flows.

Let us now consider how to extend this discussion to stably stratified wall-bounded flows. Using equation (116) and evoking the turbulent-viscosity hypothesis, it is straightforward to show that the turbulent viscosity (for the log-law region) is given by

$$\nu_t = \frac{u_\tau^2}{S}\left(1 - \frac{z}{D}\right), \tag{118}$$

where $u_\tau = (\tau_w/\rho)^{1/2}$ is the friction velocity. Furthermore, using the formulation by Osborn (1980), the turbulent diffusivity (κ_t) is commonly assumed to be given by

$$\kappa_t = \Gamma \frac{\epsilon}{N^2}, \tag{119}$$

where ϵ is the dissipation rate of the turbulent kinetic energy (k) and Γ is the mixing efficiency and is related to R_f as

$$\Gamma = \frac{R_f}{1 - R_f}. \tag{120}$$

It is worth noting here that Osborn's formulation for the turbulent diffusivity assumes stationarity and has been shown to be an oversimplification of the mixing problem by Smyth *et al.* (2001) and a number of other more recent studies (e.g. Mashayek *et al.* 2013). However, it is a widely used formulation for quantifying mixing in oceanic flows. With this caveat in mind, we retain this formulation and proceed by dividing equation (118) by equation (119) to get an expression for the stratified component of the turbulent Prandtl number (Pr_t) as follows

$$Pr_t = \frac{u_\tau^2 / S\left(1 - \frac{z}{D}\right)}{\Gamma(\epsilon / N^2)}. \tag{121}$$

Durbin & Pettersson Reif (2011) discuss that in the constant-stress (log-law) region, the equilibrium assumption holds between the production rate of the turbulent kinetic energy (P) and the dissipation rate of the turbulent kinetic energy (ϵ), i.e. $P = \epsilon$. This implies that for unstratified channel flow, ϵ can be expressed as

$$\epsilon = \frac{u_\tau^3}{\kappa z}, \tag{122}$$

where κ is the von Kármán constant (assumed to be ≈ 0.40 in this study). Similarly, evoking the equilibrium assumption between the production rate of the turbulent kinetic energy (P), the dissipation rate of the turbulent kinetic energy (ϵ) and the buoyancy flux (B) in the logarithmic region of a stably stratified wall-bounded flow yields

$$P + B = P\left(1 - R_f\right) = \epsilon, \tag{123}$$

which can be rearranged to get the dissipation rate (ϵ) as

$$\epsilon = \left(1 - R_f\right) \frac{u_\tau^3}{\kappa z}. \tag{124}$$

Substituting equation (124) into equation (121), gives Pr_t as

$$Pr_t = \frac{N^2}{R_f}\left(\frac{\kappa z}{u_\tau}\right)\frac{1}{S}\left(1-\frac{z}{D}\right). \tag{125}$$

From the classical log-law, the mean velocity gradient is given by

$$S = \frac{\partial \overline{U}}{\partial z} = \frac{u_\tau}{\kappa z}. \tag{126}$$

This can now be substituted into equation (125) to get

$$Pr_t = \frac{N^2}{S^2}\frac{1}{R_f}\left(1-\frac{z}{D}\right) = \frac{Ri_g}{R_f}\left(1-\frac{z}{D}\right). \tag{127}$$

Analogous to homogeneous Pr_t (equation 111) which is a combination (algebraic sum) of the stratified Pr_t (i.e. Ri_g/R_f) and neutral turbulent Prandtl number (Pr_{t0}) in conjunction with the discussion above, we propose a Pr_t for stably stratified wall-bounded flows, by combining the wall-bounded stratified Pr_t (equation 127) and unstratified wall-bounded Pr_t (i.e. Pr_{tw0} in equation 117) as follows

$$Pr_t = \left(1-\frac{z}{D}\right)\frac{Ri_g}{R_f} + \left(1-\frac{z}{D}\right)Pr_{twd0} + Pr_{t0}. \tag{128}$$

In equation (128), the effect of the buoyancy is considered through Ri_g/R_f term and the wall effect is taken into account by using $(1 - z/D)$. In this paper, we show that it is important to take this behavior of Pr_t into account when modeling stably stratified wall-bounded flows in order to simultaneously predict the mean velocity and density profiles correctly.

With any given parameterization for Pr_t, we need to make use of either ν_t or κ_t to calculate one from the other. It is common for the turbulent viscosity (ν_t) to be parameterized. Hence, accurate parameterization of the turbulent viscosity (ν_t) in a RANS model is very important. For an unstratified fully developed turbulent channel flow with a hydrostatic pressure distribution and a logarithmic velocity profile, it can be mathematically shown that the turbulent viscosity (ν_t) is simply a parabolic function of depth given by (Rodi 1993)

$$\nu_{t0} = \kappa u_\tau z(1 - z/D). \tag{129}$$

This equation only takes into account the effect of boundaries in generating the turbulence and is appropriate for a zero-equation RANS model. Equation (129) is the turbulent viscosity (ν_t) for a neutrally stable flow and thus does not incorporate the effect of density stratification. MA argued that as $Ri_g \to 0$, $\nu_t \to \nu_{t0}$ and when $Ri_g \to \infty$, $\nu_t \to 0$. Based on these arguments, they provided a simple modification to account for density stratification as a function of Ri_g. Here, we adopt their formulation to modify the parabolic turbulent viscosity (ν_t) to equation (130) for a stably stratified flow as a function of Ri_g given by

$$\nu_t = \kappa u_\tau z(1 - z/D)\,(1 + \beta Ri_g)^\alpha\,, \tag{130}$$

where β and α are empirical constants with values of 10 and $-1/2$, respectively (MA).

In more sophisticated turbulence closure models such as the standard k-ϵ model, additional transport equations are solved to evaluate ν_t. In the standard k-ϵ model, the turbulent viscosity is given by

$$\nu_t = (1 - R_f)\, C_\mu \frac{k^2}{\epsilon}, \tag{131}$$

where $C_\mu = (|\overline{u'w'}|/k)^2$ is the turbulent viscosity parameter and is usually considered to be roughly 0.09 (Karimpour & Venayagamoorthy 2013). The transport equation of k for a stratified inhomogeneous flow in the standard k-ϵ closure scheme is given by

$$\frac{\partial k}{\partial t} + \overline{U_j}\frac{\partial k}{\partial x_j} = P - \epsilon + B + \frac{\partial}{\partial x_j}\left(\frac{\nu_t}{\sigma_k}\frac{\partial k}{\partial x_j}\right), \tag{132}$$

where the last term is the transport of k due to existence of solid wall which is modeled using the gradient-diffusion hypothesis with σ_k as the turbulent Prandtl number for k. Furthermore, in the standard k-ϵ model the dissipation rate of the turbulent kinetic energy (ϵ) is obtained through an empirical transport equation. This equation is a dimensionally consistent analogy to the transport equation of k (Durbin & Pettersson Reif 2011) and for high-Reynolds-number flows is given by

$$\frac{\partial \epsilon}{\partial t} + \overline{U_j}\frac{\partial \epsilon}{\partial x_j} = C_{\epsilon 1} P \frac{\epsilon}{k} - C_{\epsilon 2}\epsilon\frac{\epsilon}{k} + C_{\epsilon 3} B \frac{\epsilon}{k} + \frac{\partial}{\partial x_j}\left(\frac{\nu_t}{\sigma_\epsilon}\frac{\partial \epsilon}{\partial x_j}\right). \tag{133}$$

In equation (133), $C_{\epsilon 1}$, $C_{\epsilon 2}$ and $C_{\epsilon 3}$ are empirical constants for the 'production of dissipation', 'dissipation of dissipation' and 'buoyancy flux of dissipation', respectively. Also, σ_ϵ is an empirical dissipation turbulent Prandtl number. All of the constants in the k-ϵ model except for $C_{\epsilon 3}$ have standard values as follows: $C_{\epsilon 1}$=1.44; $C_{\epsilon 2}$=1.92; σ_k=1.0 and σ_ϵ=1.3. In contrast to the other constants that have more or less universal values as shown above, there is still no consensus on the value of the buoyancy parameter ($C_{\epsilon 3}$). However, Rodi (1987) has shown that $C_{\epsilon 3} \approx 0$ is a reasonable value based on some successful numerical simulations of stratified flows. Following his work, we have also used $C_{\epsilon 3} = 0$ in our k-ϵ based RANS simulations. We discuss this more in section 5.2.

In this study, we employ the MA formulation for the turbulent viscosity (ν_t) as well as the standard k-ϵ closure scheme and use the proposed formulation for Pr_t in equation (128) to highlight the importance of considering the effect of the wall in modeling the scalar transport. We do this by comparing numerical simulations results for a one-dimensional fully developed channel flow case with results from three-dimensional DNS of channel flow of García-Villalba & del Álamo (2011).

5.1.3. Numerical Model. A one-dimensional fully developed smooth-wall channel flow similar to DNS channel flow of García-Villalba & del Álamo (2011) at a friction Reynolds number of $Re_\tau = u_\tau D/\nu = 550$ is simulated in this study using both turbulent viscosity (ν_t) proposed by MA as well as the standard k-ϵ model. Two different stratifications with friction Richardson numbers of $Ri_\tau = \Delta\rho g D/\rho_0 u_\tau^2 = 60$ and 120 are used, where $\Delta\rho$ is the density difference between the top and bottom of the channel. The RANS results are compared with the DNS data of García-Villalba & del Álamo (2011). To our knowledge this is the only available highly resolved DNS database of stably stratified turbulent channel flow.

We do this by solving the 1-D RANS momentum and scalar transport equations. The 1-D RANS momentum equation with the Boussinesq approximation is given by

$$\frac{\partial \overline{U}}{\partial t} = -\frac{1}{\rho_0}\frac{\partial \overline{p}}{\partial x} + \nu\frac{\partial^2 \overline{U}}{\partial z^2} - \frac{\partial}{\partial z}\left(\overline{u'w'}\right), \tag{134}$$

which using the turbulent-viscosity hypothesis can be rewritten as

$$\frac{\partial \overline{U}}{\partial t} = -\frac{1}{\rho_0}\frac{\partial \overline{p}}{\partial x} + \nu\frac{\partial^2 \overline{U}}{\partial z^2} + \frac{\partial}{\partial z}\left(\nu_t \frac{\partial \overline{U}}{\partial z}\right). \tag{135}$$

For simplicity, a pressure-driven flow (i.e. constant pressure gradient) is assumed so that the pressure can be decoupled from the velocity. Using the hydrostatic pressure distribution, the pressure term is then given by

$$-\frac{1}{\rho_0}\frac{\partial \overline{p}}{\partial x} = -\frac{1}{\rho_0}\frac{\partial(\rho_0 g h)}{\partial x} = -g\frac{\partial h}{\partial x} = -gS, \tag{136}$$

where $S = -u_\tau^2/gD$ is the slope of the free-stream. The one-dimensional RANS scalar transport equation is given by

$$\frac{\partial \overline{\rho}}{\partial t} = \kappa_m \frac{\partial^2 \overline{\rho}}{\partial z^2} - \frac{\partial}{\partial z}\left(\overline{\rho' w'}\right), \tag{137}$$

and can be simplified using the gradient-diffusion hypothesis as

$$\frac{\partial \overline{\rho}}{\partial z} = \kappa_m \frac{\partial^2 \overline{\rho}}{\partial z^2} + \frac{\partial}{\partial z}\left(\kappa_t \frac{\partial \overline{\rho}}{\partial z}\right). \tag{138}$$

The above RANS equations cannot be solved analytically and require a numerical solution methodology. To perform a numerical simulation, the governing equations have to be discretized in space and in time in order to convert the partial differential equations into a set of algebraic equations. In this study, a second-order accurate central difference scheme using the finite volume method is employed for spatial discretization. The temporal terms are discretized using a semi-implicit θ-method, where θ is the implicitness parameter that can range from 0–1. The θ-method can be represented as

$$\frac{\partial T}{\partial t} = \theta f\left(T^{n+1}\right) + (1-\theta) f\left(T^n\right), \tag{139}$$

where T is an arbitrary variable (e.g. $\overline{U}$), dependent on time and space and f shows a spatial function. The θ-method improves the stability and/or accuracy of the method through the weighting of the explicit and implicit terms, using the implicitness parameter θ (Casulli

& Cattani 1994). For example, when $\theta = 0$ the method is first-order accurate and fully explicit while for $\theta = 1$ the method is fully implicit, with first-order accuracy. When $\theta = 0.5$, the scheme is usually known as Crank-Nicolson method (Moin 2010), and is a semi-implicit, second-order accurate scheme that evenly distributes the weighting of the explicit and implicit terms. The channel flow governing equations are stable for $0.5 \leq \theta \leq 1$. For this study, $\theta \approx 0.7$ is used since it yielded stable solutions with no oscillations.

A no-slip boundary condition at the solid wall (i.e. $\overline{U} = 0$) and free-slip boundary condition at the free-surface (i.e. $\partial\overline{U}/\partial z = 0$) are imposed. The no-slip boundary condition requires modeling the very thin boundary layer region (the so-called near-wall region where $z^+ < 30$). A commonly used technique is to apply the velocity boundary condition at some distance away from the wall, where the logarithmic velocity profile begins (i.e. $z^+ > 30$). Assuming the existence of a logarithmic velocity profile and using a linear shear stress distribution, the solid wall boundary condition can be represented as

$$\frac{\partial\overline{U_1}}{\partial z} = \frac{C_D}{\nu_t}|\overline{U_1}|\overline{U_1}, \tag{140}$$

where $\overline{U_1}$ is the velocity at the first grid point of the flow domain and C_D can be interpreted as a drag coefficient as

$$C_D = \left[\frac{1}{\kappa}\ln\left(\frac{z_1}{z_0}\right)\right]^{-2}, \tag{141}$$

where z_0 is the roughness height such that the logarithmic velocity profile goes to zero, while z_1 is the physical distance of the first grid point from the wall, located in the log-law region.

Similarly, the standard k-ϵ model is incapable of modeling the near-wall region due to excessive overprediction of turbulent viscosity (ν_t) in this intricate near-wall region (Karimpour & Venayagamoorthy 2013). In the standard k-ϵ closure scheme, modeling the near-wall region is avoided by employing wall-functions. The wall-functions impose the boundary conditions at some distance away from the wall in the log-law region. Assuming the existence of a logarithmic velocity profile, the boundary condition for the mean velocity at the first

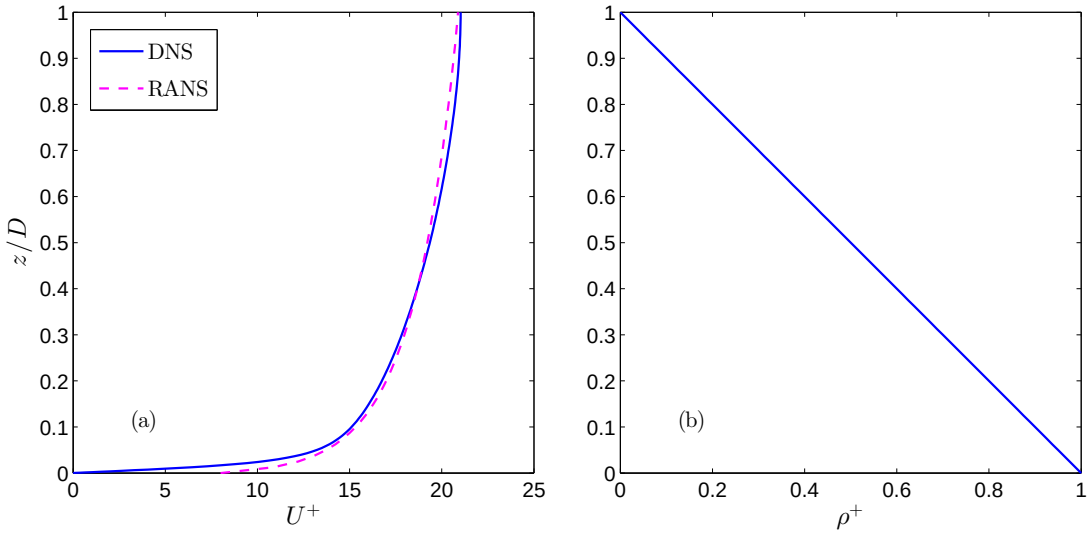

FIGURE 5.2. (a) Fully developed unstratified velocity profile; and (b) initial density profile.

grid point is given by

$$\overline{U_1} = \frac{u_\tau}{\kappa} \ln\left(\frac{z_1}{z_0}\right). \tag{142}$$

Consequently, the boundary conditions for the turbulent kinetic energy (k) and ϵ (i.e. at the first point (z_1)) are given by

$$k_1 = \frac{u_\tau^2}{\sqrt{C_\mu}}, \tag{143}$$

and

$$\epsilon_1 = \frac{u_\tau^3}{\kappa z_1}. \tag{144}$$

The natural boundary condition for the density would be a Neumann boundary condition at both or at least one of the boundaries (i.e. $\partial\overline{\rho}/\partial z = 0$). However, applying a Neumann boundary condition results in a fully mixed density field ($\partial\overline{\rho}/\partial z = 0$) across the whole water column. In order to be able to evaluate the effect of the stable stratification and also the efficacy of the proposed Pr_t's, the density profile is kept constant at both boundaries (i.e. Dirichlet boundary conditions) and the density field is allowed to evolve in the interior of the channel. We note that Dirichlet boundary conditions were also used in the simulations of García-Villalba & del Álamo (2011).

The flow is initialized first from rest and allowed to spin up until a fully developed turbulent velocity profile is obtained before the linear density stratification is imposed. Figure (5.2) shows the comparison of the unstratified velocity profile from the zero-equation RANS simulation to the unstratified DNS channel flow velocity profile of García-Villalba & del Álamo (2011) along with the initial density stratification. The velocity is normalized as $U^+ = \overline{U}/u_\tau$ and the density is normalized as $\rho^+ = (\rho_m - \rho_t)/(\rho_b - \rho_t)$, where $\rho_m = \rho_0 + \overline{\rho}$. Also, ρ_t and ρ_b represent the density at the top and bottom boundaries of the channel, respectively. As it can be seen, the agreement between the RANS simulation and the DNS results are excellent.

5.1.4. Results and Discussion. In this section, the results of the RANS numerical simulations using different turbulent Prandtl number formulations are presented and discussed. We note that for the zero-equation model, the simulations use the modified turbulent viscosity (ν_t) proposed by MA as discussed in section 5.1.2. The results obtained from using the homogeneous Pr_t's given in equation (111) as well as the MA formulation for Pr_t given by equation (145) are compared with the modified Pr_t given by equation (128). The MA proposition is given by

$$Pr_t = Pr_{t0}\frac{(1+\beta Ri_g)^\alpha}{(1+\beta_\rho Ri_g)^{\alpha_\rho}}, \tag{145}$$

where $\beta = 10$, $\alpha = -1/2$, $\beta_\rho = 10/3$ and $\alpha_\rho = -3/2$ are empirical constants.

First, the fully developed velocity and density profiles using the zero-equation closure scheme and the homogeneous Pr_t formulations given by equations (111) and also (145) for $Ri_\tau = 60$ are shown in Figure (5.3a) and (b). Superimposed on these plots are the profiles obtained from the DNS of García-Villalba & del Álamo (2011). It is evident that the homogeneous Pr_t formulations permit excessive mixing of the density and consequently a velocity profile similar to the unstratified case is obtained. On the other hand, the results of the RANS simulation using the modified Pr_t given by equation (128) show a much improved prediction of both momentum and scalar, especially a much closer agreement with the DNS density profile, thus highlighting the effect of the $(1-z/D)$ correction that has been proposed.

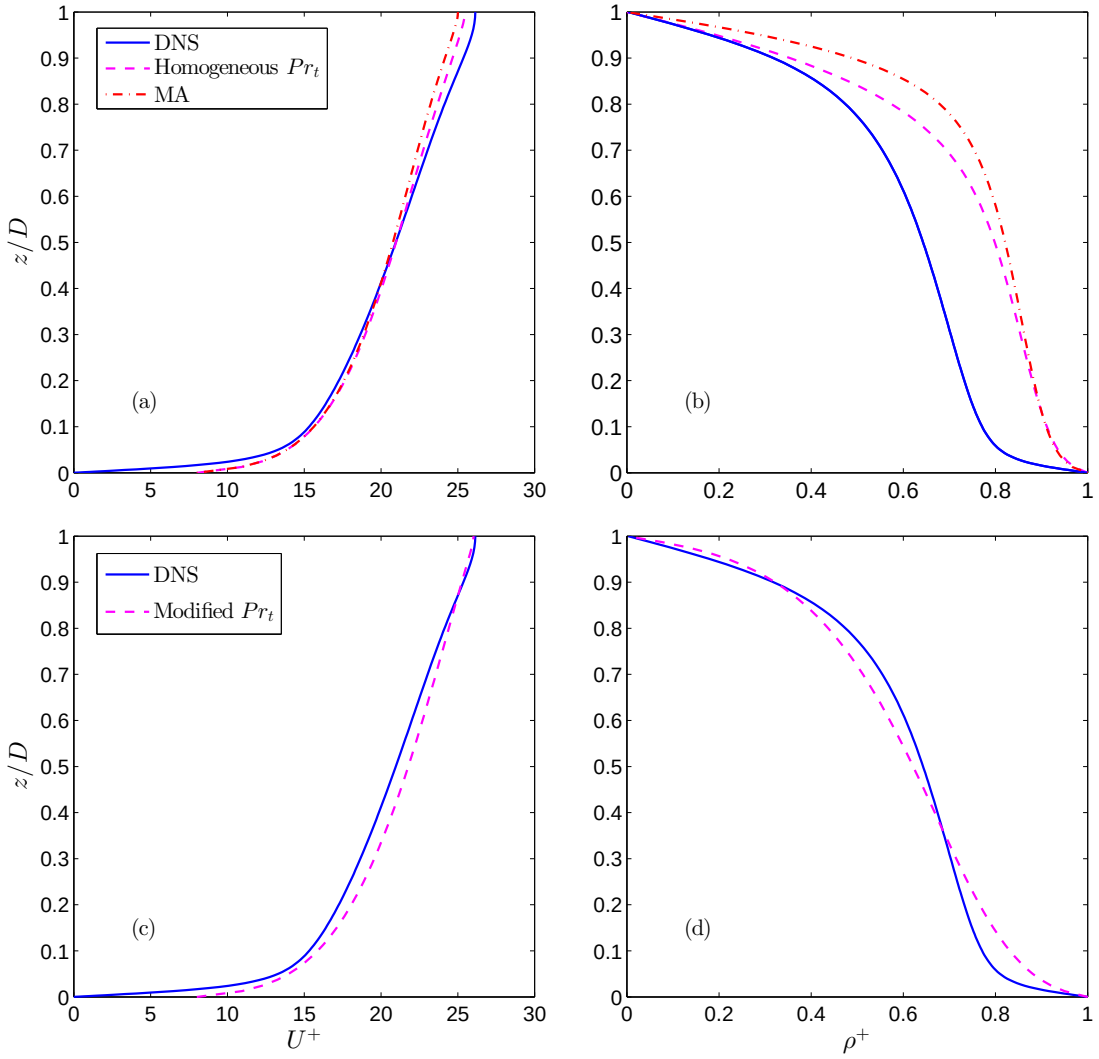

FIGURE 5.3. Left panel: velocity profiles; right panel: density profiles; for $Ri_\tau = 60$ and $Re_\tau = 550$ obtained from the zero-equation closure scheme using: (a,b) the Pr_t formulations given by equations (111) and (145); (c,d) the modified Pr_t formulation (equation 128) compared with the channel flow DNS data of García-Villalba & del Álamo (2011).

Furthermore, to better assess the robustness of the proposed correction, we make use of the modified Pr_t given by equation (128) to simulate a flow with a stronger stratification of $Ri_\tau = 120$. The results are shown in Figure (5.4) and compared with the channel flow DNS data. The formulation shows good prediction of the density and velocity profiles.

In order to assess the applicability of the modified Pr_t in more sophisticated RANS closure schemes, the channel flow simulation is performed using the standard k-ϵ model.

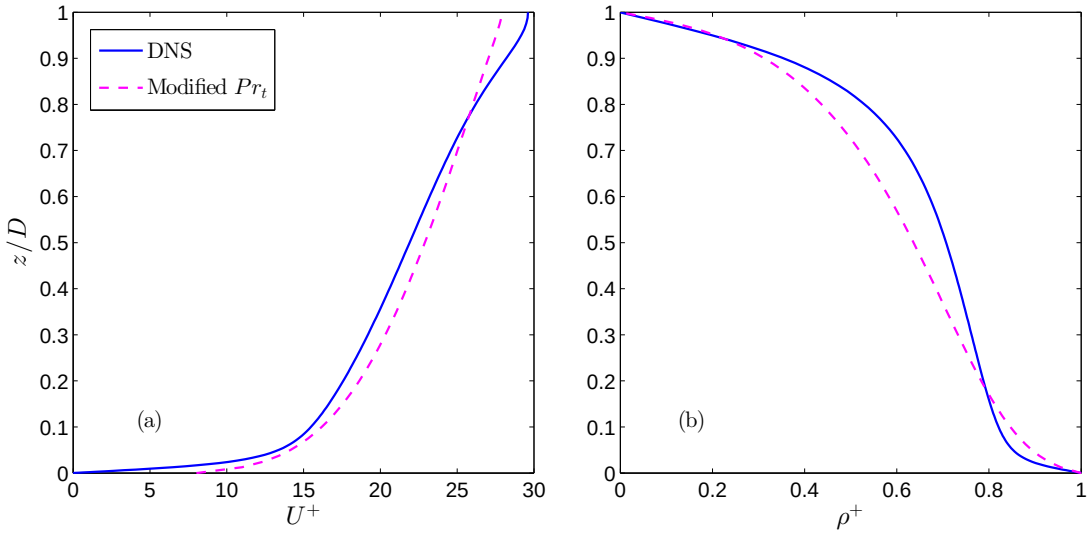

FIGURE 5.4. Comparisons of (a) velocity profiles; and density profiles for $Ri_\tau = 120$ and $Re_\tau = 550$ obtained from the zero-equation closure scheme using the modified proposition for Pr_t shown in equation (128) with the channel flow DNS data of García-Villalba & del Álamo (2011).

Figure (5.5) shows the prediction of velocity and density profiles for $Ri_\tau = 60$ compared to the DNS profiles using the standard k-ϵ model for both the homogeneous Pr_t's given in equations (111) and (145) and the modified parameterization given by equation (128). Similar to the prediction shown in Figure (5.3), the homogeneous Pr_t formulations show overmixing of density and different velocity profiles compared to the DNS profile as shown in Figure (5.5a) and (b), respectively. Interestingly (but as expected), the modified proposition substantially improves the prediction of the density profile and consequently the velocity profile as can be seen in Figure (5.5c) and (5.5d), respectively. This highlights the need for the proposed $(1 - z/D)$ correction and the applicability of the modified Pr_t in more sophisticated turbulence models.

5.1.5. CONCLUDING REMARKS. In this study, we have investigated the use of homogeneous turbulent Prandtl number (Pr_t) parameterizations to predict the mixing of momentum and density in a stably stratified channel flow. We have made use of the stratified parabolic turbulent viscosity formulation proposed by MA as well as the standard k-ϵ model and

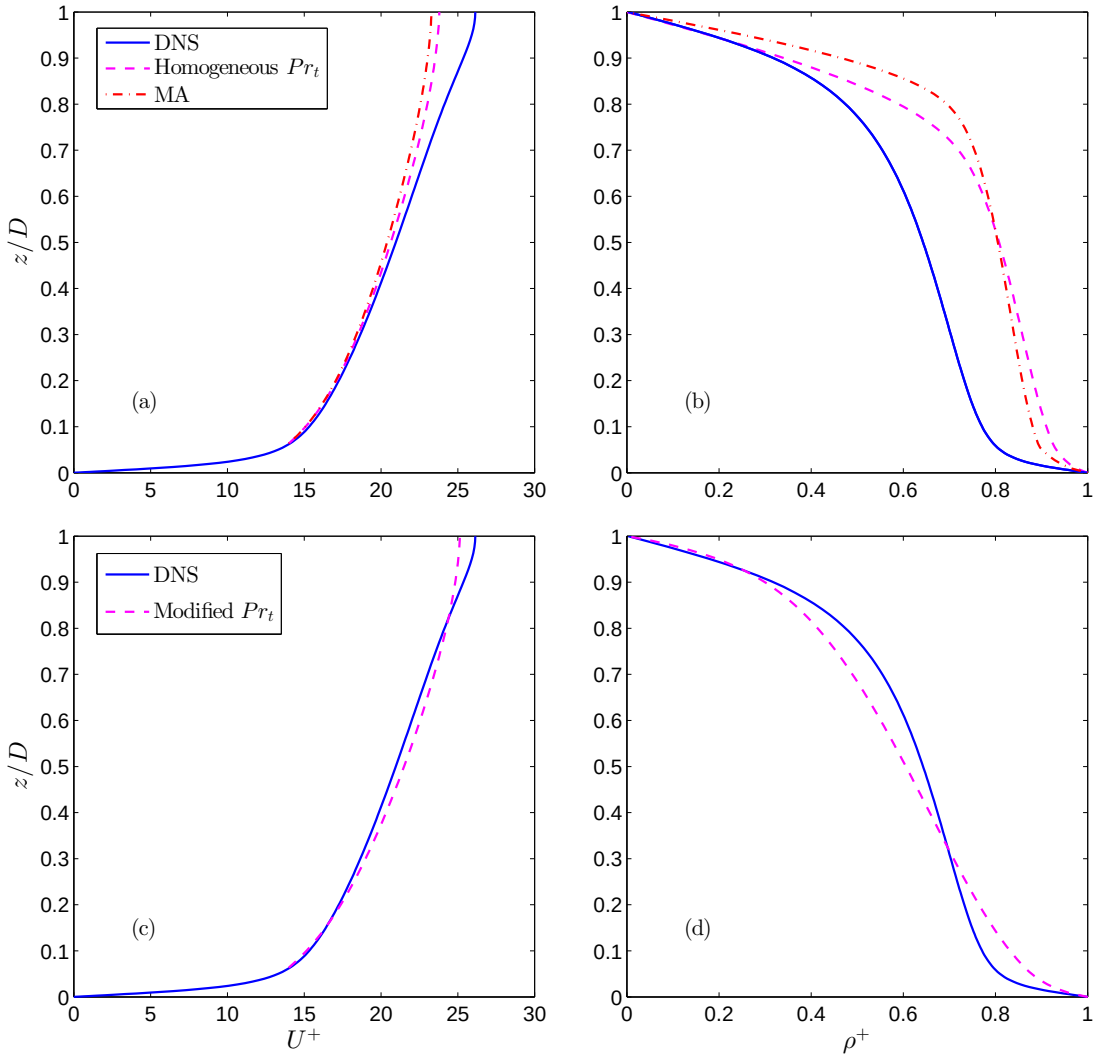

FIGURE 5.5. Left panel: velocity profiles; right panel: density profiles; for $Ri_\tau = 60$ and $Re_\tau = 550$ obtained from the standard k-ϵ closure scheme using: (a,b) the Pr_t formulations given by equations (111) and (145); (c,d) the modified Pr_t formulation (equation 128) compared with the channel flow DNS data of García-Villalba & del Álamo (2011).

tested the efficacy of the homogeneous Pr_t's in the context of one-dimensional RANS closure schemes. The comparison of the RANS results with data from DNS of stratified channel flow clearly shows the inadequacy of the homogeneous Pr_t formulations for correctly simulating a stratified channel flow. In order to account for the effect of the wall boundary, we have proposed a reasonable modification to the homogeneous Pr_t formulation by introducing a linear correction based on the distance from the wall $(1 - z/D)$. This proposition was

motivated in part by observed trends of the turbulent Prandtl number in unstratified wall-bounded flows from a number of studies such as those of Kawamura *et al.* (1998), Crimaldi *et al.* (2006) and Srinavasan & Papavassiliou (2010) as well as some modeling reasoning. The RANS results using the modified formulations compare well with the DNS data, highlighting the utility of the proposed modification.

In essence, these results highlight the need to modify the homogeneous turbulent Prandtl number formulations for wall-bounded flows. To this end, the simple correction presented in this study has shown remarkable improvement in predicting both momentum and scalar mixing. We believe these findings will be useful in numerical modeling of many geophysical flows influenced by wall effects.

In the following section, we extend our discussion to the standard k-ϵ closure scheme and specifically investigate the buoyancy parameter ($C_{\epsilon 3}$).

5.2. Improvement of the k-ϵ model[2]

5.2.1. Introduction. Stably stratified wall-bounded turbulent flows are common in nature such as in estuaries, lakes, oceans and the atmosphere. Hence, development of numerical models with the ability to correctly predict such flows is of great importance. With the increase of the computational power in recent decades, different numerical methods have been developed and used for modeling turbulent flows. Direct numerical simulation (DNS) and large-eddy simulation (LES) are two methods which have been used to fundamentally study stratified wall-bounded flows. DNS directly solves the highly non-linear Navier-Stokes equations together with the continuity and scalar (density) transport equations without recourse to any turbulence models. DNS is capable of resolving the temporal and spatial scales

[2]The results presented in this section will be submitted in substantial part as a paper entitled "Evaluation of the standard k-ϵ closure scheme for modeling stably stratied wall-bounded turbulent flows" by F. Karimpour, A. Garanaik and S. K. Venayagamoorthy, to *Ocean Modelling*. This chapter is written in a collective "we" tense to acknowledge collaborative work with the co-authors. Amrapalli Garanaik performed some RANS simulations to confirm some of the results.

of the flow from the Kolmogorov scale (η) assumed as the smallest scale where the molecular viscosity (ν) dominates, to the energy-containing scales. LES can resolve the large scales of the flow but relies on turbulence models to predict small scales of the fluid flow. However, both DNS and LES are very expensive for most practical problems and are still limited to the low- to moderate-Reynolds-number flows with idealized geometries.

Reynolds-averaged Navier-Stokes (RANS) simulation is another numerical method which is widely used for modeling turbulent flows. RANS applies Reynolds decomposition and averaging to the governing equations of the fluid flow. This process results in additional terms known as turbulent momentum fluxes (Reynolds stresses) and turbulent scalar fluxes in momentum and scalar transport equations, respectively. These extra terms imply that the number of the unknowns is greater than the number of equations leading to an undetermined system of equations commonly referred to as the closure problem. To resolve this severe shortcoming, the turbulent-viscosity and gradient-diffusion hypotheses are used to model these extra terms. The turbulent-viscosity hypothesis links the Reynolds stresses with the mean shear rate ($d\overline{U}/dz$) through the turbulent viscosity (ν_t). Similarly, the gradient-diffusion hypothesis links the turbulent scalar fluxes with the mean scalar gradient ($d\overline{\rho}/dz$) using the turbulent diffusivity (κ_t). In a uni-directional shear flow, the turbulent viscosity (ν_t) is given by

$$\nu_t = \frac{-\overline{u'w'}}{\partial\overline{U}/\partial z}, \tag{146}$$

and the turbulent diffusivity (κ_t) is defined as

$$-\overline{\rho'w'} = \kappa_t \frac{\partial\overline{\rho}}{\partial z}, \tag{147}$$

where $\overline{u'w'}$ is the Reynolds stress, $\overline{U}$ is the mean (time-averaged) velocity along the main axis, z is the vertical distance from the wall, $\overline{\rho'w'}$ is the turbulent scalar flux and $\overline{\rho}$ is the mean scalar (density).

The turbulent viscosity (ν_t) and the turbulent diffusivity (κ_t) cannot be defined explicitly and need to be parameterized. For this reason, different turbulence closure schemes are

introduced to model ν_t and κ_t. The standard k-ϵ closure scheme, first developed by Jones & Launder (1972), is one of the most popular RANS models (Pope 2000). In this model, k denotes the turbulent kinetic energy per unit mass and is defined as

$$k = \frac{1}{2}(\overline{u'^2} + \overline{v'^2} + \overline{w'^2}), \tag{148}$$

and ϵ is the dissipation rate of the turbulent kinetic energy, given by

$$\epsilon = \nu \left(\overline{\frac{\partial u_i'}{\partial x_j} \frac{\partial u_i'}{\partial x_j}} + \overline{\frac{\partial u_i'}{\partial x_j} \frac{\partial u_j'}{\partial x_i}} \right). \tag{149}$$

In the standard k-ϵ closure scheme, the turbulent viscosity (ν_t) is given by

$$\nu_t = (1 - R_f)\, C_\mu \frac{k^2}{\epsilon}, \tag{150}$$

where $C_\mu = (|\overline{u'w'}|/k)^2$ is the turbulent viscosity parameter commonly assumed to be 0.09 (Karimpour & Venayagamoorthy 2013). Also, R_f is the flux Richardson number which is defined as

$$R_f = \frac{-B}{P}, \tag{151}$$

where $B = (-g/\rho_0)\overline{\rho' w'}$ is the buoyancy flux.

The momentum equation is coupled with the density transport equation through the buoyancy term. Hence, it is important to propose suitable parameterizations for the turbulent diffusivity to correctly predict the mixing of density. Stability functions such as those introduced by Galperin *et al.* (1988), Kantha & Clayson (1994) and Canuto *et al.* (2001) describe the shear and stratification effects on the turbulent viscosity and diffusivity through complex empirical functions. A common approach is to employ the turbulent Prandtl number (Pr_t) which links the turbulent viscosity and diffusivity as

$$Pr_t = \frac{\nu_t}{\kappa_t}. \tag{152}$$

In most turbulence models such as the standard k-ϵ model, the turbulent viscosity and the turbulent Prandtl number (Pr_t) are calculated explicitly using appropriate parameterizations. The turbulent diffusivity (κ_t) is then computed subsequently. The turbulent Prandtl number is parameterized using experiments and DNS data, usually in terms of the gradient Richardson number (Ri_g) such as propositions of Munk & Anderson (1948), Webster (1964), Baum & Caponi (1992), Schumann & Gerz (1995) and Venayagamoorthy & Stretch (2010).

Most parameterizations for the turbulent Prandtl number are developed for homogeneous shear flows. Hence, the effect of the solid wall is neglected. Karimpour & Venayagamoorthy (2014, see also section 5.1) proposed an appropriate Pr_t formulation for a turbulent channel flow as

$$Pr_t = \left(1 - \frac{z}{D}\right) \frac{Ri_g}{R_f} + \left(1 - \frac{z}{D}\right) Pr_{twd0} + Pr_{t0}. \tag{153}$$

Here, (Ri_g) is the gradient Richardson number which is a measure of the stratification strength and is defined as

$$Ri_g = \frac{N^2}{S^2}, \tag{154}$$

where $N = \sqrt{-(g/\rho_0)(d\overline{\rho}/dz)}$ is the Brunt-Väisälä or buoyancy frequency and $S = \partial\overline{U}/\partial z$ is the mean shear rate. In equation (153), the flux Richardson number $R_f = R_{f\infty}[1 - exp(-7.5Ri_g)]$ and $Pr_{twd0} \approx 0.4$ is the difference between the neutral turbulent Prandtl number at the wall (Pr_{tw}) and that at the free-stream. The efficacy of the proposed Pr_t has been verified via numerical simulations using different RANS closure schemes. The RANS results using this formulation for Pr_t compared well with the DNS data of stably stratified wall-bounded turbulent flow highlighting its suitability for modeling stably stratified wall-bounded turbulent flows.

In this study, we assess the efficacy of the standard k-ϵ closure scheme for modeling stably stratified channel flows by revisiting the buoyancy parameter ($C_{\epsilon 3}$). Simulations are performed in the same one-dimensional water column model that is used in section 5.1 and the effect of the buoyancy parameter ($C_{\epsilon 3}$) is tested. In these simulations, we make use of

the Pr_t proposed by Karimpour & Venayagamoorthy (2014). In section 5.2.2 a review of the standard k-ϵ model will be presented followed by a discussion on the parameterization of $C_{\epsilon 3}$. In section 5.2.3 the standard k-ϵ RANS simulation results of the stably stratified channel flow are shown and compared with the stably stratified channel flow DNS data of García-Villalba & del Álamo (2011). Finally, in section 5.2.4 the concluding remarks of the study are presented.

5.2.2. Standard k-ϵ Model. The standard k-ϵ closure scheme solves the transport equations of k and ϵ to estimate the turbulent viscosity (ν_t) as shown in equation (150). With the Boussinesq approximation, the transport equation of k for a stratified inhomogeneous flow is given by

$$\frac{\partial k}{\partial t} + \overline{U_j}\frac{\partial k}{\partial x_j} = P - \epsilon + B + T_k, \tag{155}$$

where $P = -\overline{u_i' u_j'}(\partial \overline{U_i}/\partial x_j)$ is the production rate of k and $B = (-g/\rho_0)\overline{\rho' w'}$ is the buoyancy flux. T_k represents the transport of k arising from inhomogeneity due to the existence of the solid wall. In the standard k-ϵ model, the transport equation of the turbulent kinetic energy for high-Reynolds-number flows is modeled as

$$\frac{\partial k}{\partial t} + \overline{U_j}\frac{\partial k}{\partial x_j} = P - \epsilon + B + \frac{\partial}{\partial x_j}\left(\frac{\nu_t}{\sigma_k}\frac{\partial k}{\partial x_j}\right), \tag{156}$$

where the transport term is modeled using the gradient-diffusion hypothesis and σ_k is the turbulent Prandtl number for k. For a one-dimensional channel flow, the transport equation of the turbulent kinetic energy can be recast as

$$\frac{\partial k}{\partial t} = P - \epsilon + B + \frac{\partial}{\partial z}\left(\frac{\nu_t}{\sigma_k}\frac{\partial k}{\partial z}\right). \tag{157}$$

Using the turbulent-viscosity and the gradient-diffusion hypotheses, $P = \nu_t(\partial \overline{U}/\partial z)^2$ and $B = -\kappa_t N^2$. In the standard k-ϵ model, ϵ is obtained through an empirical transport

equation which for high-Reynolds-number flows is given by

$$\frac{\partial \epsilon}{\partial t} + \overline{U_j}\frac{\partial \epsilon}{\partial x_j} = C_{\epsilon 1} P \frac{\epsilon}{k} - C_{\epsilon 2}\epsilon\frac{\epsilon}{k} + C_{\epsilon 3} B \frac{\epsilon}{k} + \frac{\partial}{\partial x_j}\left(\frac{\nu_t}{\sigma_\epsilon}\frac{\partial \epsilon}{\partial x_j}\right). \tag{158}$$

This equation for a one-dimensional flow can be recast as

$$\frac{\partial \epsilon}{\partial t} = C_{\epsilon 1} P \frac{\epsilon}{k} - C_{\epsilon 2}\epsilon\frac{\epsilon}{k} + C_{\epsilon 3} B \frac{\epsilon}{k} + \frac{\partial}{\partial z}\left(\frac{\nu_t}{\sigma_\epsilon}\frac{\partial \epsilon}{\partial z}\right). \tag{159}$$

$C_{\epsilon 1}$, $C_{\epsilon 2}$ and $C_{\epsilon 3}$ are empirical constants for the 'production of dissipation', 'dissipation of dissipation' and 'buoyancy flux of dissipation', respectively. Also, σ_ϵ is an empirical dissipation turbulent Prandtl number.

As shown in equation (150), by assuming equilibrium between the production rate of k, the dissipation rate of k and the buoyancy flux (B) as $P \approx \epsilon - B$, the turbulent viscosity for the standard k-ϵ closure scheme can be calculated as $\nu_t = (1 - R_f)C_\mu k^2/\epsilon$ (Rodi 1987). The empirical constants used in the standard k-ϵ model are represented in table 5.1.

C_μ	$C_{\epsilon 1}$	$C_{\epsilon 2}$	σ_k	σ_ϵ
0.09	1.44	1.92	1.0	1.3

TABLE 5.1. Values of constants in the standard k-ϵ model

In contrast to other constants in the standard k-ϵ model, there is still no consensus on the value of the buoyancy parameter ($C_{\epsilon 3}$). In next section, $C_{\epsilon 3}$ is investigated by using analytical discussions.

5.2.2.1. *Parameterization of $C_{\epsilon 3}$.* The modeled transport equation of ϵ shown in equation (158) was first introduced by Jones & Launder (1972), while the buoyant dissipation term was later added by Launder & Spalding (1972). In contrast to other empirical parameters in the standard k-ϵ closure scheme, it is found that $C_{\epsilon 3}$ depends on the flow condition. Hence, different values are proposed for $C_{\epsilon 3}$. Durbin & Pettersson Reif (2011) discussed that P and B are linked as $B = -PR_f$, which reduces the transport equation of the turbulent kinetic energy (k) as $Dk/Dt = P(1 - R_f) - \epsilon + T_k$. Analogous to the transport equation of k, they argued that equal weighting factor should be considered for the contribution from the

production and buoyancy terms in the transport equation of ϵ. This implies that $C_{\epsilon 3} = C_{\epsilon 1}$ for both stable and unstable stratifications.

However, most of the proposed models describe $C_{\epsilon 3}$ as a function of stratification. Under unstable stratification where buoyancy is a source of production of k, $C_{\epsilon 3} = 1$ is usually chosen (Rodi 1987), while for stable stratifications no universal value is defined yet. Numerous studies have been carried out to parameterize $C_{\epsilon 3}$ for stably stratified flows. For example, Rodi (1987) suggests to choose $C_{\epsilon 3} \approx 0$ considering some successful calculations but still questions the universality of this proposition for all types of turbulence. To describe the behavior of $C_{\epsilon 3}$, Burchard & Baumert (1995) have considered the idealized case of neglecting the transport terms compared to P, ϵ and B (i.e. homogeneous flows or equilibrium layer of wall-bounded flows). Hence, the transport equation of k can be rewritten as

$$\begin{aligned} \frac{\partial k}{\partial t} &= P - \epsilon + B \\ &= C_\mu \left(1 - R_f\right) \frac{k^2}{\epsilon} S^2 - \epsilon - C'_\mu \left(1 - R_f\right) \frac{k^2}{\epsilon} N^2, \end{aligned} \tag{160}$$

where $C'_\mu = C_\mu / Pr_t$. Similarly, the transport equation of ϵ is

$$\begin{aligned} \frac{\partial \epsilon}{\partial t} &= C_{\epsilon 1} P \frac{\epsilon}{k} - C_{\epsilon 2} \epsilon \frac{\epsilon}{k} + C_{\epsilon 3} B \frac{\epsilon}{k} \\ &= C_{\epsilon 1} C_\mu \left(1 - R_f\right) \frac{k^2}{\epsilon} S^2 \frac{\epsilon}{k} - C_{\epsilon 2} \epsilon \frac{\epsilon}{k} - C_{\epsilon 3} \left(1 - R_f\right) C'_\mu \frac{k^2}{\epsilon} N^2 \frac{\epsilon}{k}. \end{aligned} \tag{161}$$

They solved for $d(\epsilon/k)/dt$ using equations (160) and (161) as

$$\begin{aligned}
\frac{d(\epsilon/k)}{dt} &= \frac{1}{k}\frac{d\epsilon}{dt} - \frac{\epsilon}{k^2}\frac{dk}{dt} \\
&= \frac{1}{k}\left(C_{\epsilon 1}C_\mu\left(1-R_f\right)\frac{k^2}{\epsilon}S^2\frac{\epsilon}{k} - C_{\epsilon 2}\epsilon\frac{\epsilon}{k} - C_{\epsilon 3}C'_\mu\left(1-R_f\right)\frac{k^2}{\epsilon}N^2\frac{\epsilon}{k}\right) \\
&\quad -\frac{\epsilon}{k^2}\left(C_\mu\left(1-R_f\right)\frac{k^2}{\epsilon}S^2 - \epsilon - C'_\mu\left(1-R_f\right)\frac{k^2}{\epsilon}N^2\right) \\
&= \underbrace{\left(1-R_f\right)\left(C_{\epsilon 1}C_\mu S^2 - C_\mu S^2 + C'_\mu N^2 - C_{\epsilon 3}C'_\mu N^2\right)}_{a(t)} \\
&\quad \underbrace{-\frac{\epsilon^2}{k^2}\left(C_{\epsilon 2}-1\right)}_{b(t)}. \qquad (162)
\end{aligned}$$

They concluded that as $b(t)$ is always negative, therefore negative values of $a(t)$ can lead to non-admissible negative values for k and ϵ. Therefore, the sufficient condition for k and ϵ to be positive is $a(t) \geq 0$. As the flux Richardson number is normally considered to be $R_f \leq 1$, it can be concluded that

$$C_\mu S^2\left(C_{\epsilon 1}-1\right) + C'_\mu N^2\left(1-C_{\epsilon 3}\right) \geq 0. \qquad (163)$$

Using $Pr_t = Ri_g/R_f$ for a homogeneous flow, equation (163) results in

$$C_{\epsilon 3} < 1 \quad , \quad R_f \geq R_f^- = \frac{C_{\epsilon 1}-1}{C_{\epsilon 3}-1}, \qquad (164)$$

where R_f^- is a limiting flux Richardson number and sets a lower bound for R_f.

This discussion can be further extended by assuming local equilibrium (i.e. $P = \epsilon - B$) and also using stationarity for equation (161) (i.e. $\partial\epsilon/\partial t = 0$). Using such assumptions, equation (161) will be simplified as

$$C_{\epsilon 1}P - C_{\epsilon 2}\epsilon + C_{\epsilon 3}B = C_{\epsilon 1}P - C_{\epsilon 2}P - C_{\epsilon 2}B + C_{\epsilon 3}B = 0. \qquad (165)$$

It follows from the turbulent-viscosity hypothesis that $P = \nu_t S^2$. Also, from the gradient-diffusion hypothesis we can write the buoyancy flux as $B = -\kappa_t N^2$. Using these two formulations for P and B, equation (165) can be rearranged as

$$\kappa_t N^2 (C_{\epsilon 2} - C_{\epsilon 3}) = \nu_t S^2 (C_{\epsilon 2} - C_{\epsilon 1}), \tag{166}$$

which leads to

$$Ri_g^{st} = Pr_t \frac{C_{\epsilon 2} - C_{\epsilon 1}}{C_{\epsilon 2} - C_{\epsilon 3}}, \tag{167}$$

where Ri_g^{st} is the stationary gradient Richardson number. Consequently, a stationary flux Richardson number can be inferred as

$$R_f^{st} = \frac{C_{\epsilon 2} - C_{\epsilon 1}}{C_{\epsilon 2} - C_{\epsilon 3}}. \tag{168}$$

By rearranging equation (168), $C_{\epsilon 3}$ can be obtained as

$$C_{\epsilon 3} = C_{\epsilon 2} - \frac{C_{\epsilon 2} - C_{\epsilon 1}}{R_f^{st}}. \tag{169}$$

Investigators have used different values for Ri_g^{st} such as Baum & Caponi (1992) that introduced $C_{\epsilon 3} = 1.14$ which implies $Ri_g^{st} \approx 0.6$. However, there are evidences such as the work of Rohr *et al.* (1988) which show $Ri_g^{st} \approx 0.25$ (Burchard & Bolding 2001). The corresponding stationary flux Richardson number (R_f^{st}) is required to determine $C_{\epsilon 3}$. There are various studies and parameterizations which estimate the flux Richardson number. For example, for the value of $Ri_g = 0.25$, Mellor & Yamada (1982) empirical model suggests a value of $R_f \approx 0.22$, Nakanishi (2001) model returns a value of $R_f \approx 0.23$ and a modified formula of Townsend (1958) which is calibrated and validated with the experimental atmospheric data gives $R_f = 0.25$ (Pardyjak *et al.* 2002). Burchard & Baumert (1995) have proposed that $R_f^{st} \approx 0.25$ can be a fair estimate when $Ri_g \approx 0.25$.

Using the stationary gradient Richardson number (Ri_g^{st}) and consequently the stationary flux Richardson number (R_f^{st}), researchers such as Burchard & Baumert (1995), Burchard

et al. (1998), Burchard & Petersen (1999) and Baumert & Peters (2000) proposed negative values for $C_{\epsilon 3}$. Burchard & Bolding (2001) evaluated the $C_{\epsilon 3}$ using the stability functions of Kantha & Clayson (1994), Rodi (1980), Hossain (1980), Canuto *et al.* (2001). They assumed that Ri_g^{st} can have different values other than 0.25 in a homogeneous flow and concluded that negative values for $C_{\epsilon 3}$ should be used for these models. In a more recent work, Warner *et al.* (2005) discussed that in the k-ϵ model, the contribution of the buoyancy term in the transport equation of ϵ is relatively low compared to the production and dissipation terms. Therefore, models such as DELFT3D (1999) switch off $C_{\epsilon 3}$ for stable stratifications (i.e. $C_{\epsilon 3} = 0$). It can simply be shown from equation (169) that $C_{\epsilon 3} = 0$ when $Ri_g^{st} \approx R_f^{st} \approx 0.25$. In section 5.2.3, RANS simulations for $C_{\epsilon 3} = 0$ and also positive and negative values are performed and results are compared with DNS data of stably stratified channel flow.

5.2.3. Results. In this section, the results of RANS simulations are presented and the influence of $C_{\epsilon 3}$ on simulating stably stratified wall-bounded flows is evaluated. As mentioned earlier, the turbulent Prandtl number (Pr_t) formulation proposed by Karimpour & Venayagamoorthy (2014) is used in these simulations. The RANS simulation results are compared with the DNS data of stably stratified channel flow.

5.2.3.1. *Evaluation of* $C_{\epsilon 3}$. In this section, the effect of $C_{\epsilon 3}$ is investigated. To do this, we make use of three different values of $C_{\epsilon 3} = -1.44, 0.0, 1.44$. The RANS results are compared with exact DNS data of García-Villalba & del Álamo (2011) for $Ri_\tau = 60$ and $Re_\tau = 550$ and are represented in Figure (5.6).

It can be seen that for the velocity profile, $C_{\epsilon 3} = -1.44$ predicts a higher velocity compared to DNS data, while $C_{\epsilon 3} = 1.44$ yields a velocity profile similar to an unstratified case. It is evident that $C_{\epsilon 3} = 0$ results in a well-predicted velocity profile.

For $C_{\epsilon 3} = \pm 1.44$, the density profiles do not compare well with the DNS density. While for $C_{\epsilon 3} = -1.44$ the density profile shows excessive mixing, $C_{\epsilon 3} = 1.44$ results in a less mixed density profile compared to the DNS results. As it is expected, using $C_{\epsilon 3} = 0$ results in a good prediction of the density profile.

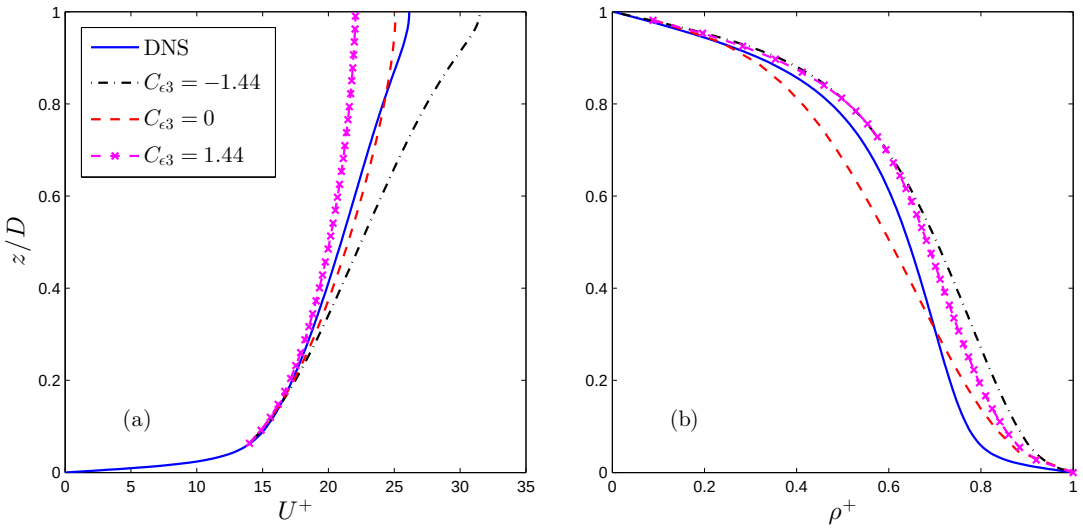

FIGURE 5.6. a) Comparisons of (a) the velocity profiles; and (b) the density profiles for $Ri_\tau = 60$ and $Re_\tau = 550$, obtained from the standard k-ϵ closure scheme for $C_{\epsilon 3} = -144, 0.0, 1.44$, compared with the DNS data of García-Villalba & del Álamo (2011).

These findings show that in the standard k-ϵ model, $C_{\epsilon 3} = 0$ is a suitable value for modeling of stably stratified wall-bounded turbulent flows.

5.2.4. CONCLUDING REMARKS. In this study, we have evaluated the efficacy of $C_{\epsilon 3}$ for simulating the mixing of momentum and scalar in a stably stratified wall-bounded turbulent flow using the standard k-ϵ model. We have used the model introduced in section 5.1.3 and the Pr_t parameterization of Karimpour & Venayagamoorthy (2014) for modeling stably stratified wall-bounded flows. Using the concept of the stationary gradient and flux Richardson numbers (Ri_g^{st} and R_f^{st}) and neglecting the transport terms, we have proposed $C_{\epsilon 3} = 0$ for a stably stratified wall-bounded turbulent flow. We have tested this proposition as well as negative and positive values for $C_{\epsilon 3}$ by performing RANS simulations to evaluate the effect of $C_{\epsilon 3}$. The RANS simulation results are remarkably good for $C_{\epsilon 3} = 0$, while other values for $C_{\epsilon 3}$ result in poor prediction of the density and velocity. We believe these findings are helpful for simulating stably stratified wall-bounded turbulent flows.

5.3. Summary

In this chapter, analytical arguments were made and one-dimensional RANS simulations were performed to investigate the mixing in a stably stratified turbulent channel flow. Simulations were implemented in a code developed in MATLAB. A new formulation for Pr_t was proposed to model stably stratified wall-bounded flows. Also, $C_{\epsilon 3} = 0$ was suggested. The results from numerical simulations were compared to the DNS data of stably stratified channel flow and showed remarkably good comparisons. Additionally, homogeneous formulations for Pr_t were used to examine their efficacy for modeling stratified wall-bounded flows. Results from numerical simulations showed deficiency of these formulations.

CHAPTER 6

Conclusions

6.1. Summary of the Study

There have been various studies for describing and modeling wall-bounded flows. However, there is a great deal of ambiguity about wall-bounded flows and the efficacy of available RANS schemes especially in the presence of stratifications for modeling such flows. This study focuses on how the solid wall affects the turbulence, particularly in the near-wall region and in the presence of stratification. Also, some models which can be appropriate for simulating such flows are introduced.

In this dissertation, wall-bounded flow turbulence is studied using analytical arguments as well as performing one-dimensional numerical simulations for both unstratified and stably stratified wall-bounded turbulent flows. The results are presented in chapters 3, 4 and 5.

In chapter 3, we have used the equilibrium assumption (i.e. $P \approx \epsilon$) to study near-wall turbulence of an unstratified flow. Using dimensional analysis, the relevant scales of the flow in the context of the turbulent-viscosity hypothesis were derived. Also, the effect of the equilibrium assumption which is widely used for deriving the turbulent viscosity (ν_t) in RANS closure schemes was revisited by using theoretical discussions. It was shown that assuming equilibrium results in failure of such models for simulating near-wall turbulence. Different DNS and experimental datasets of unstratified wall-bounded turbulent flows were used to perform *'a priori'* tests to examine the validity of the propositions.

In chapter 4, the turbulent mixing in a stably stratified channel flow was studied. Again, the equilibrium assumption was used to analyze the turbulent mixing in a stably stratified turbulent channel flow. The turbulent viscosity and diffusivity were revisited and also the efficiency of the turbulent mixing in stably stratified wall-bounded flows was investigated. *'A priori'* tests were performed by using stably stratified channel flow DNS data.

Numerical modeling of stably stratified wall-bounded turbulent flows was performed in chapter 5. The efficacy of commonly used homogeneous turbulent Prandtl numbers for

modeling stratified flows was assessed. Analytical discussions were made to propose a suitable Pr_t for wall-bounded flows and its efficacy was tested by implementing RANS simulations. Also, the buoyancy parameter ($C_{\epsilon 3}$) in the standard k-ϵ model was revisited.

6.2. Main Conclusions

The following is a brief description of the important results obtained from this study:

- Using the equilibrium assumption to analyze unstratified near-wall turbulence showed that the relevant length scale of turbulent flow in the context of the turbulent-viscosity hypothesis (TVH) is $L_S = L_c = (\epsilon/S^3)^{1/2}$. Also, it was shown that the relevant time scale is $T_S = 1/S$. This is in contrary to the common assumption in most turbulence models which use $T_L = k/\epsilon$ as the time scale.
- Analyzing the consequences of assuming equilibrium showed that turbulent viscosities which are based on the equilibrium assumption as well as the turbulent kinetic energy (k) are not suitable for modeling near-wall turbulence. The ν_t formulation of the standard k-ϵ closure scheme is a good example of such turbulent viscosities. The analyses revealed that the characteristic scales embedded in the turbulent viscosity of such models are only comparable with the exact scales of the flow in the context of TVH, when equilibrium holds. The results also showed that the normal velocity fluctuation ($\overline{w'^2}^{1/2}$) is a more appropriate velocity scale than $k^{1/2}$ to describe near-wall turbulence.
- Assessing the turbulent mixing in stably stratified wall-bounded flows showed that it is suitable to assume $P \approx \epsilon + \epsilon_{PE}$ which implies that the transport terms are substantially impeded by the presence of stable stratification. Using channel flow DNS data, it is shown that the flux Richardson number (R_f) is almost equal to an irreversible flux Richardson number (R_f^*), when the mean shear rate is dominant. However, it is shown that assuming equilibrium between the buoyancy flux (B) and the dissipation rate of the turbulent potential energy (ϵ_{PE}) as $-B \approx \epsilon_{PE}$ is not as valid as assuming $P \approx \epsilon + \epsilon_{PE}$ in stably stratified wall-bounded flows.

- Numerical simulations showed that homogeneous turbulent Prandtl numbers are not suitable for modeling wall-bounded stratified flows. Theoretical analysis as well as numerical simulations showed that a correction of $(1 - z/D)$ has to be made to homogeneous turbulent Prandtl number formulations in wall-bounded flows. Also, by analyzing the transport equations of the standard k-ϵ in conjunction with numerical modeling results of stably stratified channel flow, it is found that $C_{\epsilon 3} \approx 0$.

6.3. Suggestions for Future Research

The results discussed in this dissertation are limited to smooth-wall turbulent flows. In such flows, the drag is existing due to friction while the form drag is absent. Hence, the next logical (but complicated) step is to extend the present study to rough-wall turbulent flows.

Also, modeling stratified near-wall flow could be a useful extension of this work. An appropriate model can be sought in the context of the model of Durbin (1991) to simulate stratified near-wall turbulence.

Moreover, all the results in this dissertation are constrained to stationary flows where the flow is invariant with the change of time. However, most of the flows in nature are dynamic in time. While seeking and analyzing some exact DNS channel flow data for time-varying flows as well as introducing models that are capable of correctly changing with time might look too ambitious, it is definitely a very valuable work which could change our perception of wall-bounded turbulence.

Finally, there is much more to explore about the turbulent mixing by using the equilibrium assumption. This study has built the foundation for investigating the equilibrium assumption by focusing on a pressure-driven stratified flow over a smooth wall. More sophisticated LES and DNS works can be used to explore turbulent mixing in the vicinity of solid wall such as investigating the turbulent mixing arising from breaking of internal waves when interacting with undersea ridges. For such flows, near-wall turbulence and turbulent mixing can be investigated and the validity of invoking the equilibrium assumption needs to be verified.

References

Adkins, J. F., McIntyre, K., & Schrag, D. P. 2002. The salinity, temperature, and δ^{18}O of the glacial deep ocean. *Science*, **298**, 1769–1773.

Aguilar, D. A., & Sutherland, B. R. 2006. Internal wave generation from rough topography. *Phys. Fluids*, **18**, 066603.

Armenio, V., & Sarkar, S. 2002. An investigation of stably stratified turbulent channel flow using large-eddy simulation. *J. Fluid Mech.*, **459**, 1–42.

Armi, L., & Farmer, D. M. 1988. The flow of Atlantic water through the Strait of Gibraltar. *Prog. Ocean.*, **21**, 1–103.

Arya, S. P. S. 1975. Buoyancy effects in a horizontal flat-plate boundary layer. *J. Fluid Mech.*, **68**, 321–343.

Barad, M. F., & Fringer, O. B. 2010. Simulations of shear instabilities in interfacial gravity waves. *J. Fluid Mech.*, **644**, 61–95.

Barrett, T. K., & Van Atta, C. W. 1991. Experiments on the inhibition of mixing in stably stratified decaying turbulence using laser Doppler anemometry and laser-induced fluorescence. *Phys. Fluids*, **3**, 1321–1332.

Baum, E., & Caponi, E. A. 1992. Modeling the effects of buoyancy on the evolution of geophysical boundary layers. *J. Geophys. Res.: Oceans*, **97**, 15513–15527.

Baumert, H., & Peters, H. 2000. Second-moment closures and length scales for weakly stratified turbulent shear flows. *J. Geophys. Res.: Oceans*, **105**, 6453–6468.

Bouruet-Aubertot, P., Koudella, C., Staquet, C., & Winters, K. B. 2001. Particle dispersion and mixing induced by breaking internal gravity waves. *Dyn. Atm. Oceans*, **33**, 95–134.

Briggs, D. A., Ferziger, J. H., Koseff, J. R., & Monismith, S. G. 1998. Turbulent mixing in a shear-free stably stratified two-layer fluid. *J. Fluid Mech.*, **354**, 175–208.

Burchard, H. 2002. *Applied turbulence modelling in marine waters*. Vol. 100. Springer.

Burchard, H., & Baumert, H. 1995. On the performance of a mixed-layer model based on the k-ϵ turbulence closure. *J. Geophys. Res.: Oceans*, **100**, 8523–8540.

Burchard, H., & Bolding, K. 2001. Comparative analysis of four second-moment turbulence closure models for the oceanic mixed layer. *J. Phys. Ocean.*, **31**, 1943–1968.

Burchard, H., & Petersen, O. 1999. Models of turbulence in the marine environment-A comparative study of two-equation turbulence models. *J. Mar. Sys.*, **21**, 29–53.

Burchard, H., Petersen, O., & Rippeth, T. P. 1998. Comparing the performance of the Mellor-Yamada and the k-ϵ two-equation turbulence models. *J. Geophys. Res.: Oceans*, **103**, 10543–10554.

Canuto, V. M., Howard, A., Cheng, Y., & Dubovikov, M. S. 2001. Ocean turbulence. Part I: One-point closure model-momentum and heat vertical diffusivities. *J. Phys. Ocean.*, **31**.

Casulli, V., & Cattani, E. 1994. Stability, accuracy and efficiency of a semi-implicit method for three-dimensional shallow water flow. *Comp. Math. App.*, **27**, 99–112.

Chen, C., Hsu, J. R., Cheng, M., & Chen, C. 2008. Experiments on mixing and dissipation in internal solitary waves over two triangular obstacles. *Env. Fluid Mech.*, **8**, 199–214.

Corrsin, S. 1958. Local isotropy in turbulent shear flow. *NACA*, **RM 58B11**, 1–15.

Crimaldi, J. P., Koseff, J. R., & Monismith, S. G. 2006. A mixing-length formulation for the turbulent Prandtl number in wall-bounded flows with bed roughness and elevated scalar sources. *Phys. Fluids*, **18**, 095102.

Daly, B. J. 1967. Numerical study of two fluid Rayleigh-Taylor instability. *Phys. Fluids*, **10**, 297.

Deardorff, J. W. 1970. A numerical study of three-dimensional turbulent channel flow at large Reynolds numbers. *J. Fluid Mech.*, **41**, 453–480.

del Álamo, J. C., Jiménez, J., Zandonade, P., & Moser, R. D. 2004. Scaling of the energy spectra of turbulent channels. *J. Fluid Mech.*, **500**, 135–144.

Dimotakis, P. E. 2005. Turbulent mixing. *Annu. Rev. Fluid Mech.*, **37**, 329–356.

Durbin, P. A. 1991. Near-wall turbulence closure modeling without damping functions. *Theoret. Comput. Fluid Dyn.*, **3**, 1–13.

Durbin, P. A., & Pettersson Reif, B. A. 2011. *Statistical Theory and Modeling for Turbulent Flows*. John Wiley and Sons.

Eckart, C. 1948. An analysis of the stirring and mixing processes in incompressible fluids. *J. Mar. Res.*, **7**, 265–275.

Eckelmann, H. 1974. The structure of the viscous sublayer and the adjacent wall region in a turbulent channel flow. *J. Fluid Mech.*, **65**, 439–459.

Ellison, T. H. 1957. Turbulent transport of heat and momentum from an infinite rough plane. *J. Fluid Mech.*, **2**, 456.

Eriksen, C. C. 1985. Implications of ocean bottom reflection for internal wave spectra and mixing. *J. Phys. Ocean.*, **15**, 1145–1156.

Fringer, O. B., & Street, R. L. 2003. The dynamics of breaking progressive interfacial waves. *J. Fluid Mech.*, **494**, 319–353.

Fritts, D. C., Wang, L., Werne, J., Lund, T., & Wan, K. 2009a. Gravity wave instability dynamics at high Reynolds numbers. Part I: Wave field evolution at large amplitudes and high frequencies. *J. Atm. Sci.*, **66**, 1126–1148.

Fritts, D. C., Wang, L., Werne, J., Lund, T., & Wan, K. 2009b. Gravity wave instability dynamics at high Reynolds numbers. Part II: Turbulence evolution, structure, and anisotropy. *J. Atm. Sci.*, **66**, 1149–1171.

Gad-el-Hak, M., & Bandyopadhyay, P. R. 1994. Reynolds number effects in wall-bounded turbulent flows. *Appl. Mech. Rev.*, **47**, 307–365.

Galperin, B., Kantha, L. H., Hassid, S., & Rosati, A. 1988. A quasi-equilibrium turbulent energy model for geophysical flows. *J. Atm. Sci.*, **45**, 55–62.

Galperin, B., Sukoriansky, S., & Anderson, P. S. 2007. On the critical Richardson number in stably stratified turbulence. *Atm. Sci. Lett.*, **8**, 65–69.

García-Villalba, M., & del Álamo, J. C. 2011. Turbulence modification by stable stratification in channel flow. *Phys. Fluids*, **23**, 045104.

Garg, R. P., Ferziger, J. H., Monismith, S. G., & Koseff, J. R. 2000. Stably stratified turbulent channel flows. I. Stratification regimes and turbulence suppression mechanism. *Phys. Fluids*, **12**, 2569.

Garrett, C., & Gilbert, D. 1988. *Estimates of vertical mixing by internal waves reflected off a sloping bottom.* Elsevier.

George, W. K. 2007. Is there a universal log law for turbulent wall-bounded flows? *Phil. Trans. R. Soc. A*, **365**, 789–806.

Germano, M., Piomelli, U., Moin, P., & Cabot, W. H. 1991. A dynamic subgrid-scale eddy viscosity model. *Phys. Fluids*, **3**, 1760.

Gossard, E. 1990. Radar research on the atmospheric boundary layer. *Radar in meteorology(A 90-39376 17-47). Boston, MA, American Meteorological Society, 1990*, 477–527.

Gregg, M. C. 1987. Diapycnal mixing in the thermocline: A review. *J. Geophys. Res.: Oceans*, **92**, 5249–5286.

Gullbrand, J., & Chow, F. K. 2003. The effect of numerical errors and turbulence models in large-eddy simulations of channel flow, with and without explicit filtering. *J Fluid Mech.*, **495**, 323–341.

Hanjalić, K., & Launder, B. E. 1976. Contribution towards a Reynolds-stress closure for low-Reynolds-number turbulence. *J. Fluid Mech.*, **74**, 593–610.

Helfrich, K. R. 1992. Internal solitary wave breaking and run-up on a uniform slope. *J. Fluid Mech.*, **243**, 133–133.

Hossain, M. S. 1980. *Mathematische Modellierung von turbulenten Auftriebsströmungen.* Ph.D. thesis, Univ. Karlsruhe, Germany.

Howard, L. N. 1961. Note on a paper of John W. Miles. *J. Fluid Mech.*, **10**, 509–512.

Hoyas, S., & Jiménez, J. 2006. Scaling of the velocity fluctuations in turbulent channels up to $Re_\tau = 2003$. *Phys. Fluids*, **18**, 011702.

Hult, E. L., Troy, C. D., & Koseff, J. R. 2011a. The mixing efficiency of interfacial waves breaking at a ridge: 1. Overall mixing efficiency. *J. Geophys. Res.: Oceans*, **116**.

Hult, E. L., Troy, C. D., & Koseff, J. R. 2011b. The mixing efficiency of interfacial waves breaking at a ridge: 2. Local mixing processes. *J. Geophys. Res.: Oceans*, **116**.

Ivey, G. N., & Nokes, R. I. 1989. Vertical mixing due to the breaking of critical internal waves on sloping boundaries. *J. Fluid Mech.*, **204**, 479–500.

Ivey, G. N., Winters, K. B., & Koseff, J. R. 2008. Density stratification, turbulence, but how much mixing? *Ann. Rev. Fluid Mech.*, **40**, 169.

Jiménez, J. 2012. Cascades in wall-bounded turbulence. *Annu. Rev. Fluid Mech.*, **44**, 27–45.

Jiménez, J. 2013. How linear is wall-bounded turbulence? *Phys. Fluids*, **25**, 110814.

Jiménez, J., & Moser, R. D. 2007. What are we learning from simulating wall turbulence? *Phil. Trans. R. Soc. A*, **365**, 715–732.

Jiménez, J., Hoyas, S., Simens, M. P., & Mizuno, Y. 2010. Turbulent boundary layers and channels at moderate Reynolds numbers. *J. Fluid Mech.*, **657**, 335–360.

Jones, M. B., Nickels, T. B., & Marusic, I. 2008. On the asymptotic similarity of the zero-pressure-gradient turbulent boundary layer. *J. Fluid Mech.*, **616**, 195–203.

Jones, W. P., & Launder, B. E. 1972. The prediction of laminarization with a two-equation model of turbulence. *Int. J. Heat Mass Transfer*, **15**, 301–314.

Jones, W. P., & Launder, B. E. 1973. The calculation of low-Reynolds-number phenomena with a two-equation model of turbulence. *Int. J. Heat Mass Transfer*, **16**, 1119–1130.

Kalitzin, G., Medic, G., Iaccarino, G., & Durbin, P. 2005. Near-wall behavior of RANS turbulence models and implications for wall functions. *J. Comput. Phys.*, **204**, 265–291.

Kantha, L. H., & Clayson, C. A. 1994. An improved mixed layer model for geophysical applications. *J. Geophys. Res.: Oceans*, **99**, 25235–25266.

Kao, T. W., Pan, F., & Renouard, D. 1985. Internal solitons on the pycnocline: Generation, propagation, and shoaling and breaking over a slope. *J. Fluid Mech.*, **159**, 19–53.

Karimpour, F., & Venayagamoorthy, S. K. On turbulent mixing in stably stratified wall-bounded flows. *Phys. Fluids*, **Submitted**.

Karimpour, F., & Venayagamoorthy, S. K. A revisit of the equilibrium assumption for predicting near-wall turbulence. *J. Fluid Mech.*, **In Press**.

Karimpour, F., & Venayagamoorthy, S. K. 2013. Some insights for the prediction of near-wall turbulence. *J. Fluid Mech.*, **723**, 126–139.

Karimpour, F, & Venayagamoorthy, SK. 2014. A simple turbulence model for stably stratified wall-bounded flows. *J. Geophys. Res.: Oceans*, **119**, 870–880.

Kawai, S., & Larsson, J. 2012. Wall-modeling in large-eddy simulation: Length scales, grid resolution, and accuracy. *Phys. Fluids*, **24**, 015105.

Kawamura, H., Ohsaka, K., Abe, H., & Yamamoto, K. 1998. DNS of turbulent heat transfer in channel flow with low to medium-high Prandtl number fluid. *Int. J. Heat Fluid Flow*, **19**, 482–491.

Kays, W. M. 1994. Turbulent Prandtl number - where are we? *J. Heat Transfer*, **116**, 284–295.

Kays, W. M., Crawford, M. E., & Weigand, B. 1993. *Convective heat and mass transfer*. Vol. 3. McGraw-Hill New York.

Kim, J., Moin, P., & Moser, R. 1987. Turbulence statistics in fully developed channel flow at low-Reynolds-number. *J. Fluid Mech.*, **177**, 133–166.

Klebanoff, P. S., Tidstrom, K. D., & Sargent, L. M. 1962. The three-dimensional nature of boundary-layer instability. *J. Fluid Mech.*, **12**, 1–34.

Kolmogorov, A. N. 1942. The equations of turbulent motion in an incompressible fluid. *Izvestia Acad. Sci., USSR*, **Phys. 6**, 56–58.

Komori, S., Ueda, H., Ogino, F., & Mizushina, T. 1983. Turbulence structure in stably stratified open-channel flow. *J Fluid Mech.*, **130**, 13–26.

Koudella, C. R., & Staquet, C. 2006. Instability mechanisms of a two-dimensional progressive internal gravity wave. *J. Fluid Mech.*, **548**, 165–196.

Lam, C. K. G., & Bremhorst, K. A. 1981. A modified form of the $k-\epsilon$ model for predicting wall turbulence. *Trans. ASME I: J. Fluids Eng.*, **103**, 456–460.

Laufer, J. 1948. *Investigation of turbulent flow in a two-dimensional channel*. Ph.D. thesis, California Institute of Technology.

Launder, B. E., & Sharma, B. I. 1974. Application of the energy-dissipation model of turbulence to the calculation of flow near a spinning disc. *Lett. Heat Mass Transfer*, **1**, 131–137.

Launder, B. E., & Spalding, D. B. 1972. *Mathematical Models of Turbulence*. Academic Press, New York.

Legg, S. 2004. Internal tides generated on a corrugated continental slope. Part I: Cross-slope barotropic forcing. *J. Phys. Ocean.*, **34**, 156–173.

Legg, S., & Adcroft, A. 2003. Internal wave breaking at concave and convex continental slopes. *J. Phys. Ocean.*, **33**, 2224–2246.

Lewis, D. J. 1950. The instability of liquid surfaces when accelerated in a direction perpendicular to their planes. II. *Proceedings of the Royal Society of London. Series A, Mathematical and Physical Sciences*, 81–96.

Lilly, D. K. 1966. *On the application of the eddy viscosity concept in the inertial sub-range of turbulence*. National Center for Atmospheric Research.

Lilly, D. K., Waco, D. E., & Adelfang, S. I. 1974. Stratospheric mixing estimated from high-altitude turbulence measurements. *J. Applied Meteor.*, **13**, 488–493.

Linden, P. F. 1980. Mixing across a density interface produced by grid turbulence. *J. Fluid Mech.*, **100**, 691–703.

Linden, P. F., & Redondo, J. M. 1991. Molecular mixing in Rayleigh–Taylor instability. Part I: Global mixing. *Phys. Fluids*, **3**, 1269.

Loulou, P., Moser, R. D., Mansour, N. N., & Cantwell, B. J. 1997. Direct numerical simulation of incompressible pipe flow using B-spline spectral method. *NASA Technical Memorandum 89461*, **110436**, 1–144.

Lumley, J. L. 1978. Computational modeling of turbulent flows. *Adv. in Appl. Mech.*, **18**, 123–176.

Maderich, V. S., Konovalov, O. M., & Konstantinov, S. I. 1995. Mixing efficiency and processes of restratification in a stably stratified medium. *Mixing in Geophysical Flows, edited by J. M. Redondo and O. Metais, Int. Cent. for Numer. Methods in Eng., Barcelona, Spain*, 393–401.

Marusic, I., & Perry, A. E. 1995. A wall-wake model for the turbulence structure of boundary layers. Part 2. Further experimental support. *J. Fluid Mech.*, **298**, 389–407.

Marusic, I., McKeon, B. J., Monkewitz, P. A., Nagib, H. M., Smits, A. J., & Sreenivasan, K. R. 2010. Wall-bounded turbulent flows at high Reynolds numbers: Recent advances and key issues. *Phys. Fluids*, **22**, 065103.

Mashayek, A., & Peltier, W. R. 2013. Shear-induced mixing in geophysical flows: Does the route to turbulence matter to its efficiency? *J. Fluid Mech.*, **725**, 216–261.

Mashayek, A., Caulfield, C. P., & Peltier, W. R. 2013. Time-dependent, non-monotonic mixing in stratified turbulent shear flows: Implications for oceanographic estimates of buoyancy flux. *J. Fluid Mech.*, **736**, 570–593.

McEligot, D. M., & Taylor, M. F. 1996. The turbulent Prandtl number in the near-wall region for low-Prandtl-number gas mixtures. *Int. J. Heat Mass Transfer*, **39**, 1287–1295.

McKeon, B. J., Li, J., Jiang, W., Morrison, J. F., & Smits, A. J. 2004. Further observations on the mean velocity distribution in fully developed pipe flow. *J. Fluid Mech.*, **501**, 135–147.

McKeon, B. J., Li, J., Jiang, W., Morrison, J. F., & Smits, A. J. 2004. Further observations on the mean velocity distribution in fully developed pipe flow. *J. Fluid Mech.*, **501**, 135–147.

Mellor, G. L., & Yamada, T. 1982. Development of a turbulence closure model for geophysical fluid problems. *Rev. Geophys. Space Phys.*, **20**, 851–875.

Michallet, H., & Ivey, G. N. 1999. Experiments on mixing due to internal solitary waves breaking on uniform slopes. *J. Geophys. Res.: Oceans*, **104**, 13467–13477.

Miles, J. W. 1961. On the stability of heterogeneous shear flows. *J. Fluid Mech.*, **10**, 496–508.

Moin, P. 2010. *Fundamentals of engineering numerical analysis*. Cambridge University Press.

Moser, R. D., Kim, J., & Mansour, N. N. 1999. Direct numerical simulation of turbulent channel flow up to $Re_\tau = 590$. *Phys. Fluids*, **11**, 943–945.

Moum, J. N., Farmer, D. M., Smyth, W. D., Armi, L., & Vagle, S. 2003. Structure and generation of turbulence at interfaces strained by internal solitary waves propagating shoreward over the continental shelf. *J. Phys. Ocean.*, **33**, 2093–2112.

Munk, W., & Wunsch, C. 1998. Abyssal recipes II: Energetics of tidal and wind mixing. *Deep-Sea Res. Part I*, **45**, 1977–2010.

Munk, W. H., & Anderson, E. R. 1948. Notes on the theory of the thermocline. *J. Mar. Res.*, **3**, 276–295.

Nagib, H. M., & Chauhan, K. A. 2008. Variations of von Kármán coefficient in canonical flows. *Phys. Fluids*, **20**, 101518.

Nakanishi, M. 2001. Improvement of the Mellor–Yamada turbulence closure model based on large-eddy simulation data. *Boundary-layer Meteor.*, **99**, 349–378.

Nieuwstadt, F. T. M. 2005. Direct numerical simulation of stable channel flow at large stability. *Boundary-layer Meteor.*, **116**, 277–299.

Nikuradse, J. 1929. *Untersuchungen über die Strömungen des Wassers in konvergenten und divergenten Kanälen: Aus d. Kaiser Wilhelm-Institut f. Strömungsforschg, Göttingen.* VDI-Verlag.

Oakey, N. S. 1982. Determination of the rate of dissipation of turbulent energy from simultaneous temperature and velocity shear microstructure measurements. *J. Phys. Ocean.*, **12**, 256–271.

Ohya, Y., Neff, D. E., & Meroney, R. N. 1997. Turbulence structure in a stratified boundary layer under stable conditions. *Boundary-Layer Meteor.*, **83**, 139–162.

Osborn, T. R. 1980. Estimates of the local rate of vertical diffusion from dissipation measurements. *J. Phys. Ocean.*, **10**, 83–89.

Osborn, T. R., & Cox, C. S. 1972. Oceanic fine structure. *Geophys. Astrophys. Fluid Dyn.*, **3**, 321–345.

Österlund, J. M., Johansson, A. V., Nagib, H. M., & Hites, M. H. 2000. A note on the overlap region in turbulent boundary layers. *Phys. Fluids*, **12**, 1.

Pardyjak, E. R., Monti, P., & Fernando, H. J. S. 2002. Flux Richardson number measurements in stable atmospheric shear flows. *J. Fluid Mech.*, **459**, 307–316.

Park, N., Lee, S., Lee, J., & Choi, H. 2006. A dynamic subgrid-scale eddy viscosity model with a global model coefficient. *Phys. Fluids*, **18**, 125109.

Pasquero, C., Provenzale, A., & Babiano, A. 2001. Parameterization of dispersion in two-dimensional turbulence. *J. Fluid Mech.*, **439**, 279–303.

Patel, V. C., Rodi, W., & Scheuerer, G. 1985. Turbulence models for near-wall and low-Reynolds-number flows: A review. *AIAA*, **23**, 1308–1319.

Peltier, W. R., & Caulfield, C. P. 2003. Mixing efficiency in stratified shear flows. *Ann. Rev. Fluid Mech.*, **35**, 135–167.

Petersen, M. R., Stewart, G. R., & Julien, K. 2007. Baroclinic vorticity production in protoplanetary disks. II. Vortex growth and longevity. *The Astrophysical Journal*, **658**, 1252.

Pope, S. B. 2000. *Turbulent Flows*. Cambridge University Press.

Rahman, M. M., & Siikonen, T. 2005. An eddy viscosity model with near-wall modications. *Int. J. Numer. Meth. Fluids*, **49**, 975–997.

Reichardt, H. 1938. Messungen turbulenter Schwankungen. *Naturwissenschaften*, **26**, 404–408.

Reynolds, O. 1883. An experimental investigation of the circumstances which determine whether the motion of water shall be direct or sinuous, and of the law of resistance in parallel channels. *Proc. Royal Soc. Lond.*, **35**, 84–99.

Riley, J. J., & Lelong, M. 2000. Fluid motions in the presence of strong stable stratification. *Ann. Rev. Fluid Mech.*, **32**, 613–657.

Rodi, W. 1980. Turbulent models and their application in hydraulics–a state of the art review. *Int. Assoc. Hydr. Res., Delft.*

Rodi, W. 1987. Examples of calculation methods for flow and mixing in stratified fluids. *J. Geophys. Res.: Oceans*, **92**, 5305–5328.

Rodi, W., & Mansour, N. N. 1993. Low-Reynolds-number k-ϵ modelling with the aid of direct numerical simulation data. *J. Fluid Mech.*, **250**, 509–529.

Rohr, J. J., Itsweire, E. C., Helland, K. N., & Atta, C.W. Van. 1988. Growth and decay of turbulence in a stably stratified shear flow. *J. Fluid Mech.*, **195**, 77–111.

Rudnick, D. L., Boyd, T. J., Brainard, R. E., Carter, G. S., Egbert, G. D., Gregg, M. C., Holloway, P. E., Klymak, J. M., Kunze, E., Lee, C. M., Levine, M. D., Luther, D. S., Martin, J. P., Merrifield, M. A., Moum, J. N., Nash, J. D., Pinkel, R., Rainville, L., & Sanford, T. B. 2003. From tides to mixing along the Hawaiian Ridge. *Science*, **301**, 355–357.

s. k. Venayagamoorthy, & Stretch, D. D. 2006. Lagrangian mixing in decaying stably stratified turbulence. *J. Fluid Mech.*, **564**, 197–226.

Sandstrom, H., & Oakey, N. S. 1995. Dissipation in internal tides and solitary waves. *J. Phys. Ocean.*, **25**, 604–614.

Schultz, M. P., & Flack, K. A. 2013. Reynolds-number scaling of turbulent channel flow. *Phys. Fluids*, **25**, 025104.

Schumann, U. 1973. *Ein Verfahren zur direkten numerischen Simulation turbulenter Strömungen in Platten-und Ringspaltkanälen und über seine Anwendung zur Untersuchung von Turbulenzmodellen*. Ph.D. thesis, Univ. Karlsruhe.

Schumann, U., & Gerz, T. 1995. Turbulent mixing in stably stratified shear flows. *J. Appl. Meteor.*, **34**, 33–48.

Sharp, D. H. 1984. An overview of Rayleigh-Taylor instability. *Physica D: Nonlinear Phenomena*, **12**, 3–18.

Sillero, J. A., Jiménez, J., & Moser, R. D. 2013. One-point statistics for turbulent wall-bounded flows at Reynolds numbers up to $\delta^+ \approx 2000$. *Phys. Fluids*, **25**, 105102.

Slinn, D. N., & Riley, J. J. 1996. Turbulent mixing in the oceanic boundary layer caused by internal wave reflection from sloping terrain. *Dyn. Atm. Oceans*, **24**, 51–62.

Smagorinsky, J. 1963. General circulation experiments with the primitive equations: I. The basic experiment. *Monthly Weather Rev.*, **91**, 99–164.

Smits, A. J., McKeon, B. J., & Marusic, I. 2011. High-Reynolds-number wall turbulence. *Ann. Rev. Fluid Mech.*, **43**, 353–375.

Smyth, W. D., & Moum, J. N. 2012. Ocean mixing by Kelvin-Helmholtz instability. *Oceanography*, **25(2)**, 140–149.

Smyth, W. D., Moum, J. N., & Caldwell, D. R. 2001. The efficiency of mixing in turbulent patches: Inferences from direct simulations and microstructure observations. *J. Phys. Ocean.*, **31**.

Sonmor, L. J., & Klaassen, G. P. 1997. Toward a unified theory of gravity wave stability. *J. Atm. Sci.*, **54**, 2655–2680.

Srinivasan, C., & Papavassiliou, D. V. 2010. Prediction of the turbulent Prandtl number in wall flows with Lagrangian simulations. *Ind. Eng. Chem. Res.*, 8881–8891.

Staquet, C., & Bouruet-Aubertot, P. 2001. Mixing in weakly turbulent stably stratified flows. *Dyn. Atm. Oceans*, **34**, 81–102.

Staquet, C., & Sommeria, J. 2002. Internal gravity waves: From instabilities to turbulence. *Ann. Rev. Fluid Mech.*, **34**, 559–593.

Stretch, D. D., Rottman, J. W., Venayagamoorthy, S. K., Nomura, K. K., & Rehmann, C. R. 2010. Mixing efficiency in decaying stably stratified turbulence. *Dyn. Atm. Oceans*, **49**, 25–36.

Strutt, J. W. 1894. The Theory of Sound.

Sutherland, B. R. 2001. Finite-amplitude internal wavepacket dispersion and breaking. *J. Fluid Mech.*, **429**, 343–380.

Sveen, J. K., Guo, Y., Davies, P. A., & Grue, J. 2002. On the breaking of internal solitary waves at a ridge. *J. Fluid Mech.*, **469**, 161–188.

Taylor, G. I. 1950. The instability of liquid surfaces when accelerated in a direction perpendicular to their planes. I. *Proceedings of the Royal Society of London. Series A. Mathematical and Physical Sciences*, **201**, 192–196.

Taylor, J. R., Sarkar, S., & Armenio, V. 2005. Large-eddy simulation of stably stratified open channel flow. *Phys. Fluids*, **17**, 116602.

Thomson, W. 1871. Hydrokinetic solutions and observations. *Proceedings of the Royal Society*, **7**, 63.

Thorpe, S. A. 1971. Experiments on the instability of stratified shear flows: Miscible fluids. *J. Fluid Mech.*, **46**, 299–319.

Townsend, A. A. 1958. The effects of radiative transfer on turbulent flow of a stratified fluid. *J. Fluid Mech.*, **4**, 361–375.

Townsend, A. A. 1961. Equilibrium layers and wall turbulence. *J. Fluid Mech.*, **11**, 97–120.

van Driest, E. R. 1956. On turbulent flow near a wall. *J. Aero. Sci.*, **23**, 1007–1011.

Venayagamoorthy, S. K., & Fringer, O. B. 2012. Examining breaking internal waves on a shelf slope using numerical simulations. *Oceanography*, **25**, 132–139.

Venayagamoorthy, S. K., & Stretch, D. D. 2010. On the turbulent Prandtl number in homogeneous stably stratified turbulence. *J. Fluid Mech.*, **644**, 359–369.

von Helmholtz, H. L. F. 1868. On discontinuous movements of fluids. *The London, Edinburgh, and Dublin Philosophical Magazine and Journal of Science*, **36**, 337–346.

Vreman, A. W. 2004. An eddy-viscosity subgrid-scale model for turbulent shear flow: Algebraic theory and applications. *Phys. Fluids*, **16**, 3670.

W. L. Hydraulics Delft. 1999. *Delft3D-FLOW user manual*. Delft Hydraulics, Delft, The Netherlands.

Warner, J. C., Sherwood, C. R., Arango, H. G., & Signell, R. P. 2005. Performance of four turbulence closure models implemented using a generic length scale method. *Ocean Model.*, **8**, 81–113.

Webster, C. A. G. 1964. An experimental study of turbulence in a density-stratified shear flow. *J. Fluid Mech.*, **19**, 221–245.

Wilson, J. D. 2012. An Alternative Eddy-Viscosity Model for the Horizontally Uniform Atmospheric Boundary Layer. *Boundary-Layer Meteor.*, **45**, 165–184.

Woods, J. D. 1968. Wave-induced shear instability in the summer thermocline. *J. Fluid Mech.*, **32**, 791–800.

Wu, X., & Moin, P. 2008. A direct numerical simulation study on the mean velocity characteristics in turbulent pipe flow. *J. Fluid Mech.*, **608**, 81–112.

Wüest, A., Piepke, G., & Van Senden, D. C. 2000. Turbulent kinetic energy balance as a tool for estimating vertical diffusivity in wind-forced stratified waters. *Limnol. Ocean.*, **45**, 1388–1400.

Wunsch, C., & Ferrari, R. 2004. Vertical mixing, energy, and the general circulation of the oceans. *Annu. Rev. Fluid Mech.*, **36**, 281–314.

You, D., & Moin, P. 2007. A dynamic global-coefficient subgrid-scale eddy-viscosity model for large-eddy simulation in complex geometries. *Phys. Fluids*, **19**, 065110.

Zagarola, M. V., & Smits, A. J. 1998. Mean-flow scaling of turbulent pipe flow. *J. Fluid Mech.*, **373**, 33–79.

Zanoun, E.-S., Nagib, H., Durst, F., & Monkewitz, P. 2002. Higher Reynolds number channel data and their comparison to recent asymptotic theory. *In: 40th AIAA-1102, Aerospace Sciences Meeting, Reno.*

APPENDIX A

Inference of the Dissipation Rate in Wall-Bounded Turbulence[1]

In this chapter, a novel formulation for ν_t will be proposed. In section A.2, the appropriate scales of the wall-bounded turbulent flow are derived in the context of the turbulent-viscosity hypothesis (TVH) and then the new turbulent viscosity is introduced. Also, *'a priori'* tests are performed to examine the efficacy of the proposed formulation. The results presented in this chapter will be used in future for inference of the dissipation rate of the turbulent kinetic energy.

A.1. Introduction

The turbulent viscosity (ν_t) is commonly used to link the turbulent momentum fluxes ($\overline{u'w'}$) with the mean shear rate as

$$\nu_t = \frac{-\overline{u'w'}}{d\overline{U}/dz}, \tag{170}$$

where $\overline{U}$ is the mean streamwise velocity and z is the normal distance from the wall. As discussed in section 3.1, Karimpour & Venayagamoorthy (2013) assumed equilibrium between the rates of production (P) and dissipation (ϵ) of the turbulent kinetic energy (k) for a turbulent wall-bounded flow (i.e. $P \approx \epsilon$) and proposed the turbulent viscosity (ν_t) as

$$\nu_t \approx \epsilon / S^2. \tag{171}$$

This proposed formulation for the turbulent viscosity (ν_t) has shown excellent agreement with the exact turbulent viscosity (ν_t) calculated from DNS data for different types of wall-bounded flows. Furthermore, as we previously discussed, by using the turbulent-viscosity

[1]The results presented in this chapter will be submitted in substantial part as "A methodology for inference of the dissipation rate in wall-bounded turbulent flows" by F. Karimpour, J. M. Wilson and S. K. Venayagamoorthy, to *Physics of Fluids*. This chapter is written in a collective "we" tense to acknowledge collaborative work with the co-authors. Jordan M. Wilson contributed by providing some constructive discussions.

hypothesis (TVH), ν_t can be recast in terms of velocity (U_{TVH}), length (L_{TVH}) and time (T_{TVH}) scales as

$$\nu_t = U_{TVH} L_{TVH} = U_{TVH}^2 T_{TVH} = L_{TVH}^2 / T_{TVH}. \tag{172}$$

Pope (2000) suggested $U_{TVH} = (-\overline{u'w'})^{1/2}$, which implies $L_{TVH} = (-\overline{u'w'})^{1/2}/S$ and $U_{TVH} = 1/S$. Once again, using the equilibrium assumption, Karimpour & Venayagamoorthy (2013) deduced the pertinent scales of velocity (U_S), length (L_S) and time (T_S), given by

$$U_{TVH} \approx U_s = \left(\frac{\epsilon}{S}\right)^{1/2}, \tag{173}$$

$$L_{TVH} \approx L_s = \left(\frac{\epsilon}{S^3}\right)^{1/2}, \tag{174}$$

$$T_{TVH} = T_s = \frac{1}{S}. \tag{175}$$

L_S is the Corrsin scale introduced by Corrsin (1958) and is the smallest eddy deformed by the mean shear rate (S). This scale is the upper end of the inertial subrange and could be considered as a length scale for equilibrium (i.e. $L_S = L_{TVH}$ where $P = \epsilon$). As shown in Figure (A.1), the propositions by Karimpour & Venayagamoorthy (2013) compare remarkably well with the exact DNS data. Note that 'the plus sign' ("+") denotes non-dimensionalized quantities, where the non-dimensional turbulent viscosity is $\nu_t^+ = \nu_t/\nu$, the non-dimensional velocity scale is $U_{TVH}^+ = U_{TVH}/u_\tau$ and the normalized length scale is $L_{TVH}^+ = L_{TVH}/(\nu/u_\tau)$, with u_τ defined as the friction velocity. While the propositions of Karimpour & Venayagamoorthy (2013) compare well with DNS results using *'a priori'* tests, it ignores the prevailing transport terms in the near-wall region which implies that the nonlinear behavior of P/ϵ is neglected.

In this chapter, our main goal is to introduce a novel proposition for ν_t which is able to properly capture the P/ϵ behavior in the near-wall turbulence. In section A.2, we discuss

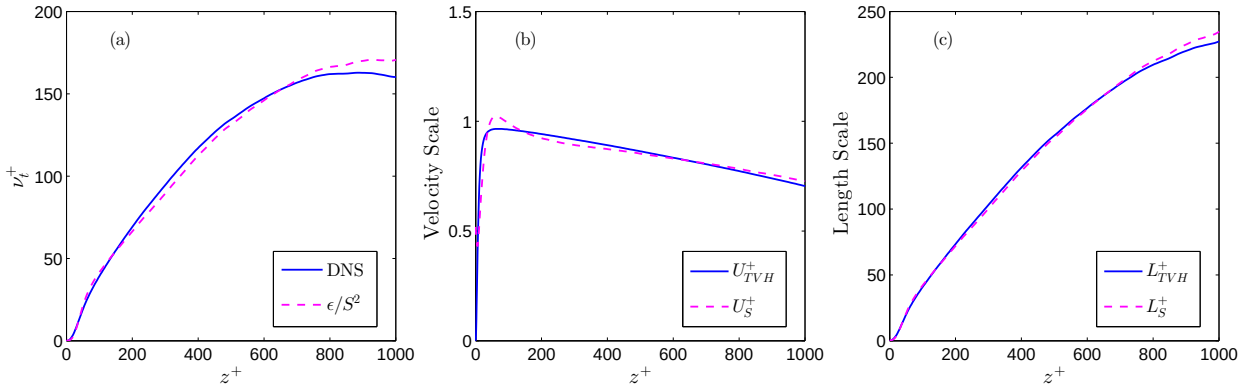

FIGURE A.1. Comparison of (a) the turbulent viscosity from equation (171); (b) U_S; and (c) L_S with the exact ν_t, U_{TVH} and L_{TVH} in a turbulent channel flow at Re_τ=2003, computed from the DNS data of Hoyas & Jiménez (2006).

the near-wall region behavior and propose appropriate scales in the context of the turbulent-viscosity hypothesis (TVH), using the insights provided by Karimpour & Venayagamoorthy (2013). Furthermore, we develop an appropriate turbulent viscosity (ν_t) for the near-wall region which captures the correct behavior of P/ϵ. *'A priori'* tests are performed to verify the propositions using channel flow DNS datasets of Moser *et al.* (1999) for $Re_\tau \approx 395$ and 590, del Álamo *et al.* (2004) for $Re_\tau \approx 950$ and Hoyas & Jiménez (2006) for $Re_\tau \approx 2003$, where $Re_\tau = u_\tau \delta/\nu$ is the friction Reynolds number and δ is half of the channel depth. Finally, conclusions are given in section A.3.

A.2. Parameterization of the Turbulent Viscosity

In this section, we discuss the appropriate scales suitable for describing the wall-bounded turbulent flows. We also introduce an appropriate turbulent viscosity (ν_t) for modeling near-wall turbulence. Furthermore, *'a priori'* tests using DNS data are performed to validate our propositions.

A.2.1. Relevant Characteristic Scales. As discussed, Karimpour & Venayagamoorthy (2013) invoked the equilibrium assumption (i.e. $P \approx \epsilon$) to introduce the turbulent viscosity as $\nu_t = \epsilon/S^2$ and derive the relevant scales. Although their propositions provide valuable insights for describing the turbulent near-wall region, it is clear that equilibrium

does not hold between P and ϵ in the near-wall region. To this end, we need to modify the velocity and the length scales to obtain an appropriate turbulent viscosity (ν_t) that captures the correct behavior of P/ϵ in the near-wall region. Since modification of both scales is difficult, we focus our efforts on recasting the most dominant scale in the turbulent viscosity (ν_t). For this purpose, we evaluate the ratio of the non-dimensional (normalized) length scale to velocity scale. The ratio of L^+_{TVH}/U^+_{TVH} is given by

$$\frac{L^+_{TVH}}{U^+_{TVH}} = \frac{(-\overline{u'w'}^{1/2}/S)/(\nu/u_\tau)}{-\overline{u'w'}^{1/2}/u_\tau} = \frac{L^+_S}{U^+_S} = \frac{(\epsilon/S^3)^{1/2}/(\nu/u_\tau)}{(\epsilon/S)^{1/2}/u_\tau} = \frac{u_\tau^2}{\nu}\frac{1}{S} = \frac{1}{S^+}. \tag{176}$$

S^+ is the non-dimensional (normalized) mean shear rate and it can be shown that for a fully developed channel flow it lies in the range of $0 \leq S^+ \leq 1$, with $S^+ = 1$ at the wall (i.e. $z = 0$) and $S^+ = 0$ at the channel mid-depth (Pope 2000). It is obvious from equation (176) that the length scale is the dominant scale and is much larger than the velocity scale. Consequently, it is much more important to modify the proposed length scale (L_S) introduced by Karimpour & Venayagamoorthy (2013) than their velocity scale (U_S). This fact is also presented in Figure (A.2) which shows that the ratio of these two scales (i.e. L^+_{TVH}/U^+_{TVH}) rapidly grows with distance from the wall. Here, $z^+ = zu_\tau/\nu$ is the wall unit.

Now, in order to modify L_S, we first start by considering the linear distribution of the shear stress (τ). To infer the linear shear stress distribution, it is required to consider the streamwise RANS momentum equation of the fully developed wall-bounded turbulent flow, which is given by

$$0 = -\frac{\partial \overline{p}}{\partial x} + \rho\frac{\partial}{\partial z}\left(\nu\frac{\partial \overline{U}}{\partial z}\right) - \rho\frac{\partial(\overline{u'w'})}{\partial z}, \tag{177}$$

where $\overline{p}$ is the mean pressure, x denotes the streamwise direction and ρ is the fluid density. From the cross-stream RANS momentum equation, it can be shown that the mean pressure ($\overline{p}$) is independent of z (George 2007) and its streamwise gradient is uniform (invariant) across the flow depth (i.e. $\partial\overline{p}/\partial x = \partial\overline{p}_w/\partial x = c$, where c is a constant and 'w' denotes the value of the variable at the wall). As the flow has no acceleration, the pressure forces are balanced by the shear forces, which implies that $\partial\overline{p}/\partial x = \partial\tau/\partial z$ with τ defined as the total

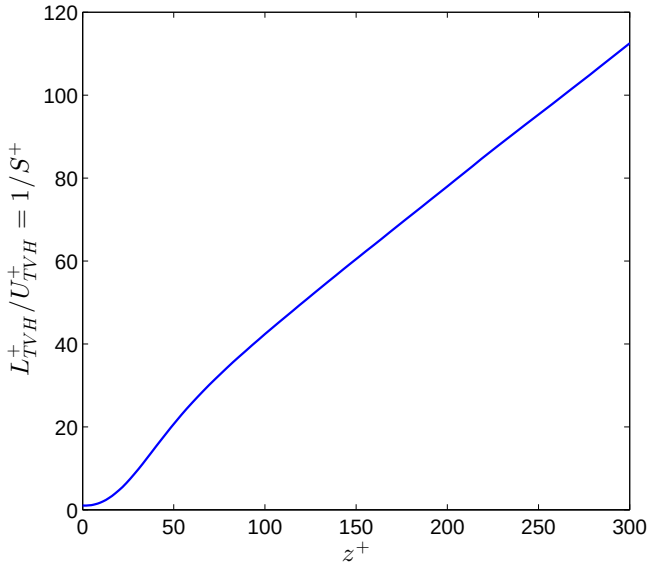

FIGURE A.2. Ratio of L^+_{TVH}/U^+_{TVH} in a turbulent channel flow at Re_τ=2003, computed from the DNS data of Hoyas & Jiménez (2006).

shear stress at a given level z. Hence, equation (177) can be recast as

$$\frac{\partial \tau}{\partial z} = \rho \frac{\partial}{\partial z}\left(\nu \frac{\partial \overline{U}}{\partial z}\right) - \rho \frac{\partial(\overline{u'w'})}{\partial z}. \tag{178}$$

Integrating equation (178) with respect to z, the shear stress distribution can be derived as

$$\tau = \rho \nu S - \rho \overline{u'w'}. \tag{179}$$

It can be deduced from equation (179) that $\tau = \tau_w$ at the wall ($z = 0$) and $\tau = 0$ in the free-stream ($z = \delta$). Therefore, knowing that the pressure gradient is linear in the streamwise direction, this implies that $\partial\overline{p}/\partial x = \partial\overline{p}_w/\partial x = \partial\tau/\partial z = -\tau_w/\delta$. Consequently, the linear shear stress distribution can be inferred as

$$\tau = \tau_w \left(1 - \frac{z}{\delta}\right) = \rho u_\tau^2 \left(1 - \frac{z}{\delta}\right). \tag{180}$$

Now, let us first focus on recasting the length scale in the log-law region. In the log-law region and beyond, the viscous effects are negligible and the shear stress distribution

equation can be simplified as

$$-\overline{u'w'} \approx u_\tau^2 \left(1 - \frac{z}{\delta}\right). \tag{181}$$

Using equation (181), $L_{TVH} = (-\overline{u'w'})^{1/2}/S$ can be rearranged as

$$L_{TVH} = \frac{-\overline{u'w'}^{1/2}}{S} \approx L_P = \frac{u_\tau}{S}\left(1 - \frac{z}{\delta}\right)^{0.5}. \tag{182}$$

From the standard logarithmic velocity profile for a smooth-wall flow, we know that $U^+ = (1/\kappa)\ln(z^+) + B$, where $U^+ = \overline{U}/u_\tau$, κ is the von Kármán empirical constant normally assumed to be universal and B is a constant independent of the Reynolds number (McKeon *et al.* 2004). This logarithmic velocity profile is inferred from the asymptotic matching of the inner and outer layers in a fully developed wall-bounded flow (Nagib & Chauhan 2008). In the logarithmic velocity profile formulation, it is conventionally assumed that $\kappa \approx 0.40 - 0.41$ for smooth-wall flows. However, the precise value of κ remains unsettled. For example Österlund *et al.* (2000) suggested that $\kappa = 0.38$, Zagarola & Smits (1998) indicated that $\kappa = 0.436 \pm 0.002$, Zanoun *et al.* (2002) suggested $\kappa = 0.379$ and McKeon *et al.* (2004) argued that $\kappa = 0.421 \pm 0.002$ (A complete list of different values for κ is provided in the work of Marusic *et al.* 2010). However, using the logarithmic velocity profile, the mean shear rate (S) is given by $S = u_\tau/\kappa z$, which implies that κ is the slope of u_τ/S when plotted versus depth (z). Using this mean shear rate (S), equation (182) can be rewritten as

$$L_{TVH} \approx L_P \approx L_{\log} = \kappa z \left(1 - \frac{z}{\delta}\right)^{0.5}. \tag{183}$$

Exquisite attention has been paid to the logarithmic velocity profile and it is shown to have minor quantitative difference from the exact mean streamwise velocity. However, it appears that not much emphasis has been given to investigate the effects of the logarithmic velocity formulation on the predictions of the mean shear rate as well as turbulence scales. It is more insightful when we note that even a slight error in predicting mean shear rate (S) could result in significant differences in the prediction of L_{TVH} (i.e. L_P) and consequently ν_t.

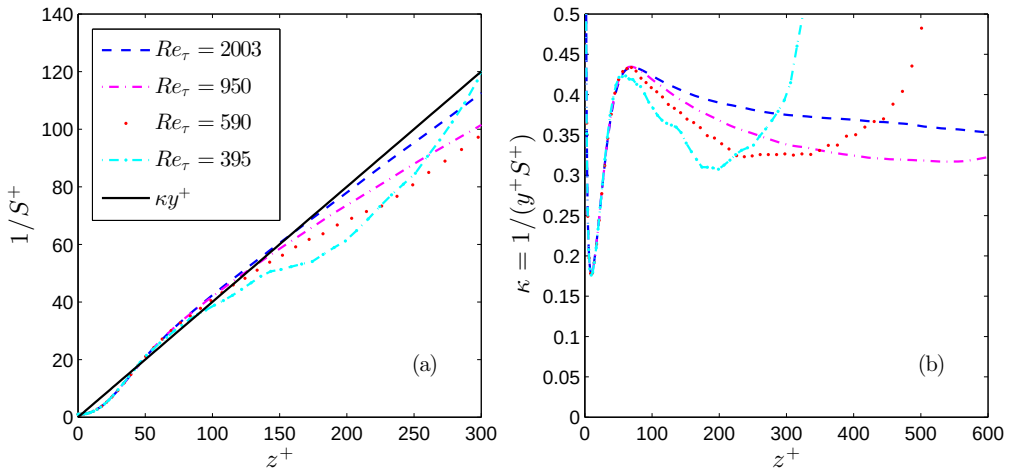

FIGURE A.3. (a) Comparison of $1/S$ from log-law with the exact $1/S$; and (b) estimation of $\kappa = 1/(S^+z^+) = u_\tau/Sz$ in a turbulent channel flow at Re_τ=2003, 950, 590 and 395, computed from the DNS data.

In order to assess the validity of the logarithmic mean shear rate ($S = u_\tau/\kappa z$), $1/S^+ = \kappa z^+$ which is inferred from log-law is compared with the inverse of the non-dimensional exact mean shear rates ($1/S^+$) using different channel flow DNS data. These mean shear rates are plotted versus wall unit (z^+) in Figure (A.3a). It is obvious from Figure (A.3a) that assuming $1/S = \kappa z/u_\tau$ only holds in the beginning of the log-law region (linear part of Figure A.3a). This clearly shows that the logarithmic region exists in a very narrow region of the flow depth, which is usually considered to extend up to 30% of the channel depth from the wall. The comparison gets worse with distance from the wall which underscores the doubt that the logarithmic velocity profile is not a fair estimation. This issue is often overlooked by only comparing with the velocity profile instead of the mean shear rate (S). Furthermore, it can be noticed that with the increase of the Reynolds number, the region of agreement between the exact $1/S$ and $\kappa z/u_\tau$ shrinks, such that for $Re_\tau = 590$ it is almost 1/6 of the flow depth from $z^+ \approx 35$ to $z^+ \approx 125$, while for $Re_\tau = 2003$ the agreement holds in almost 1/15 of the flow depth, only from $z^+ \approx 35$ to $z^+ \approx 175$.

Using the logarithmic velocity profile, the von Kármán constant can be inferred as $\kappa = u_\tau/Sz = 1/(S^+z^+)$. As shown by Hoyas & Jiménez (2006) and George (2007) and can also be seen in Figure (A.3b), κ is not a constant value even in the so-called log-law region which

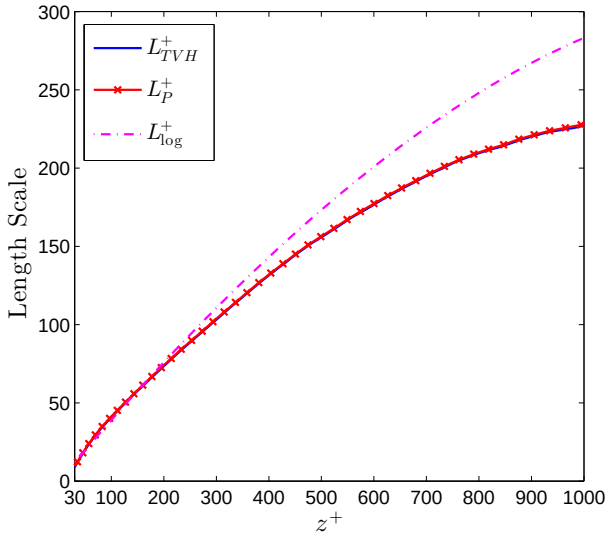

FIGURE A.4. Comparison of L_{TVH} with L_P and $L_{\log}$ in a turbulent channel flow at Re_τ=2003, computed from the DNS data of Hoyas & Jiménez (2006).

significantly varies over the flow depth. Overall, Figures (A.3 a,b) question the existence of a logarithmic region as well as a constant κ.

Furthermore, in order to elucidate the effect of the mean shear rate on predicting L_{TVH}, Figure (A.4) compares L_P introduced in equation (182) using the exact mean shear rate (S) computed from the DNS data and $L_{\log}$ introduced in equation (183) with L_{TVH}. Figure (A.4) shows that $L_{\log}$ hugely overpredicts L_{TVH} which is expected due to the incorrect estimation of the mean shear rate (S) from the logarithmic velocity profile.

In order to resolve this shortcoming, the most straightforward solution is to empirically modify $(1 - z/\delta)^{\alpha=0.5}$. To this end, we have modified the exponent α using different sets of channel flow DNS data with $Re_\tau = 590, 950$ and 2003 as shown in Figure (A.5). It is seen that using $\alpha \approx 0.75$-0.85 results in a good estimation of the modified length scale introduced as $L_{\kappa^*} = \kappa z(1 - z/\delta)^\alpha$. In this study, we have used $\alpha = 0.85$.

In the near wall-region where $z \to 0$, the proposed length scale $L_{\kappa^*} \to \kappa z$, which is well-known as Prandtl's mixing length (Pope 2000). In the near-wall region ($z^+ \leq 30$), this length scale overpredicts the length scale L_{TVH}. To overcome this shortcoming, van Driest (1956) argued that the wall has damping effects and hence the diminished fluid motion can be

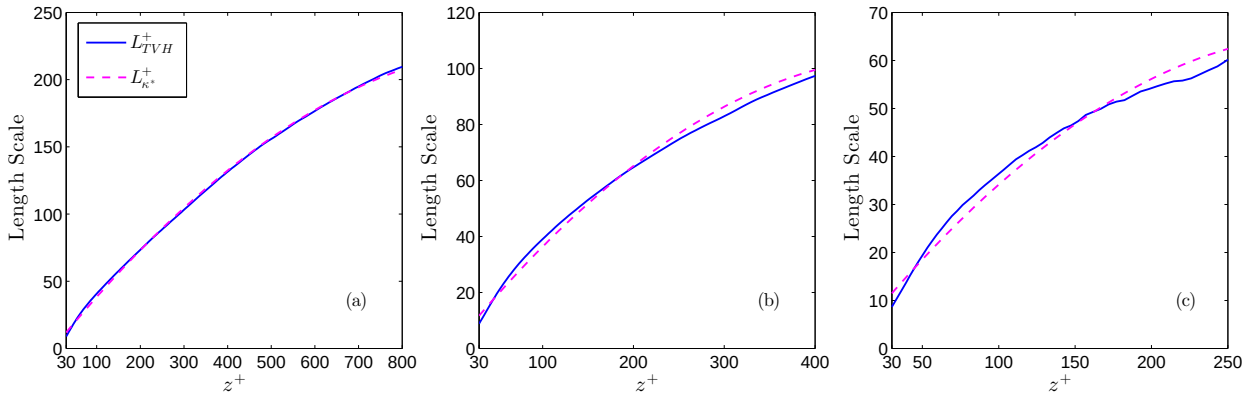

FIGURE A.5. Comparison of L_{TVH} with L_{κ^*} in a turbulent channel flow at: (a) $Re_\tau = 2003$; (b) $Re_\tau = 950$; and (c) $Re_\tau = 590$.

described with an exponential function as $1 - exp(-z^+/A^+)$. Therefore, van Driest (1956) proposed modifying Prandtl's mixing length (κz) in the near-wall region with a damping function (f_μ) given as

$$f_\mu = 1 - exp(-z^+/A^+), \tag{184}$$

where $A^+ \approx 26$. This function is zero at the wall and for $z^+ \gtrsim 100$ asymptotes to unity. Figure (A.6) shows the efficacy of the van Driest damping function (f_μ) in predicting L_{TVH} in the near-wall region for different friction Reynolds numbers of $Re_\tau = 395, 590, 950$ and 2003. It is clear that L_{TVH} is Reynolds-number-independent in the near-wall region and f_μ performs very well in capturing the near-wall length scale. Consequently, L_{κ^*} can be modified as

$$L_\kappa = f_\mu \kappa z \left(1 - \frac{z}{\delta}\right)^{0.85}. \tag{185}$$

Figure (A.7) compares L_κ with L_{TVH} and L_S. Although the difference between L_κ and L_S looks negligible, we shall later show that L_κ is the parameter of choice for modeling the correct behavior of P/ϵ in the near-wall region.

A.2.2. TURBULENT VISCOSITY. Here we extend our discussion and develop the turbulent viscosity (ν_t) using the appropriate scales. As shown in equation (172), the turbulent

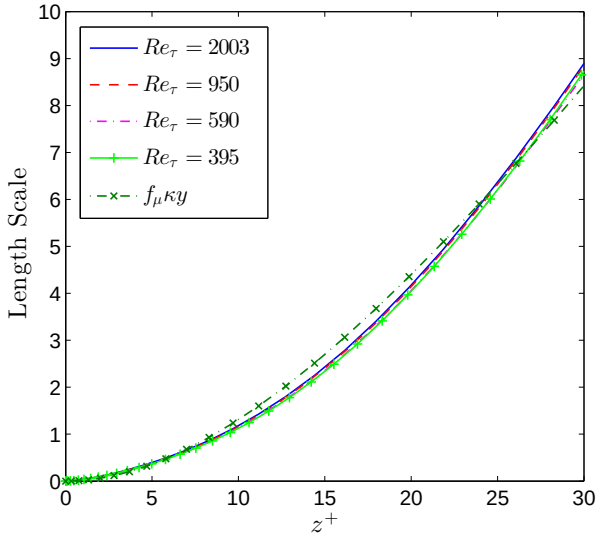

FIGURE A.6. Comparison of $f_\mu \kappa z$ with L_{TVH} in the near-wall region of a turbulent channel flow at Re_τ=2003, 950, 590 and 395, computed from the DNS data.

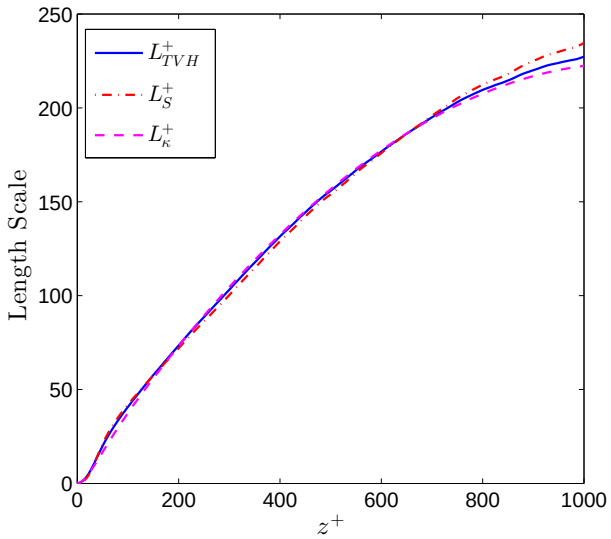

FIGURE A.7. Comparison of L_κ with L_{TVH} and L_S in a turbulent channel flow at Re_τ=2003, computed from the DNS data of Hoyas & Jiménez (2006).

viscosity (ν_t) can be defined as a product of velocity and length scales. Using L_κ introduced in equation (185) and $U_S = (\epsilon/S)^{1/2}$ shown in equation (173), the turbulent viscosity (ν_t)

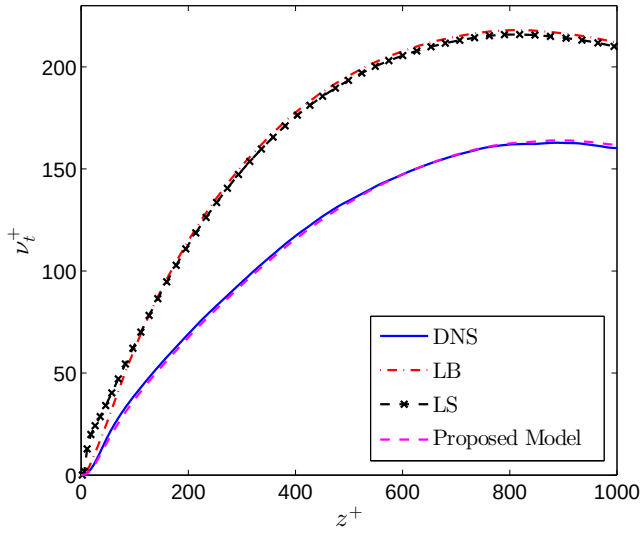

FIGURE A.8. Comparison of the turbulent viscosity (ν_t) from equation (187), formulations of LS and LB with the exact turbulent viscosity (ν_t) in a turbulent channel flow at Re_τ=2003, computed from the DNS data of Hoyas & Jiménez (2006).

can be introduced as

$$\nu_t = L_\kappa U_S = f_\mu \kappa z \left(1 - \frac{z}{\delta}\right)^{0.85} \left(\frac{\epsilon}{S}\right)^{1/2}. \tag{186}$$

Equation (186) can be rearranged in terms of L_κ and L_S as

$$\nu_t = \left(\frac{L_\kappa}{L_S}\right)(L_S U_S) = \left(\frac{L_\kappa}{L_S}\right)\frac{\epsilon}{S^2} = \frac{f_\mu \kappa z \left(1 - z/\delta\right)^{0.85}}{\left(\epsilon/S^3\right)^{1/2}} \left(\frac{\epsilon}{S^2}\right), \tag{187}$$

where ϵ/S^2 is the turbulent viscosity (ν_t) introduced by Karimpour & Venayagamoorthy (2013) using the equilibrium assumption. It is obvious that the turbulent viscosity introduced in equation (171) is modified using the ratio of (L_κ/L_S). Figure (A.8) shows the comparison of the proposed turbulent viscosity presented in equation (187) with the exact turbulent viscosity computed from the channel flow DNS data of Hoyas & Jiménez (2006). Also, the turbulent viscosity of Launder & Sharma (1974) (hereafter LS) and Lam & Bremhorst (1981) (hereafter LB) are presented. It is clear that the proposed model compares remarkably well with the exact ν_t especially in the near-wall region, while both models of LS and LB perform poorly.

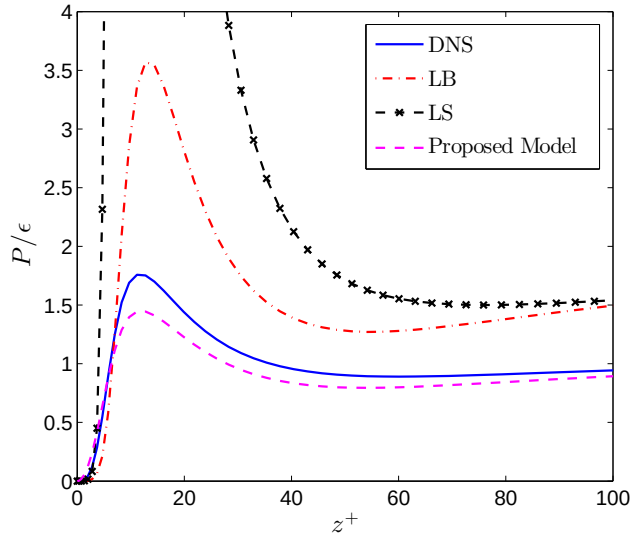

FIGURE A.9. Comparison of P/ϵ calculated by using ν_t introduced in equation (187), formulations of LS and LB with the exact P/ϵ in a turbulent channel flow at Re_τ=2003, computed from the DNS data of Hoyas & Jiménez (2006).

As discussed previously, an appropriate turbulent viscosity (ν_t) for near-wall modeling must be able to yield the correct behavior of P/ϵ in the near-wall region. In order to assess the efficacy of our proposed turbulent viscosity (ν_t), the predicted P/ϵ using the turbulent viscosity in equation (187) as well as formulations of LS and LB are compared with the exact P/ϵ computed from the DNS data of Hoyas & Jiménez (2006). This comparison is presented in Figure (A.9) and as expected the proposed model performs very well while both formulations of LS and LB highly overpredict P/ϵ, especially the model of LS. As a side note, it should be mentioned that the modeled P/ϵ is calculated using the turbulent-viscosity hypothesis (TVH) as

$$\frac{P}{\epsilon} = \frac{-\overline{u'w'}S}{\epsilon} = \frac{\nu_t S^2}{\epsilon} = \left(\frac{L_\kappa}{L_S}\right)\frac{(\epsilon/S^2)S^2}{\epsilon} = \frac{f_\mu \kappa z\left(1-z/\delta\right)^{0.85}}{\left(\epsilon/S^3\right)^{1/2}} = \frac{L_\kappa}{L_S}. \tag{188}$$

Equation (188) implies that the modeled P/ϵ is simply the ratio of L_κ/L_S. Also, it should be noted that the exact P/ϵ can be recast in terms of L_{TVH} and L_S as

$$\frac{P}{\epsilon} = \frac{-\overline{u'w'}S}{\epsilon} = \frac{-\overline{u'w'}/S^2}{\epsilon/S^3} = \left(\frac{L_{TVH}}{L_S}\right)^2. \tag{189}$$

A.3. Concluding Remarks

The aim of this study is to propose a novel turbulent viscosity which can capture the P/ϵ behavior in the near-wall region. To do this, we have employed a theoretical analysis to introduce such a formulation. This is done by deriving the corresponding velocity scale and length scale, using dimensional analysis following the work of Karimpour & Venayagamoorthy (2013). The proposed turbulent viscosity (ν_t) is a product of the proposed scales as $\nu_t = U_s.L_\kappa$.

The length scale is derived by using the linear shear stress distribution and assuming a logarithmic velocity profile. The analysis results in a theoretical length scale of $f_\mu \kappa z(1 - z/\delta)^{0.5}$. However, our study revisits the existence of a logarithmic velocity profile and hence a log-law region in a wall-bounded turbulent flow. Using different sets of DNS data as well as analysis of the mean shear rate derived from log-law (i.e. $S = \partial\overline{U}/\partial z = u_\tau/\kappa z$) reveals that a log-law region hardly exists. Also, it is found that κ is not necessarily a universal constant, which is in agreement with findings of Hoyas & Jiménez (2006) and George (2007). However, this is a subject that needs more in-depth investigation and is beyond the scope of this present study.

These shortcomings result in the failure of the derived length scale ($f_\mu \kappa z(1 - z/\delta)^{0.5}$) compared to L_{TVH}. Hence, in order to alleviate this failure, the length scale is empirically modified and introduced as $L_\kappa = f_\mu \kappa z(1 - z/\delta)^{0.85}$, which agrees with available DNS data. The velocity scale (U_S) is also derived based on the equilibrium assumption between P and ϵ. We show that as the velocity scale carries a much lighter weight than L_κ in the turbulent viscosity formulation, it is reasonable to use the equilibrium assumption for inferring U_S.

Also, *'a priori'* tests are performed to assess the validity of our propositions by comparing with the exact turbulent channel flow DNS data. The proposed formulations compare remarkably well with the exact DNS data, highlighting their accuracy. Also, the behavior of P/ϵ which is an important parameter in the near-wall region is revisited using the proposed formulation for ν_t. The comparison of the estimated P/ϵ compares very well with the exact

DNS data, as well. We believe the findings of this study can help promote a renewed interest in understanding near-wall turbulence.